University of Alberta

Improved Mathematical Models for Fading and Shadowing in Wireless Channels

by

Seyed Ali Saberali

A thesis submitted to the Faculty of Graduate Studies and Research
in partial fulfillment of the requirements for the degree of

Master of Science
in
Communications

Department of Electrical and Computer Engineering

Fall 2013
Edmonton, Alberta

Dedicated to My Beloved Parents
and
My Beloved Wife, Elaheh

Abstract

Signal shadowing and multipath fading are two challenging phenomena in wireless communications. The goal of this thesis is to improve the statistical models and the mathematical tools required for description and analysis of some specific fading scenarios, namely lognormal shadowing, two-wave with diffuse power fading and diffuse Nakagami-*m* with line-of-sight fading. For lognormal shadowing, a novel method is proposed to derive approximations to the lognormal characteristic function. For two-wave with diffuse power fading, new expressions are derived for its probability density function, cumulative distribution function and moments. Finally, a novel fading model is introduced which combines a line-of-sight with a Nakagami-*m* diffuse scatter. The new fading model is justified and expressions are derived for its statistics. The new fading distribution is compared to the Rice, Nakagami-*m* and two-wave with diffuse power distributions. Application of the results in performance analysis of wireless systems operating in Nakagami-*m* with line-of-sight fading is investigated.

Acknowledgements

This dissertation would not have been possible without the help of so many people in so many ways. I would like to express my sincere gratitude to Professor Norman Beaulieu for supervising my research in two years of my M.Sc. program and for all the academic and professional skills I learned from him. Fulfilment of this dissertation would not have been possible without his guidance and persistent care.

I wish to acknowledge Professor Ying Tsui for his kind supports and in particular for organizing my final exam. I would like to thank the members of my evaluation committee, Professor Byron Schmuland from the Mathematical and Statistical Sciences Department, Dr. Yindi Jing and Dr. Bruce Cockburn from the Electrical and Computer Engineering Department of the University of Alberta.

I thank my fellow labmates in *i*CORE Wireless Communications Laboratory: Dr. Aydin Behnad, Dr. David Young, Mahdi Karami, Samy Soliman Shokry, Chunxing Jiang, Navod Suraweera and Kasun Hemachandra for their friendship and kind supports.

Finally, my most heartfelt thanks go to my parents and to my wife for their wholehearted and endless love, sympathy and patience.

I am not able to adequately express my appreciation for all adorable people through the words and in this limited space. This formal acknowledgment was just what my mind could think, but my heart forever thanks you all!

Table of Contents

List of Tables

List of Figures

List of Abbreviations

Abbreviation	Description	First Use
CLT	Central Limit Theorem	2
i.i.d.	independent and identically distributed	2
CF	Characteristic Function	2
LOS	Line-of-Sight	3
TWDP	Two-Wave with Diffuse Power	3
PDF	Probability Density Function	3
CDF	Cumulative Distribution Function	4
BER	Bit Error Rate	4
SER	Symbol Error Rate	4
BPSK	Binary Phase Shift Keying	4
RV	Random Variable	8
MGF	Moment Generating Function	10
CCDF	Complementary CDF	30

Chapter 1

Introduction

Wireless communications is a rapidly growing technology which aims to transfer information between sources and destinations, across the wireless channels linking them together. Real world communication channels suffer from various channel impairments that can severely degrade the communications performance. Some of these phenomena have random nature. Thermal noise, cochannel interference, multipath fading and signal shadowing are examples of such phenomena. In order to design and analyze the performance of wireless systems operating in such channels, it is necessary to construct mathematical models that reflect the physical characteristics of the transmission medium [1, 2]. Because of the random nature of many of these characteristics, statistical models must be used for their description. Multipath fading and shadowing are two challenging phenomena in wireless communications and their statistical modeling has been an essential field of research in the wireless communications literature over the last decades [2]. Due to the huge effort devoted to modeling and analysis of fading and shadowing systems, numerous mathematical models have been proposed to describe them, and they have been used to analyze the behavior and the performance of various communications schemes affected by these phenomena. In the remainder of this chapter, we provide a brief review on shadowing and multipath fading. Then, we briefly summarize the contributions of this dissertation on improving the mathematical and statistical tools for modeling and analysis of shadowing and fading systems.

1.1 Lognormal Shadowing

Buildings, terrain and trees commonly exist in wireless channels, both in urban and rural areas. In such channels, the level of the transmitted signal shadows successively as it passes through the obstacles in the propagation medium. As a result, the signal level captured by the receiver can be viewed as a product of the transmitted signal level and a number

of random attenuation coefficients. This leads to random variations in the received signal level at the receiver. Due to the central limit theorem (CLT) , the distribution of a product of independent and identically distributed (i.i.d.) random variables approaches a lognormal distribution [3, Theorem 7.2]. So, the shadowing effect is commonly modeled by a lognormal random variable. Performance analysis of many wireless shadowing systems requires evaluation of the distribution of sums of independent lognormal random variables. However, no exact closed-form solution is available for the lognormal sum distribution. A standard technique that can be used to evaluate the distribution of sums of independent random variables is to evaluate the product of their characteristic functions (CFs) and then take the inverse fourier transform of the result. However, evaluation of the lognormal CF is not straightforward as there is no closed-form expression available for it either. Moreover, the infinite series solution for the lognormal CF is divergent and can be used for its evaluation over a very limited range of parameters. Numerical evaluation of the lognormal CF using its defining integral form is also tedious because of the slow decay rate and the highly oscillatory nature of the integrand.

Various methods are proposed in the literature either to facilitate numerical evaluation of the lognormal CF or to provide approximate solutions for it [4–12]. Most of the proposed solutions have tried to solve this problem based on numerical techniques for computation of the integral form of the lognormal CF, and they have been successful to facilitate the required computations to different computational complexity levels. In this thesis, however, we follow a novel approach to derive approximate solutions to the lognormal characteristic function. Instead of numerical methods, we use the CLT as a means to achieve limiting expressions for the lognormal characteristic function. In addition to their theoretical importance, the limiting expressions can be used to approximate the lognormal CF. As the basic idea of our contributions toward this problem, we used the fact that the distribution of a product of i.i.d. random variables approaches a lognormal distribution when the number of random variables increases. So, the CF of a product of i.i.d. random variables also approaches the lognormal CF in the limit; i.e., when the number of random variables tends to infinity. The proposed method provides a framework to derive approximate solutions for the lognormal CF. This framework leads to a general infinite series in terms of the mean, variance and moment generating function of an appropriate random variable. Selection of any random variable in the derived series expression leads to an specific approximate solution for the lognormal CF. Examples of such solutions are also provided in this thesis, and their advantages and shortcomings are discussed.

1.2 Two-Wave with Diffuse Power Fading

Another significant phenomenon in wireless channels is multipath fading. Multipath fading results from reception of the transmitted signal through different propagation paths as a result of reflection, scattering or diffraction. The resulting signal components at the receiver may add destructively or constructively, which causes relatively fast variations in the signal level captured by the receiver [2]. The behavior of the received signal in multipath fading is highly dependent on the physical characteristics of the wireless channel, and it is not possible to describe the multipath effect by a general mathematical model, regardless of the specific characteristics of each fading channel. As a result, numerous statistical models have been proposed for multipath fading, each one suitable for a wireless channel with certain specifications. The Rayleigh distribution is one of the commonly used fading models, which can accurately describe the behavior of the received signal envelope when a relatively large number of multipath components are captured by the receiver, and none of them is dominant. The signal components with comparable strength are called the non-specular components of the received signal [13]. The combination of non-specular components at the receiver forms the diffuse part of the received signal. The presence of a line-of-sight (LOS) between the transmitter and the receiver creates a signal component at the receiver with a relatively strong power. Such a component is referred to as a specular component of the received signal [13]. When there is a LOS between the communication points, the Rayleigh distribution is no longer a valid model for the envelope of the received signal. The presence of LOS component in addition to a Rayleigh distributed diffuse component leads to the Rice model for the distribution of the received signal envelope.

A more recent model for the multipath effect, which considers a more complicated scenario, is the two-wave with diffuse power (TWDP) fading model [13]. This model assumes that the received signal consists of two LOS components and a Rayleigh distributed diffuse component. Analysis of TWDP fading systems has attracted much attention in the recent years. This is first because TWDP fading can behave very differently from the other fading models. For example, it is shown that the signal level in TWDP fading can reach low levels, even more often than the signal level in Rayleigh fading with comparable average power [13]. The second reason for investigating TWDP fading is its capability in modeling of many real world wireless channels. One can find many examples and scenarios which lead to TWDP fading in [13, 14]. Analysis of TWDP fading systems requires the TWDP fading PDF. The only available expression for the TWDP fading PDF is the approximate

expression given in [13, eq. (17)]. Although the approximate solution in [13, eq. (17)] has been used in the analysis of many wireless fading systems, we believe that it is worthwhile to search for other expressions for the TWDP fading PDF, which may be easier to evaluate and can lead to simpler expressions for the performance metrics of TWDP fading systems. In our attempt to fulfill this goal, we derive a new expression for the TWDP fading PDF in Chapter 3 of this thesis. The derived PDF expression is an infinite series which can be evaluated recursively using basic mathematical operations; i.e., summation and multiplication, with a low-complexity algorithm. The derived expressions makes fast and accurate evaluation of the TWDP fading PDF possible, over the practical range of TWDP fading parameters. Using the derived expression for the TWDP fading PDF, we also find new expressions for the TWDP cumulative distribution function (CDF) and moments. It is also shown that application of the derived PDF expression in performance analysis of some TWDP fading systems is straightforward. This is shown by evaluation of the integral of the complementary error function against the TWDP fading PDF, which is a building block for evaluating the bit error rate (BER) and the symbol error rate (SER) of fading systems. The derived expression for this integral is used for evaluating the BER of a BPSK system operating in TWDP fading.

1.3 Diffuse Nakagami-*m* with LOS Fading

The Nakagami-*m* distribution is another widely-used statistical model for multipath fading. According to many experimental measurements, the Nakagami-*m* distribution shows a better fit to the empirical data, compared to Rayleigh and Rice distributions [15, 16]. As a result, analysis of the performance of wireless systems operating in Nakagami-*m* fading has been thoroughly investigated in the literature. In some references, it is conjectured that the Nakagami-*m* fading can model the received signal envelope both in the presence and in the absence of a LOS component [16]. To the best of the author's knowledge, the behavior of combination of Nakagami-*m* diffuse fading and a LOS component has not yet been directly investigated in the literature.

In the last part of this thesis, we investigate diffuse Nakagami-*m* with LOS fading as a new fading model. We show that this model can behave significantly different from both the Rice and Nakagami-*m* fading models. We have also compared the new fading model to TWDP fading. It is shown that although TWDP fading shows a closer behavior to diffuse Nakagami-*m* with LOS fading, its behavior does not always match the diffuse Nakagami-*m* with LOS fading behavior. In our contributions regarding the diffuse Nakagami-*m* with

LOS fading model, we derive expressions for its PDF, CDF, moment generating function and moments. We develop efficient numerical algorithms for the low-complexity evaluation of the derived expressions. Application of the results for the performance analysis of fading systems is investigated. In particular, the BER of a BPSK system operating in diffuse Nakagami-*m* with LOS fading is derived and is compared to the BER of the same system operating in the TWDP and Nakagami-*m* fading environments.

1.4 Organization of the Thesis

The remainder of this thesis is organized in four chapters. Our contributions on the problem of calculating the lognormal CF are presented in Chapter 2. This chapter consists of two parts. The first part includes our paper, "New approximations to the lognormal characteristic function" [17], which was accepted and published in the proceedings of the *IEEE GC'12* conference. This paper contains our main contributions regarding the derivation of new approximate solutions for the lognormal CF. In the second part of Chapter 2, we provide a brief supplementary discussion about the paper and we explain our future work regarding this problem. Chapter 3 of this dissertation presents our contributions on the derivation of new expressions for the TWDP fading statistics. This chapter includes our paper "New Expressions for TWDP Statistics" [18] which has been published in *IEEE Wireless Communications Letters*. Chapter 3 also includes a brief supplementary discussion about some of the results obtained in the paper and proposes some the future research directions. Investigation of the diffuse Nakagami-*m* with LOS fading model is presented in Chapter 4 of this dissertation. This chapter presents our paper "A Novel Line-of-Sight Plus Diffuse Fading Model" [19] which was submitted to *IEEE Transactions on Information Theory*. Chapter 5 concludes the dissertation.

As the final point regarding the organization of this thesis, note that this thesis is paper-based and therefore the references used in each chapter are presented in the bibliography at the end of that chapter. So, the bibliography numbers given in each chapter of the dissertation are local to that chapter and are not preserved in the other chapters of the manuscript.

Bibliography

[1] J. G. Proakis, *Digital Communications,* 4th ed., New York: McGraw-Hill, 2001.

[2] M. K. Simon and M. S. Alouini, *Digital Communications over Fading Channels*, Wiley, 2005.

[3] A. Papoulis and S. U. Pillai, *Probability, Random Variables and Stochastic Processes*, New York: McGraw-Hill, 2002.

[4] R. Barakat, "Sums of independent lognormally distributed random variables," *J. Opt. Soc. Amer.,* vol. 66, no. 3, pp. 211-216, 1976.

[5] J. A. Gubner, "A new formula for lognormal characteristic functions," *IEEE Trans. Veh, Technol.*, vol. 55, no. 5, pp. 1668-1671, Sep. 2006.

[6] N. C. Beaulieu, "Fast convenient numerical computation of lognormal characteristic functions," *IEEE Trans. Commun.*, vol. 56, no. 3, pp. 331-333, Mar. 2008.

[7] N. C. Beaulieu, "A simple integral form of lognormal characteristic functions convenient for numerical computation," in *Proc. IEEE GLOBECOM '06,* San Francisco, CA, Nov. 2006, pp. 1-3.

[8] N. B. Mehta, J. Wu, A. F. Molisch and J. Zhang, "Approximating a sum of random variables with a lognormal," *IEEE Trans. Wireless Commun.*, vol. 6, no. 7, pp. 2690-2699, July 2007.

[9] N. C. Beaulieu, "A power series expansion for the truncated lognormal characteristic function," *25th Biennial Symp. Commun.*, May 2010.

[10] R. B. Leipnik, "On lognormal random variables: I - the characteristic function," *J. Austral. Math. Ser. B,* vol. 32, pp. 327-347, 1991.

[11] N. C. Beaulieu and Q. Xie, "An optimal lognormal approximation to lognormal sum distributions," *IEEE Trans. Veh. Technol.*, vol. 53, no. 2, pp. 479-489, Mar. 2004.

[12] C. Tellambura and D. Senaratne, "Accurate computation of the MGF of the lognormal distribution and its application to sum of lognormals," *IEEE Trans. Commun.*, vol. 58, no. 5, pp. 1568-1577, May 2010.

[13] G. D. Durgin, T. S. Rappaport, and D. A. Wolf, "New analytical models and probability density functions for fading in wireless communications," *IEEE Trans. Commun.,* vol. 50, no. 6, pp. 1005-1015, June 2002.

[14] J. Frolik, "A case for considering hyper-Rayleigh fading channels," *IEEE Trans. Wireless Commun.,* vol. 6, no. 4, pp. 1235-1239, Apr. 2007.

[15] M. Nakagami, " The m-distribution, a general formula of intensity of rapid fading," in *Statistical Methods in Radio Wave Propgation,* W. G. Hoffman, Ed. Oxford, England Pergamon, 1960.

[16] H. Suzuki, "A statistical model for urban radio propagation," *IEEE Trans. Commun.,* vol. 25, no. 7, pp. 673-680, July 1977.

[17] S. A. Saberali and N. C. Beaulieu, "New approximations to the lognormal characteristic function," *in proceedings of IEEE GC' 12,* pp. 2168-2172, Dec. 2012.

[18] S. A. Saberali and N. C. Beaulieu, "New expressions for TWDP fading statistics," *IEEE Wireless Commun. Lett.,* available in *IEEE* early access articles, Sep. 2013.

[19] N. C. Beaulieu and S. A. Saberali, "A novel line-of-sight plus diffuse fading model," *submitted to IEEE Trans. Info. Theory,* Sep. 2013.

Chapter 2

Approximation of the Lognormal Characteristic Function

In this chapter, we present our results on proposing new approximations to the lognormal CF. Sec. 2.1 covers our main contributions regarding this problem and includes our paper "New approximations to the lognormal characteristic function". Sec. 2.2 provides a supplementary discussion about the results obtained in Sec. 2.1, and briefly introduces our future research directions regarding the problem of approximating the lognormal CF.

2.1 New Approximations to the Lognormal Characteristic Function[1]

Authors: S. A. Saberali and N. C. Beaulieu

Published in the proceedings of IEEE GC'12

2.1.1 Introduction

Lognormal random variables (RVs) are used to describe a variety of phenomena in various fields of science and technology, such as biology, medicine, finance and communications [1]. As a result of the central limit theorem (CLT), a product of independent identically distributed (i.i.d.) positive RVs approaches a lognormal RV in distribution, as the number of RVs increases [2, Ch. 7]. This fact causes the lognormal distribution to arise widely in practice. In particular, the lognormal distribution appears in numerous problems in the modeling and analysis of communication systems. For instance, the effect of shadowing on the received signal in wireless communications is described by a lognormal RV. Furthermore, a sum of lognormal RVs is used to model cochannel interference in cellular networks and to evaluate outage probabilities [3].

[1] A version of this chapter has been published in the Proceedings of the IEEE GLOBECOM 2012 Conference, pp. 2168 - 2172, Anaheim, CA, Dec. 2012. Digital Object Identifier: 10.1109/GLOCOM.2012.6503436.

Throughout this paper we will denote by Z, a lognormal RV, with $Z \sim LN(\mu, \sigma^2)$ where μ and σ^2 are the mean and the variance of the corresponding normal RV. The probability density function (PDF) of Z is given by [2]

$$f_Z(z) = \frac{1}{\sqrt{2\pi}\sigma z} e^{-\frac{(\ln(z)-\mu)^2}{2\sigma^2}}, \quad z > 0. \tag{2.1}$$

The CF of a RV is a powerful tool in analysis involving RVs as it completely defines the PDF of the RV and often provides an effective way to analyze systems involving random parameters. As a significant case, one can calculate the CF of a sum of independent RVs by calculating the product of the summands' CFs [2]. Since lognormal RVs and their sums arise in many problems in wireless and optical communication systems, calculation of the lognormal CF is an essential element in the analysis of these systems. Unfortunately, this task is not straightforward as there exists no closed-form relationship for the lognormal CF [4]. Much effort has been devoted in the literature to find convenient methods for the evaluation of the lognormal CF [5–11].

Direct calculation of the lognormal CF through the defining integral

$$\phi_Z(\omega) = E(e^{j\omega Z}) = \int_0^\infty \frac{1}{\sqrt{2\pi}\sigma z} e^{-\frac{(\ln(z)-\mu)^2}{2\sigma^2}} e^{j\omega z} dz \tag{2.2}$$

is difficult as the integrand is highly oscillatory and the tail of the lognormal PDF decays very slowly [12]. Therefore, the integral (2.2) is not suitable for the common quadrature techniques [12]. Numerous integral representations and integration techniques have been proposed in the literature to facilitate calculation of the lognormal CF through numerical integration [6–9]. A standard approach for evaluating the lognormal CF would be to exploit infinite series representations. Divergence or poor convergence is the main drawback of this approach as usually the terms in such a series either diverge, or oscillate widely and grow to inordinate amplitude before "settling down" to decreasing amplitude. Nonetheless, various infinite series for evaluation of the lognormal CF were derived in [5, 10] which are convergent for specific ranges of parameters.

In this paper, we derive two novel approximations in terms of well-known mathematical functions to evaluate the lognormal CF. Each approximation is accurate and convenient for calculation over a specific range of lognormal RV parameters. Note that the ranges of parameters of lognormal RVs vary in different applications. In optical communications, for instance, σ is typically small and ranges from 10^{-2} to 1 [13]. In wireless communication applications, σ typically ranges from 2 dB to 13 dB (0.46 to 3) [14, 15].

This paper is organized as follows. In Sec. 2.1.2, we derive a novel closed-form approximation to the lognormal CF based on applying a Taylor series expansion in a nontraditional

place. The resulting approximation is accurate only for values of σ smaller than 0.3. In Sec. 2.1.3, we follow a new approach based on the CLT to approximate the lognormal CF with an infinite series. The infinite series is in terms of the moment generating function (MGF) of an appropriate ancillary RV. In Sec. 2.1.4, we propose an ancillary RV whose MGF leads to a finite series approximation to the lognormal CF which is given in terms of the generalized hypergeometric functions. These functions are available in most mathematical and engineering algebraic systems including MATLAB, Mathematica and Maple. The new approximation is accurate and convenient for calculating the CF for values of σ up to 10 dB. The theoretical results are tested by computer simulations in Sec. 2.1.5. Sec. 2.1.6 concludes the paper.

2.1.2 A Closed-Form Approximation to the Lognormal CF for Small Values of σ

In this section, we derive a simple approximation to the lognormal CF when σ is small ($\sigma < 0.3$). With no loss of generality we assume $\mu = 0$ in this section since it can easily be shown that the CF of a RV $W \sim LN(\mu, \sigma^2)$ is related to the CF of $Z \sim (0, \sigma^2)$ by [6]

$$\phi_W(\omega) = \phi_Z\left(e^{\mu}\omega\right). \tag{2.3}$$

Following the definition of the lognormal CF in (2.2) and then changing the dummy variable of integration to $z = e^{\sigma u}$, we can rewrite the lognormal CF in the form

$$\phi_Z(\omega) = \int_{-\infty}^{\infty} \frac{1}{\sqrt{2\pi}} e^{-\frac{u^2}{2}} \exp\left(j\omega e^{\sigma u}\right)\, du. \tag{2.4}$$

For small values of σ, one can approximate $e^{\sigma u}$ with the first three terms of the Taylor expansion of the exponential function; i.e. $e^{\sigma u} \approx 1 + \sigma u + \frac{1}{2}(\sigma^2 u^2)$. Although this approximation is not accurate when u gets large, because $e^{-u^2/2}$ decays very fast, the magnitude of the integrand for large u is close to zero, and therefore the approximation of the integral remains accurate. Using this approximation in (2.4) leads to

$$\begin{aligned}
\phi_Z(\omega) &\simeq \int_{-\infty}^{\infty} \frac{1}{\sqrt{2\pi}} e^{-\frac{u^2}{2}} \exp\left[j\omega\left(1 + \sigma u + \frac{1}{2}\sigma^2 u^2\right)\right] du \\
&= \frac{e^{j\omega}}{\sqrt{2\pi}} \int_{-\infty}^{\infty} e^{-\frac{1}{2}(1 - j\omega\sigma^2)u^2 + j\omega\sigma u}\, du \\
&= \frac{e^{j\omega}}{\sqrt{1 - j\sigma^2\omega}} \exp\left(-\frac{\sigma^2\omega^2}{2(1 - j\sigma^2\omega)}\right)
\end{aligned} \tag{2.5}$$

where we have used [16, eq. (3.323.2)]

$$\int_{-\infty}^{\infty} e^{-px^2 \pm qx}\, dx = \exp\left(\frac{q^2}{4p}\right)\sqrt{\frac{\pi}{p}}, \quad \Re\{p\} > 0 \tag{2.6}$$

to solve the last integral. Eq. (2.5) gives an approximate formula for evaluation of the lognormal CF. This approximation has a simple form and its calculation is easy and fast. Empirically, we have found that this approximation reaches visual precision for $\sigma < 0.3$. Thus, this new approximation will be useful for some applications in optical communication systems [13].

2.1.3 A General Series Approximation to the Lognormal CF

The approximation derived in the previous section is accurate for a limited range of parameters of the lognormal RV. So, we require another way to approximate the lognormal CF for larger values of σ. In this section, we derive a general infinite series for the lognormal CF based on the CLT for RVs. Using the results of this section, we will derive an approximation to the lognormal CF in Section IV which remains accurate for a wider range of values of σ.

Let $\{Y_i\}_{i=1}^n$ be a set of n positive i.i.d. random variables. Define

$$X_i = \ln Y_i, \quad i = 1, 2, ..., n \tag{2.7}$$

as a set of n new random variables with common means μ_x and common variances σ_x^2. Also define the RV

$$p_n = Y_1 Y_2 ... Y_n \tag{2.8}$$

as the product of the Y_is. According to the CLT for the product of positive i.i.d. RVs, as n gets large the distribution of p_n approaches a lognormal distribution with parameters $(n\mu_x, n\sigma_x^2)$ [2, p. 284]; i.e.

$$f_{p_n}(z) \simeq \frac{1}{\sqrt{2n\pi}\sigma_x z} e^{-\frac{(\ln(z)-n\mu_x)^2}{2n\sigma_x^2}}, \quad z > 0. \tag{2.9}$$

If we normalize the product in (2.8) as

$$P_n = p_n^{\frac{\sigma}{\sigma_x\sqrt{n}}} \exp\left(-\frac{\sigma\sqrt{n}}{\sigma_x}\mu_x + \mu\right) \tag{2.10}$$

then

$$\begin{aligned} P_n &= (Y_1 Y_2 ... Y_n)^{\frac{\sigma}{\sigma_x\sqrt{n}}} \exp\left(-\frac{\sigma\sqrt{n}}{\sigma_x}\mu_x + \mu\right) \\ &= \exp\left[\frac{\sigma}{\sigma_x\sqrt{n}}\left(X_1 + X_2 + ... + X_n - n\mu_x\right) + \mu\right]. \end{aligned} \tag{2.11}$$

As n gets large, the term in the exponent approaches a normal distribution with mean μ and variance σ^2. Therefore P_n approaches $Z \sim LN(\mu, \sigma^2)$ in its distribution. For n sufficiently large, one can approximate the CF of Z with the CF of P_n; i.e.

$$\phi_Z(\omega) = E\left(e^{j\omega Z}\right) \simeq E\left(e^{j\omega P_n}\right) = \phi_{P_n}(\omega). \tag{2.12}$$

To fulfill this goal we have to derive a relationship for the CF of P_n. Following the definition of the CF, we can write

$$\begin{aligned}
\phi_{P_n}(\omega) =& E(e^{j\omega P_n}) = E\left[\sum_{k=0}^{\infty}\frac{(j\omega P_n)^k}{k!}\right] \\
=& \sum_{k=0}^{\infty}\frac{(j\omega)^k}{k!}E\left\{\left[(Y_1Y_2...Y_n)^{\frac{\sigma}{\sigma_x\sqrt{n}}}\exp(-\frac{\sigma\sqrt{n}}{\sigma_x}\mu_x+\mu)\right]^k\right\} \\
=& \sum_{k=0}^{\infty}\frac{\left[j\omega\exp(-\frac{\sigma\sqrt{n}}{\sigma_x}\mu_x+\mu)\right]^k}{k!}E\left[(Y_1Y_2...Y_n)^{\frac{\sigma k}{\sigma_x\sqrt{n}}}\right] \\
=& \sum_{k=0}^{\infty}\frac{\left[j\omega\exp(-\frac{\sigma\sqrt{n}}{\sigma_x}\mu_x+\mu)\right]^k}{k!}\left[E(Y_i^{\frac{\sigma k}{\sigma_x\sqrt{n}}})\right]^n \\
=& \sum_{k=0}^{\infty}\frac{\left[j\omega\exp(-\frac{\sigma\sqrt{n}}{\sigma_x}\mu_x+\mu)\right]^k}{k!}\left[E(e^{\frac{\sigma}{\sigma_x\sqrt{n}}kX_i})\right]^n \\
=& \sum_{k=0}^{\infty}\frac{\left[j\omega\exp(-\frac{\sigma\sqrt{n}}{\sigma_x}\mu_x+\mu)\right]^k}{k!}\left[M_X(\frac{\sigma k}{\sigma_x\sqrt{n}})\right]^n
\end{aligned} \tag{2.13}$$

where $M_X(s)$ is the MGF of X_i defined as [2]

$$M_X(s) = E\left(e^{sX_i}\right) = \int_{-\infty}^{\infty} f_{X_i}(x)e^{sx}dx. \tag{2.14}$$

Eq. (2.13) gives a general relationship between the CF of the product of n i.i.d RVs and the MGF of the logarithm of each RV. For different choices of the RV Y (or equivalently X), eq. (2.13) results in different approximations to the lognormal CF.

We have two considerations in the selection of X. First, since s admits values from 0 to ∞ in (2.13), the region of convergence of $M_X(s)$, which is the Laplace transform of $f_{X_i}(x)$, should include the non-negative real line. As a result, the family of gamma-distributed RVs (exponential, chi-square and gamma) are not good choices for X as their MGFs are not defined over the entire non-negative real line. The second consideration is the convergence of the infinite series in (2.13). Substitution of some RVs in (2.13) may result in a divergent infinite series. As a special example, suppose we select X to be a normal RV with mean 0 and variance 1. Then, the MGF of X will be $M_X(s) = \exp(\frac{1}{2}s^2)$ [2]. Now consider $n = 1$. In this case, we will have $Y \sim LN(0,1)$ and $P_n \sim LN(\mu,\sigma^2)$. Thus,

(2.13) leads to an exact relationship for the lognormal CF as

$$\begin{aligned}\phi_Z(\omega) = \phi_{P_n}(\omega) &= \sum_{k=0}^{\infty} \frac{(j\omega e^{\mu})^k}{k!} e^{\frac{1}{2}(\sigma k)^2} \\ &= \sum_{k=0}^{\infty} \frac{(j\omega)^k}{k!} e^{\mu k + \frac{1}{2}\sigma^2 k^2} \end{aligned} \tag{2.15}$$

which is the well-known divergent infinite series representation of the lognormal CF. The terms in this series grow exponentially as $k^2 - k \ln k$. So, for any value of μ, the series rapidly diverges.

By taking these considerations in account, we will derive a new approximation to the lognormal CF using (2.13), in the next section.

2.1.4 A finite series approximation[2] to the lognormal CF for larger values of σ

Let X be a uniform random variable in the interval $[a, b]$; i.e. $X \sim U(a, b)$. The mean, variance and MGF of a uniform RV are given by [2]

$$E(X) = \frac{a+b}{2} \tag{2.16}$$

$$Var(X) = \frac{(b-a)^2}{12} \tag{2.17}$$

$$M_X(s) = \begin{cases} \dfrac{\exp(sb) - \exp(sa)}{s(b-a)}, & s \neq 0 \\ 1 \quad , & s = 0 \end{cases}. \tag{2.18}$$

Observe that the MGF is defined over the entire non-negative real line. Substitution of (2.16)-(2.18) in (2.13) leads to

$$\phi_{P_n}(\omega) = 1 + \sum_{k=1}^{\infty} \frac{\left(j\omega e^{-\sqrt{3n}\,\frac{b+a}{b-a}\,\sigma}\right)^k}{k!} \left[\frac{e^{\sqrt{\frac{12}{n}}\,\frac{b}{b-a}\,\sigma k} - e^{\sqrt{\frac{12}{n}}\,\frac{a}{b-a}\,\sigma k}}{\sqrt{\frac{12}{n}}\,\sigma\, k} \right]^n \tag{2.19}$$

[2] It is not an accurate statement to call (2.22) a finite series approximation as the generalized hypergeometric functions are themselves defined by infinite series expressions [25, Sec. 9.14]. So, we modify this title to "A finite sum approximation to the lognormal CF in terms of the generalized hypergeometric functions for larger values of σ. (This footnote is added to the thesis and was not included in the paper.)

where we assumed that $\mu = 0$ as justified in Sec. 2.1.2. By using the binomial expansion of $(x+y)^n$ we can rewrite (2.19) as

$$\begin{aligned}\phi_{P_n}(\omega) =& 1 + \left(\frac{n}{12\sigma^2}\right)^{\frac{n}{2}} \sum_{k=1}^{\infty} \left\{ \frac{\left[j\omega e^{-\sqrt{3n}\frac{b+a}{b-a}\sigma}\right]^k}{k!\, k^n} \right. \\ & \left. \times \sum_{l=0}^{n} \binom{n}{l} (-1)^l e^{\sqrt{\frac{12}{n}}\frac{b}{b-a}\sigma k(n-l)} e^{\sqrt{\frac{12}{n}}\frac{a}{b-a}\sigma k l} \right\} \\ =& 1 + \left(\frac{n}{12\sigma^2}\right)^{\frac{n}{2}} \sum_{l=0}^{n} \binom{n}{l} (-1)^l \sum_{k=1}^{\infty} \frac{\left[j\omega e^{(\sqrt{3n}-\sqrt{\frac{12}{n}}\, l)\sigma}\right]^k}{k!\, k^n}. \end{aligned} \tag{2.20}$$

The infinite series in (2.20) can be represented in closed-form[3] as

$$\begin{aligned}\sum_{k=1}^{\infty} \frac{x^k}{k!\, k^n} &= x \sum_{k=1}^{\infty} \frac{x^{k-1}}{k! k^n} = x \sum_{k=0}^{\infty} \frac{x^k}{k!\, (k+1)^{n+1}} \\ &= x\ {}_{n+1}F_{n+1}\left(1, ..., 1; 2, ..., 2; x\right) \end{aligned} \tag{2.21}$$

where ${}_{n+1}F_{n+1}(1, ..., 1; 2, ..., 2; x)$ is the generalized hypergeometric function. We have used its infinite series representation given in [17] in the derivation of (2.21). Using (2.21), we can rewrite (2.20) as

$$\begin{aligned}\phi_{P_n}(\omega) = 1 + j\omega e^{\sqrt{3n}\,\sigma} \left(\frac{n}{12\sigma^2}\right)^{\frac{n}{2}} \times \sum_{l=0}^{n} \left\{ \binom{n}{l} (-1)^l e^{-\sqrt{\frac{12}{n}}\sigma\, l} \right. \\ \left. {}_{n+1}F_{n+1}\left(1, ..., 1; 2, ..., 2; j\omega e^{(\sqrt{3n}-\sqrt{\frac{12}{n}}\, l)\sigma}\right) \right\}. \end{aligned} \tag{2.22}$$

Eq. (2.22) gives an approximate finite series representation for the lognormal CF in terms of the generalized hypergeometric functions. As n increases, the approximation in (2.22) rapidly converges to the true CF since the distribution of a sum of uniform RVs rapidly converges to a normal distribution [2, 18]. Consequently, the product RV in (2.8) is approximately lognormally distributed even for small values of n ($n \geq 3$).

To evaluate the CF for $0 \leq \omega \leq \omega_m$, we have to calculate the generalized hypergeometric function for values of the argument as large as $j\omega_m e^{\sqrt{3n}\,\sigma}$. This argument grows exponentially with $\sqrt{n}$. One should note that the calculation of the generalized hypergeometric function gets more difficult as the argument gets larger. So the value of n cannot be

[3] According to some definitions for a closed-form expression, a generalized hypergeometric function cannot generally be considered as a closed-form expression, as it cannot be converted into an expression containing only elementary functions, combined by a finite amount of rational operations and compositions. So, we modify our statement here by removing the word "closed-form". (This footnote is added to the thesis and was not included in the paper.)

selected arbitrarily large. On one hand, selecting a large value for n leads to a more precise CF, while on the other hand, the computational complexity increases as n gets large. Thus there is a tradeoff in the selection of n between the accuracy of the approximation and the computational complexity. Also note that the term in the exponent of the argument of the hypergeometric function is linearly proportional to σ. Thus computation of (2.22) becomes more difficult as σ gets larger. A more detailed discussion about this issue will follow in Sec. 2.1.5.

2.1.5 Simulation Results

In this section, we present some examples for evaluation of the lognormal CF using the derived formulas in (2.5) and (2.22). Results obtained from computer simulations are also presented to test the accuracy of the theoretical results. In the simulations, $\mu = 0$ is assumed without loss of generality according to (2.3).

The first three examples are motivated by optical communication applications where σ ranges from 10^{-2} to 1. Figs. 2.1-2.3 show the calculated lognormal CFs for $\sigma = 0.05, 0.3$ and 0.7, respectively. For the first two cases, the values of σ are small and we can use both the formulas in (2.5) and (2.22) to approximate the CF. Empirically, we have found that the approximation in (2.5) is accurate only for $\sigma < 0.3$. The CFs obtained from computer simulations are also presented in the figures. For each case, computer simulation results are achieved by generating $N_s = 10^7$ samples of a lognormal RV with the specified parameters. By denoting the set of samples as $\{z_k\}_{k=1}^{N_s}$, we can evaluate the CF empirically by

$$\phi_Z(\omega) \approx \frac{1}{N_s} \sum_{k=1}^{N_s} e^{j\omega z_k}. \tag{2.23}$$

The figures illustrate excellent agreement between the approximation curves and the simulation results. As we see, small values of σ result in oscillatory CFs for the lognormal RV. To track the oscillations of the CF for small values of σ, we need to use more terms in the summation in (2.22). Empirically, we have found that for $\sigma < 0.5$ it suffices to set n equal to 5 or 6 to achieve accurate results. Figs. 2.1 and 2.2 are plotted for $n = 5$. Note that to calculate the CF when $\sigma < 0.3$, it is preferred to use (2.5) instead of (2.22) since (2.5) provides more accurate results with less computational complexity.

In Fig. 2.3, we use only (2.22) to approximate the CF since (2.5) is not accurate for $\sigma > 0.3$. To achieve the approximate curve in Fig. 2.3 we set $n = 5$ in (2.22). We see that the real and imaginary parts of the CF are less oscillatory. As a result, the match between

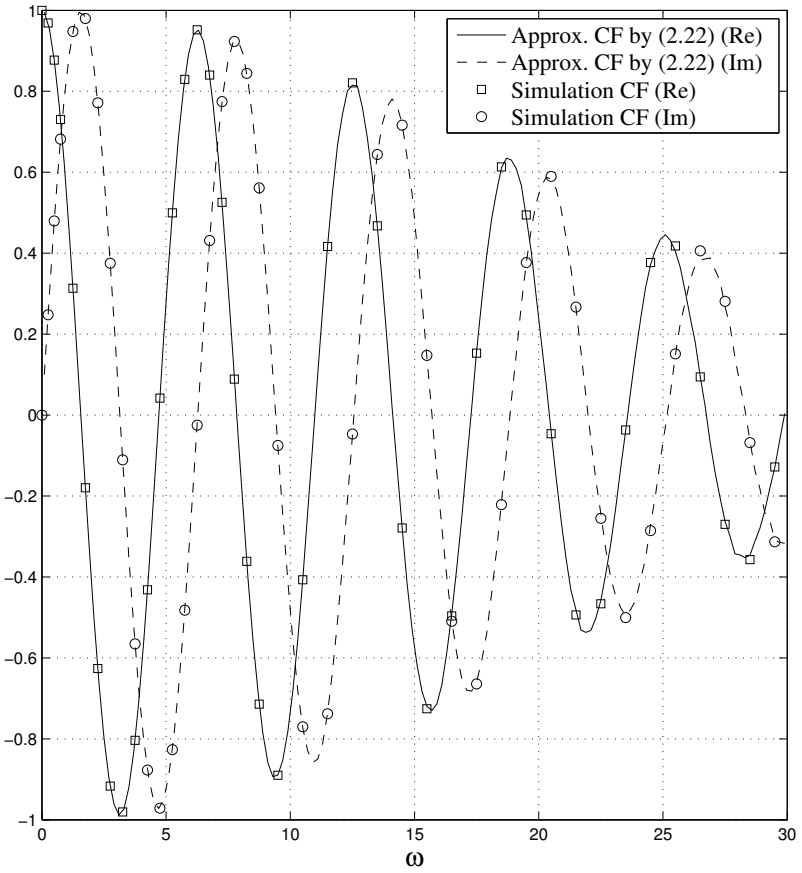

Figure 2.1. Approximation and simulation CFs for a lognormal RV with $\sigma = 0.05$. Six terms are used ($n = 5$) for the approximation in (2.22).

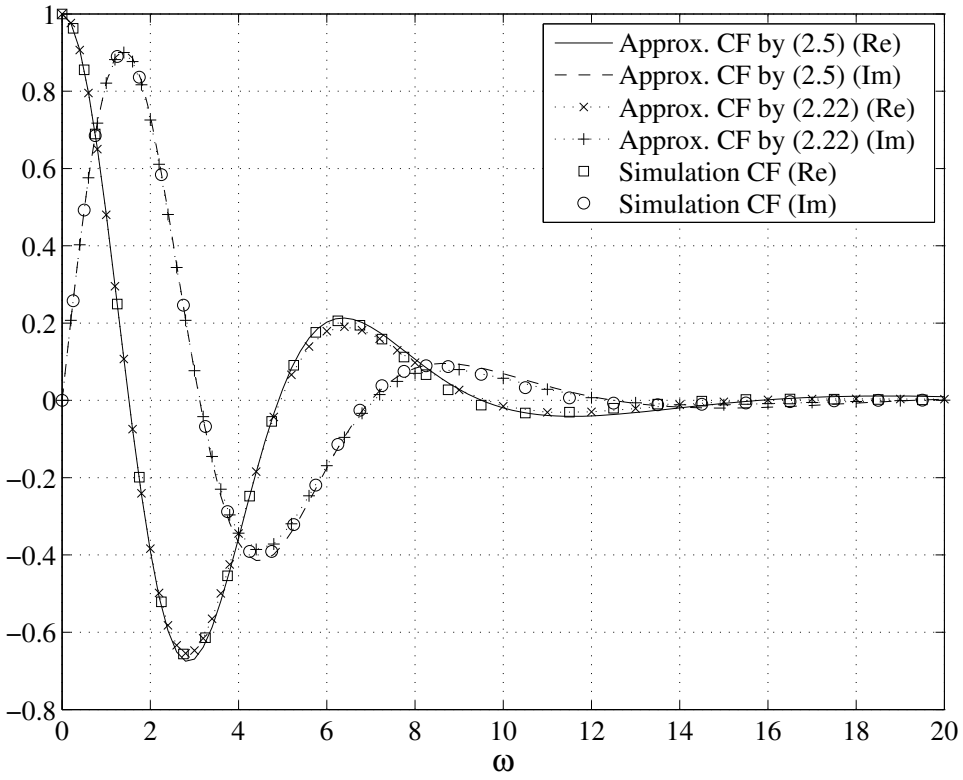

Figure 2.2. Approximation and simulation CFs for a lognormal RV with $\sigma = 0.3$. Six terms are used ($n = 5$) for the approximation in (2.22).

the simulation CF and the approximation CF using (2.22) is better in Fig. 2.3 compared to Figs. 2.1 and 2.2.

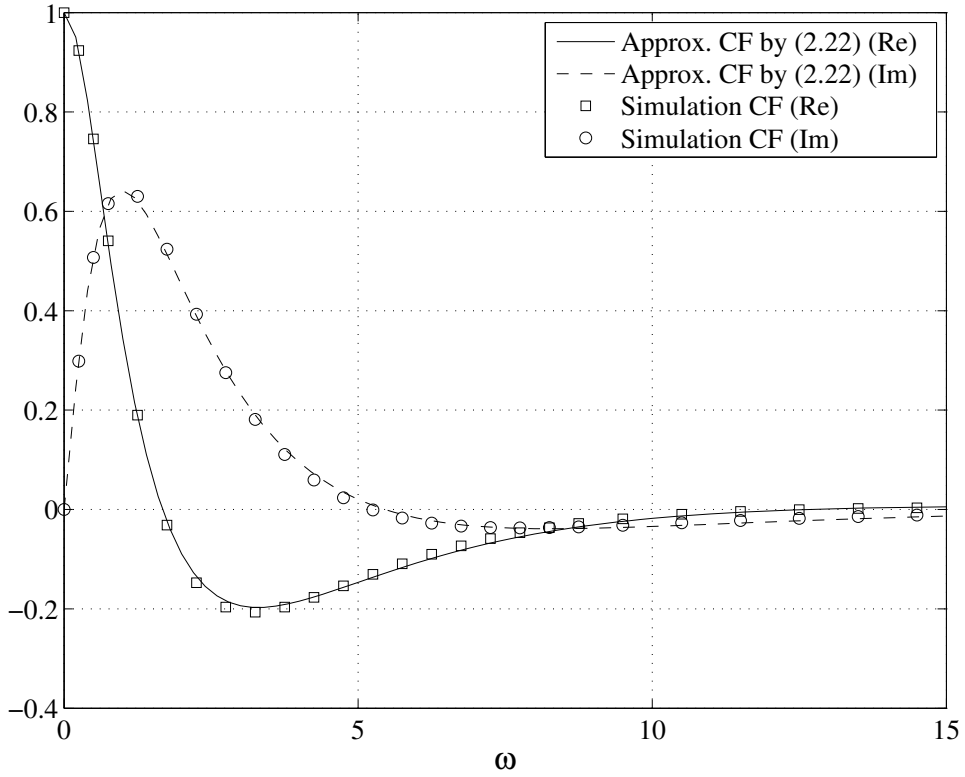

Figure 2.3. Approximation and simulation CFs for a lognormal RV with $\sigma = 0.7$. Six terms are used ($n = 5$) for the approximation in (2.22).

The remaining examples are selected as lognormal CFs with parameters that arise in wireless communication applications. Figs. 2.4 and 2.5 show the CFs for lognormal RVs with σ_{dB} equal to 6 dB ($\sigma = 1.382$) and 10 dB ($\sigma = 2.3$), respectively. Note that σ_{dB} and σ are related by $\sigma = 0.1 \ln 10 \times \sigma_{dB}$ [19]. We observe that as σ increases, the CF decays slower and shows less oscillatory behavior.

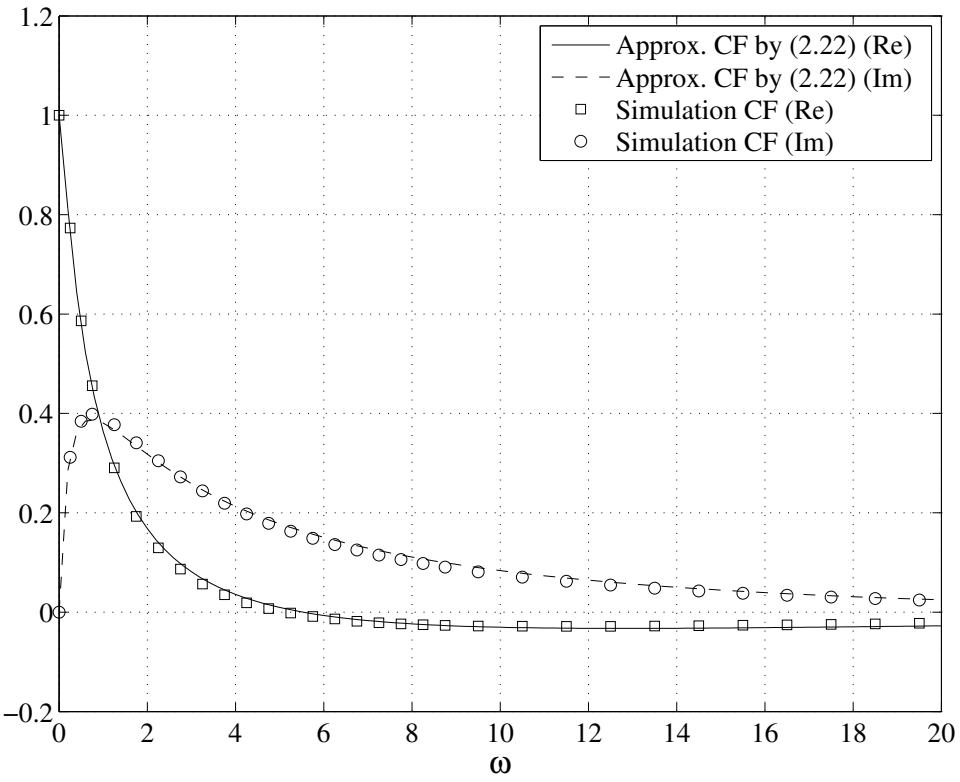

Figure 2.4. Approximation and simulation CFs for a lognormal RV with $\sigma_{dB} = 6$ dB ($\sigma = 1.382$). Five terms are used ($n = 4$) for the approximation in (2.22).

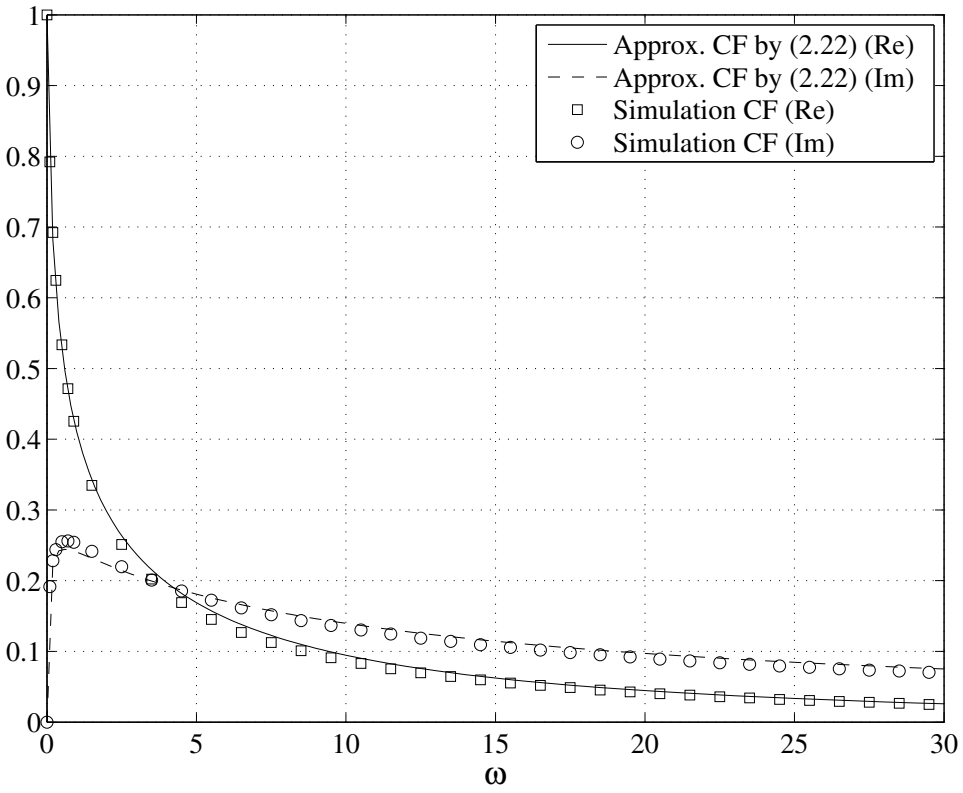

Figure 2.5. Approximation and simulation CFs for a lognormal RV with $\sigma_{dB} = 10$ dB ($\sigma = 2.3$). Four terms are used ($n = 3$) for the approximation in (2.22).

In Sec. 2.1.4 we argued that the argument of the generalized hypergeometric function, i.e. $j\omega e^{\sqrt{3n}\sigma}$, grows more rapidly as σ increases. This makes evaluation of the generalized hypergeometric function more complex for large values of σ, and therefore increases the calculation time of the CF using (2.22). On the other hand, for large values of σ, the CF is less oscillatory and the approximate relationship in (2.22) converges more rapidly to the true CF. Therefore, in order to decrease the rate of growth of the argument, we can select a smaller value for n, compared to the case of small σ. In Figs. 2.4 and 2.5 we used $n = 4$ and $n = 3$ to achieve the approximate curves, respectively. Unfortunately, we find that for values of σ larger than 10 dB, the evaluation of (2.22) becomes very time consuming. This constrains the use of (2.22) to approximate the lognormal CF to values of σ not larger than 10 dB.

2.1.6 Conclusion

In this paper we derived two approximations for the lognormal CF, each one useful for a specific range of values of σ. One approximation is in terms of elementary mathematical

functions and is valid for small values of σ. Calculation of this approximate formula is simple and fast. The other approximate formula for the lognormal CF is in terms of the generalized hypergeometric functions and gives accurate results over a much larger range of values of σ. Calculation of the latter approximation is fast for small values of σ, but becomes slow as σ becomes large. The accuracy of the theoretical results was demonstrated by computer simulations.

2.2 Supplementary Discussion

In this section, we derive another limiting expression for the lognormal CF using the method proposed in Sec. 2.1.3. Then, we discuss our future works.

2.2.1 Another Limiting Expression for the Lognormal CF

As was discussed in the paper, one can derive approximate solutions other than (2.22) by choosing X in (2.13) to have a distribution other than the uniform distribution. For example, let $X = -W$, where $W \sim \mathcal{G}(\alpha, \lambda)$, be a gamma RV with parameters $\alpha > 0$ and $\lambda > 0$ and the MGF [2]

$$M_W(s) = \frac{1}{(1 - \frac{s}{\lambda})^{\alpha}}, \quad \Re\{s\} < \lambda. \tag{2.24}$$

Note that the region of convergence of $M_W(s)$ does not include the entire non-negative real line. So, to use (2.13), we defined X as $-W$ to have $M_X(s) = M_W(-s)$. The region of convergence of $M_X(s)$ is $\Re\{s\} > -\lambda$ which includes the non-negative real line. Also note that $\mu_X = -\frac{\alpha}{\lambda}$ and $\sigma_X = \frac{\sqrt{\alpha}}{\lambda}$ [2]. Substitution of these parameters in (2.13) yields

$$\phi_{P_n^{(2)}}(\omega) = \sum_{k=0}^{\infty} \frac{\left[j\omega e^{\sigma\sqrt{\alpha n}+\mu}\right]^k}{k!(1 + \frac{\sigma k}{\sqrt{\alpha n}})^{\alpha n}} = \sum_{k=0}^{\infty} \frac{\left[j\omega e^{\sigma\sqrt{m}+\mu}\right]^k}{k!(1 + \frac{\sigma k}{\sqrt{m}})^{m}} \tag{2.25}$$

where $m \triangleq \alpha n$. Note that since a gamma distribution with $\alpha = 1$ is an exponential distribution, (2.28) can be seen as the resulting series obtained by choosing X_is to be m i.i.d. negative-exponential RVs, instead of n i.i.d. negative-gamma RVs. Following the standard series convergence tests, one can easily show that (2.25) is convergent. For example, for the real part of (2.25), we have

$$\Re\left\{\phi_{P_n^{(2)}}(\omega)\right\} = \sum_{k=0}^{\infty} \underbrace{\frac{(-1)^k \left[\omega e^{\sigma\sqrt{m}+\mu}\right]^{2k}}{(2k)!(1 + \frac{2\sigma k}{\sqrt{m}})^{m}}}_{\triangleq a_k}. \tag{2.26}$$

Applying the ratio test for the convergence of the infinite series to (2.26) yields

$$\lim_{k\to\infty} \left|\frac{a_{k+1}}{a_k}\right| = \frac{\omega^2}{4} \exp(2\sigma\sqrt{m} + 2\mu) \lim_{k\to\infty} \frac{1}{(k+1)(k+1/2)} \left(1 - \frac{2\sigma}{\sqrt{m} + 2\sigma k + 2\sigma}\right) = 0 < 1 \tag{2.27}$$

which shows that the series is convergent. Similarly, one can show that the imaginary part of (2.25) is convergent. Although the ratio test in (2.27) shows that (2.25) is convergent, the constant value behind the second limit in (2.27) shows that the ratio of successive coefficients in the series grows exponentially with σ, μ and $\sqrt{m}$, and therefore the series needs

more terms to settle as these parameters increase. This means that to evaluate the infinite series approximation in (2.25), a larger truncation order must be selected as σ, μ and $\sqrt{m}$ increase. As was the case for the infinite series in (2.20), the evaluation of (2.25) with a large truncation order is not straightforward. So we express (2.25) in terms of known mathematical functions, as their efficient evaluation is more investigated. Fortunately, when m is an integer, the series (2.25) can be expressed as a generalized hypergeometric function as [16]

$$\phi_{P_n^{(2)}}(\omega) = {}_mF_m\left(\frac{\sqrt{m}}{\sigma}, ..., \frac{\sqrt{m}}{\sigma}; 1 + \frac{\sqrt{m}}{\sigma}, ..., 1 + \frac{\sqrt{m}}{\sigma}; j\omega e^{\sigma\sqrt{m}+\mu}\right). \tag{2.28}$$

Unfortunately, (2.28) converges only slowly to the lognormal CF, and overly large values of m must be selected to obtain an accurate approximation. Note that as m increases the order of the hypergeometric function and the values of its arguments increase. So evaluation of (2.28) becomes extremely time consuming to the extent that it becomes useless in practice. Since (2.28) gives the lognormal CF as a limiting case of the generalized hypergeometric function, it can be important from a theoretical point of view.

2.2.2 Future Work

In this chapter, we proposed a framework to derive limiting expressions for the lognormal CF. Using this framework, we derived two limiting expressions for the lognormal CF in eqs. (2.22) and (2.28), in terms of generalized hypergeometric functions. Eq. (2.28) was shown to converge slowly to the lognormal CF, and therefore was not useful in practice. However, it can be important from an academic point of view, as it represents the lognormal CF as a limiting case of a generalized hypergeometric function. The other expression in (2.22) is more suitable for practical applications as it converges to the lognormal CF very fast. Note that improvements in calculation of the hypergeometric function ${}_qF_q(\cdot;\cdot;\cdot)$ can facilitate evaluation of (2.22), and therefore, make it possible to increase the accuracy of the approximation in (2.22) by selecting larger values of n.

The use of the proposed framework for finding limiting expressions for the lognormal CF is not limited to our results in this chapter. In fact, we only examined some well-known random variables for substitution as the ancillary random variable in (2.13), and among them we selected two cases for which we could represent the resulting expressions in terms of well-known mathematical functions. One could select other random variables whose sums approach to the normal distribution faster than uniform random variables, or select a random variable in which substitution of its mean, variance and moment generating function

in (2.13) leads to a more rapidly converging infinite series. Although finding such random variable may not be straightforward, a more thorough search for them should be performed.

Bibliography

[1] E. Limpert, W. A. Stahel, and M. Abbt, "Lognormal distributions across the sciences: keys and clues," *BioScience,* vol. 51, no. 5, pp. 341-352, May 2001.

[2] A. Papoulis and S. U. Pillai, *Probability, Random Variables and Stochastic Processes*, New York: McGraw-Hill, 2002.

[3] T. S. Rappaport, *Wireless Communications - Principles and Practice*, New Jersey: Prentice Hall, 1996.

[4] N. L. Johnson, S. Kotz, and N. Balakrishnan, *Continuous Univariate Distributions,* 2nd ed, vol. 1, New York: Wiley, 1994.

[5] R. Barakat, "Sums of independent lognormally distributed random variables," *J. Opt. Soc. Amer.,* vol. 66, no. 3, pp. 211-216, 1976.

[6] J. A. Gubner, "A new formula for lognormal characteristic functions," *IEEE Trans. Veh, Technol.*, vol. 55, no. 5, pp. 1668-1671, Sep. 2006.

[7] N. C. Beaulieu, "Fast convenient numerical computation of lognormal characteristic functions," *IEEE Trans. Commun.*, vol. 56, no. 3, pp. 331-333, Mar. 2008.

[8] N. C. Beaulieu, "A simple integral form of lognormal characteristic functions convenient for numerical computation," in *Proc. IEEE GLOBECOM '06,* San Francisco, CA, Nov. 2006, pp. 1-3.

[9] N. B. Mehta, J. Wu, A. F. Molisch and J. Zhang, "Approximating a sum of random variables with a lognormal," *IEEE Trans. Wireless Commun.*, vol. 6, no. 7, pp. 2690-2699, July 2007.

[10] N. C. Beaulieu, "A power series expansion for the truncated lognormal characteristic function," *25th Biennial Symp. Commun.*, May 2010.

[11] R. B. Leipnik, "On lognormal random variables: I - the characteristic function," *J. Austral. Math. Ser. B,* vol. 32, pp. 327-347, 1991.

[12] N. C. Beaulieu and Q. Xie, "An optimal lognormal approximation to lognormal sum distributions," *IEEE Trans. Veh. Technol.*, vol. 53, no. 2, pp. 479-489, Mar. 2004.

[13] X. Zhu and J. M. Kahn, "Free-space optical communication through atmospheric turbulance channels," *IEEE Trans. Commun.*, vol. 50, no. 8, pp. 1293-1300, Aug. 2002.

[14] Y. Yeh and S. C. Schwartz, "Outage probability in mobile telephony due to multiple lognormal interferers," *IEEE Trans. Commun.,* vol. 32, no. 4, pp. 380-388, Apr. 1984.

[15] N. C. Beaulieu, "An extended limit theorem for correlated lognormal sums," *IEEE Trans. Commun.*, vol. 60, no. 1, pp. 23-26, Jan. 2012

[16] I. S. Gradshteyn and I. M. Ryzhik, *Table of Integrals, Series, and Products,* San Diego, CA: Academic Press, seventh ed., 2007.

[17] M. Abramowitz and I. A. Stegun, *Handbook of Mathematical Functions with Formulas, Graphs, and Mathematical Tables*, New York: Dover, 1970.

[18] Y. Chen and N. C. Beaulieu, "A simple polynomial approximation to the Gaussian Q-function and its application," *IEEE Commun. Lett.*, vol. 13, no. 2, pp. 124-126, Feb. 2009.

[19] S. S. Szyszkowicz and H. Yanikomeroglu, "Limit theorem on the sum of identically distributed equally and positively correlated joint lognormals," *IEEE Trans. Commun.*, vol. 57, no. 12, pp. 3538-3542, Dec. 2009.

Chapter 3

Improved Mathematical Tools for Analysis of TWDP Fading Systems

This chapter includes our contributions on the derivation of new expressions for the TWDP fading statistics, and their application in the analysis of wireless fading systems. This chapter is organized in two sections. Sec. 3.1 includes our paper "New expressions for TWDP fading statistics" which has been published in *IEEE Wireless Communications Letters*. Sec. 3.2 provides some supplementary materials regarding the results in Sec. 3.1. In this section, a brief comparison is also made between the results obtained in the paper and the results available in the TWDP literature for the performance analysis of BPSK fading systems. Sec. 3.2 also explains our future research directions regarding the analysis of TWDP systems.

3.1 New Expressions for TWDP Fading Statistics[1]

Authors: S. A. Saberali and N. C. Beaulieu

Published in IEEE Wireless Communications Letters

3.1.1 Introduction

Two-wave with diffuse power (TWDP) is a useful fading model introduced in [1]. This model has attracted much attention as it can behave very differently from the previously studied fading distributions and it models many practical wireless communication systems [1, 2]. The model assumes that the received signal has two relatively strong multipath components and numerous low power diffuse components. The mathematical TWDP fading

[1] A version of this chapter has been published in the IEEE Wireless Communication Letters and is available in IEEE early access articles. Digital Object Identifier: 10.1109/WCL.2013.090313.130541.

model is

$$\tilde{V} = V_1 e^{j\psi_1} + V_2 e^{j\psi_2} + \tilde{V}_{dif} \tag{3.1}$$

where $\tilde{V}$ is the received baseband signal and V_1, V_2, ψ_1 and ψ_2 represent the magnitudes and phases of two specular components, respectively. The phases are independent and uniformly distributed in $[0, 2\pi]$. The contribution of nonspecular components is reflected in $\tilde{V}_{dif}$ as a diffuse component whose mean-squared voltage is $2\sigma^2$, and its real and imaginary parts follow a normal distribution [1].

Knowledge of the probability density function (PDF) of TWDP fading, which is the PDF of the envelope of $\tilde{V}$, is required in the performance analysis of TWDP fading systems. This PDF was shown to have the integral form [1]

$$f_R(r) = r \int_0^\infty \exp\left(-\frac{\sigma^2\nu^2}{2}\right) J_0(r\nu) J_0(V_1\nu) J_0(V_2\nu) \nu d\nu \tag{3.2}$$

where R represents the envelope of $\tilde{V}$. Eq. (3.2) can be expressed as [3, Sec. 8.7]

$$f_R(r) = r\sigma^2 \Psi_2^{(3)}\left(1; 1, 1, 1; -\frac{\sigma^2}{2}V_1^2, -\frac{\sigma^2}{2}V_2^2, -\frac{\sigma^2}{2}r^2\right) \tag{3.3}$$

where $\Psi_2^{(n)}(\cdot;\cdot;\cdot)$ is the confluent Lauricella function [3, Sec. 2.1.1], [4, eq. (36)]. However, confluent Lauricella functions must be calculated numerically using their integral form or their three-fold infinite series form [3–5]. Moreover, integration of confluent Lauricella functions against other mathematical functions is not well studied. Therefore, (3.3) is not useful in the performance analysis of TWDP systems. Defining

$$K = \frac{V_1^2 + V_2^2}{2\sigma^2} \tag{3.4}$$

$$\Delta = \frac{2V_1V_2}{V_1^2 + V_2^2} \tag{3.5}$$

the right side of (3.2) was approximated in [1] by

$$f_R(r) \approx \frac{r}{\sigma^2} \exp\left(-\frac{r^2}{2\sigma^2} - K\right) \sum_{i=1}^{M} a_i D\left(\frac{r}{\sigma}; K, \Delta\cos\frac{\pi(i-1)}{2M-1}\right) \tag{3.6a}$$

where

$$D(x; K; \alpha) = \frac{e^{\alpha K}}{2} I_0\left(x\sqrt{2K(1-\alpha)}\right) + \frac{e^{-\alpha K}}{2} I_0\left(x\sqrt{2K(1+\alpha)}\right). \tag{3.6b}$$

$I_0(\cdot)$ is the zeroth-order Bessel function of the second kind and

$$a_i = \frac{2(-1)^i}{(2M-1)(2M-i)!(i-1)!} \int_0^{2M-1} \prod_{\substack{k=1 \\ k\neq i}}^{2M} (u-k+1) du. \tag{3.6c}$$

M is the order of the approximation in (3.6) and $M \geq \frac{1}{2}K\Delta$ is suggested in [1] as a rule of thumb. Eq. (3.6) has been used in the analysis of many TWDP wireless fading systems [5–11]. Note that (3.6) deviates from the exact PDF when K is large and Δ is close to one [1]. To keep the approximation precise, M must be increased. However, choosing large M is limited as both the order of the polynomials and the upper limit of the integral in (3.6c) increase with M. This makes numerical evaluation of (3.6c) difficult.

In this paper, we derive convergent infinite series expressions for the TWDP fading PDF and cumulative distribution function (CDF). The derived series are in terms of well known mathematical functions. An efficient algorithm is proposed for the evaluation of these series. The proposed algorithm only requires basic mathematical operations and one evaluation of the exponential function. The only source of error in evaluation of the derived series is the truncation error and higher accuracy can always be achieved by simply calculating more terms. It was found that only 110 terms are enough for the truncated series to be precise, even for values of K as large as 12 dB and values of Δ close to one. Infinite series expressions are also derived for the TWDP moments and the integral of $f_R(r)$ against the complementary error function. This series is used to derive the BER of a BPSK system operating in TWDP fading.

The remainder of this paper is organized as follows. New expressions for the TWDP statistics are derived in Sec. 3.1.2 and an efficient algorithm is proposed for their evaluation. The convergence behaviors of the derived series are discussed in Sec. 3.1.3. The performance analysis of TWDP fading systems is investigated in Sec. 3.1.4. Sec. 3.1.5 concludes the paper.

3.1.2 New Expressions for the TWDP Fading Statistics

In this section, we introduce infinite series expressions for the TWDP fading PDF, CDF and moments, and we propose an efficient algorithm for their evaluation.

In Appendix 3.A, it is shown that the TWDP fading PDF can be expressed as

$$f_R(r) = \underbrace{\frac{r}{\sigma^2}\, e^{-\frac{r^2}{2\sigma^2}}}_{\text{Rayleigh PDF}} \sum_{k=0}^{\infty} \gamma_k \mathrm{L}_k\left(\frac{r^2}{2\sigma^2}\right) \tag{3.7a}$$

where

$$\gamma_k \triangleq \frac{\left(-K\sqrt{1-\Delta^2}\right)^k}{k!} \mathrm{P}_k\left(\frac{1}{\sqrt{1-\Delta^2}}\right). \tag{3.7b}$$

In (3.7), $\mathrm{P}_k(\cdot)$ and $\mathrm{L}_k(\cdot)$ represent the k^{th} order Legendre and Laguerre polynomials, respectively [12, Secs. 8.91 and 8.97]. One can integrate (3.7) to derive the CDF of R by using the change of variable $x = \frac{r^2}{2\sigma^2}$ and [12, eq. 7.414.1]. This yields

$$F_R(r) = 1 - \underbrace{e^{-\frac{r^2}{2\sigma^2}}}_{\text{Rayleigh CCDF}} \sum_{k=0}^{\infty} \gamma_k \left[\mathrm{L}_k\left(\frac{r^2}{2\sigma^2}\right) - \mathrm{L}_{k-1}\left(\frac{r^2}{2\sigma^2}\right) \right] \tag{3.8}$$

where $\mathrm{L}_{-1}(x) \triangleq 0$. The Rayleigh PDF and complementary CDF (CCDF) are factored out of the summations in (3.7) and (3.8), respectively.

For accurate and efficient evaluation of (3.7) and (3.8) we develop a recursive numerical algorithm. Defining $\alpha_k = (-K)^k/k!$, $p_k(x) = x^k \mathrm{P}_k(\frac{1}{x})$ and $l_k(y) = \mathrm{L}_k(y)$, we use the recursive relations for both the Legendre polynomials [12, eqs. 8.914.1 and 8.912.1] and the Laguerre polynomials [12, eqs. 8.971.8 and 8.970.3] to write

$$p_{k+1}(x) = \frac{2k+1}{k+1} p_k(x) - \frac{k}{k+1} x^2 p_{k-1}(x), \quad p_0(x) = 1 \tag{3.9}$$

$$l_{k+1}(x) = \frac{2k+1-x}{k+1} l_k(x) - \frac{k}{k+1} l_{k-1}(x), \quad l_0(x) = 1. \tag{3.10}$$

Using (3.7)-(3.10), we propose Algorithm 3.1 for the evaluation of the TWDP fading PDF and CDF. In this algorithm, N is the truncation order for the evaluation of the series in (3.7)

Algorithm 3.1 Evaluation of the TWDP fading PDF and CDF

Require: $K \geq 0, 0 \leq \Delta \leq 1, \sigma > 0, N \geq 0, r \geq 0$
- $p'' \leftarrow 0, p' \leftarrow 1$
- $l'' \leftarrow 0, l' \leftarrow 1$
- $a \leftarrow 1$
- $f \leftarrow 1, F \leftarrow 1$
- **for** $k = 1$ to N **do**
  - $a \leftarrow -\frac{K}{k} \times a$
  - $p \leftarrow \left(2 - \frac{1}{k}\right) p' - \left(1 - \frac{1}{k}\right)(1 - \Delta^2) p''$
  - $l \leftarrow \left(2 - \frac{1 + r^2/(2\sigma^2)}{k}\right) l' - \left(1 - \frac{1}{k}\right) l''$
  - $f \leftarrow f + a \times p \times l, F \leftarrow F + a \times p \times (l - l')$
  - $p'' \leftarrow p', p' \leftarrow p$
  - $l'' \leftarrow l', l' \leftarrow l$
- **end for**
- $\beta = \exp\left(-\frac{r^2}{2\sigma^2}\right)$
- $f \leftarrow \frac{r}{\sigma^2} \beta \times f, F \leftarrow 1 - \beta \times F$
- **return** f, F

and (3.8). The proposed algorithm only requires basic mathematical operations and involves one evaluation of the exponential function. The number of required summations and multiplications grows as $O(N)$. Therefore, one can select large values of N to calculate (3.7) and (3.8) fast and accurately. Figs. 3.1 and 3.2 show the TWDP fading PDF and CDF curves evaluated using Algorithm 3.1 with $N = 100$. Fig. 3.1 also shows the approximate PDF using

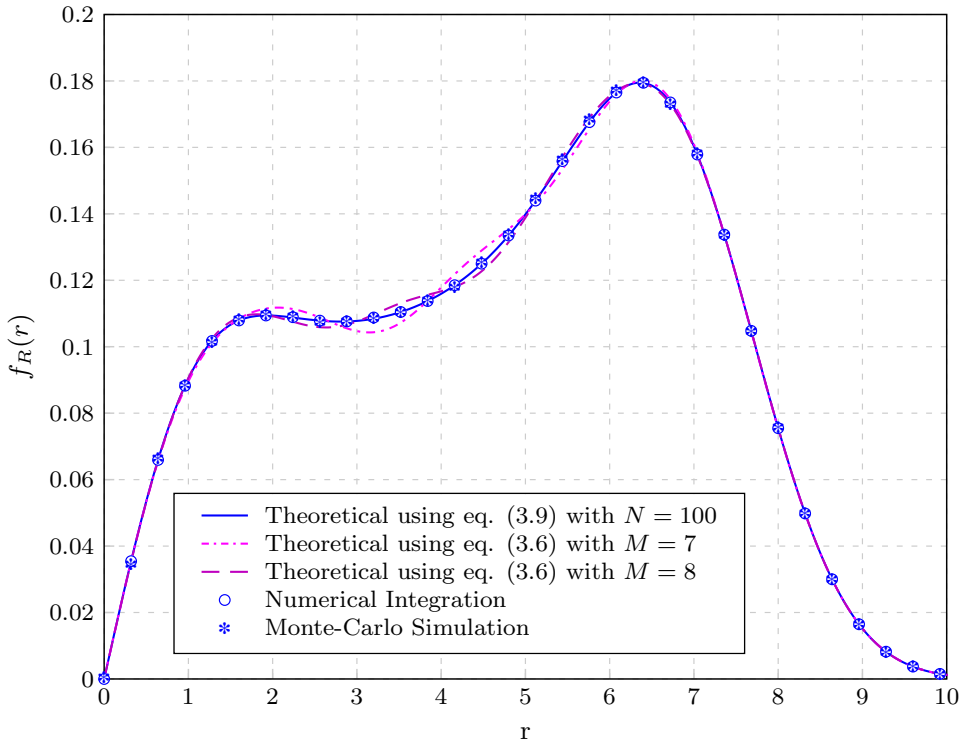

Figure 3.1. The TWDP fading PDF for $\Delta = 1$ and $K = 11$ dB.

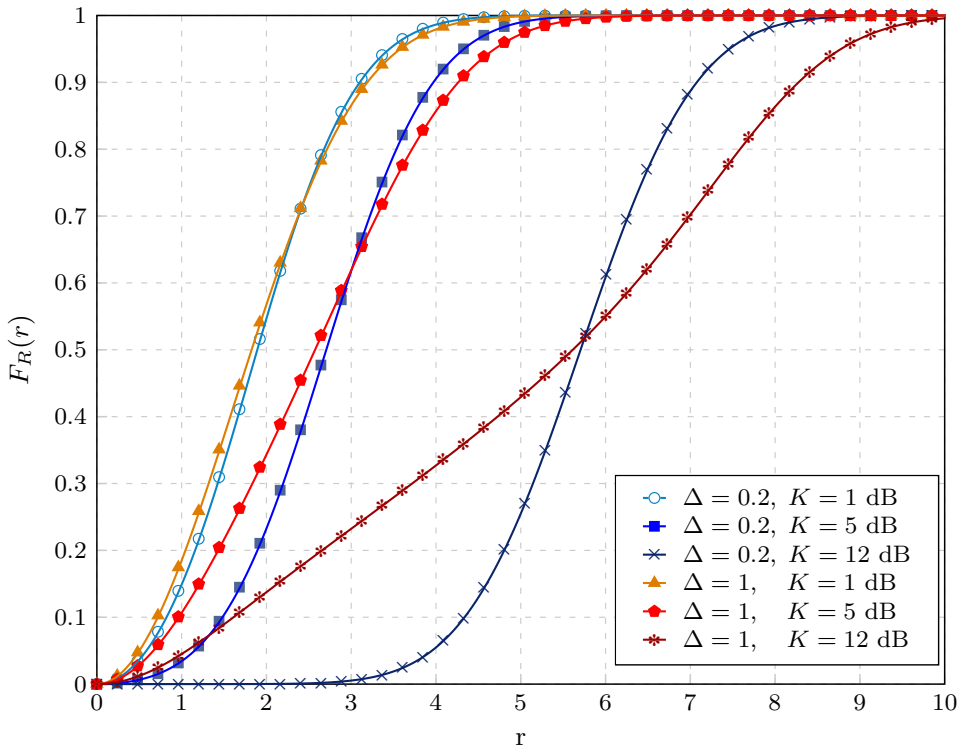

Figure 3.2. The TWDP fading CDF for various choices of parameters. The markers represent the simulation points and the solid curves are obtained by the theoretical expression in (3.8).

Table 3.1. TWDP MOMENTS EVALUATED USING (3.11) TRUNCATED AFTER 100 TERMS AND COMPUTER SIMULATIONS

		First moment		Second moment		Third moment	
K(dB)	Δ	μ_1	$\tilde{\mu}_1$	μ_2	$\tilde{\mu}_2$	μ_3	$\tilde{\mu}_3$
0	0.2	1.81	1.81	4.00	4.00	10.08	10.08
0	1	1.78	1.78	4.00	4.00	10.37	10.37
6	0.2	3.00	3.00	9.96	9.96	35.71	35.71
6	1	2.85	2.85	9.96	9.96	39.15	39.14
12	0.2	5.71	5.71	33.70	33.70	205.28	205.29
12	1	5.25	5.25	33.70	33.70	237.47	237.45

(3.6) for $M = 7, 8 > \frac{1}{2}\Delta K = 6.2946$, the PDF evaluated by numerical integration of (3.2), and the PDF curve obtained by Monte Carlo computer simulation. We observe full agreement between the derived theoretical results, numerical results and computer simulation results. Note that it is possible to increase the accuracy of (3.6) by increasing M. However, as was formerly discussed, this is at the expense of higher computational complexity for numerical evaluation of the required integrals in (3.6c). For instance, MATLAB's quadrature integration command, `quad`, cannot evaluate the integrals in (3.6c) precisely for $M > 8$, $K = 11$ dB and $\Delta = 1$. Note that for $K = 11$ dB and $\Delta = 1$, evaluation of the PDF at points $r = 0 : 0.02 : 15$ by Algorithm 3.1, eq. (3.6) and numerical integration took 3.8×10^{-3}, 4.17 and 27.67 seconds, respectively. Fig. 3.2, shows the TWDP fading CDF obtained for various choices of parameters using (3.7) and computer simulation. To achieve the simulation curves in Figs. 3.1 and 3.2, $N_s = 10^8$ samples of the TWDP distribution were generated. Then, the PDF and CDF are approximated by $f_R^{sim}(r) \approx \frac{\text{No. of samples in } (r-h/2, r+h/2)}{N_s h}$ for small h (here $h = 10^{-2}$) and $F_R^{sim}(r) \approx \frac{\text{No. of samples in (0,r)}}{N_s}$, respectively.

It is straightforward to derive the n-th moment of R using (3.7) and [13, eq. 2.13.2.3] as

$$\mu_n = \int_0^\infty r^n f_R(r)\, dr = \left(2\sigma^2\right)^{\frac{n}{2}} \Gamma\left(\frac{n}{2}+1\right) \sum_{k=0}^{\infty} \frac{\gamma_k}{k!} \left(-\frac{n}{2}\right)_k . \tag{3.11}$$

Table 3.1 shows μ_1, μ_2 and μ_3 evaluated using (3.11). These values are verified by simulation moments, $\tilde{\mu}_n$, achieved by averaging the n-th powers of 10^8 TWDP samples.

3.1.3 Convergence Analysis

In this section, we investigate the convergence behavior of (3.7) and (3.8). To prove that these series are convergent, we use the ratio test for convergence of infinite series [12,

Table 3.2. NUMBER OF TERMS REQUIRED FOR THE ACCURATE EVALUATION OF (3.7) AND (3.8)

K(dB)/Δ	0	0.2	0.4	0.6	0.8	1
-3	$10, 11$	$11, 11$	$11, 12$	$12, 12$	$12, 13$	$13, 13$
0	$13, 14$	$14, 14$	$15, 15$	$15, 16$	$16, 17$	$17, 18$
3	$18, 18$	$19, 19$	$20, 21$	$21, 22$	$22, 23$	$24, 25$
6	$25, 26$	$27, 28$	$29, 30$	$31, 32$	$33, 35$	$36, 37$
9	$37, 39$	$41, 42$	$45, 47$	$49, 51$	$54, 55$	$58, 60$
12	$60, 62$	$67, 69$	$76, 78$	$84, 86$	$93, 95$	$101, 103$

Sec. 0.222]. Denote the k^{th} term of the series in (3.7) with c_k. Both $\mathrm{P}_k(\cdot)$ and $\mathrm{L}_k(\cdot)$ are k^{th} order polynomials where $P_k(x) = \frac{1}{2^k}\frac{(2k)!}{(k!)^2}x^k + O(x^{k-1})$ and $\mathrm{L}_k(y) = \frac{(-1)^k}{k!}y^k + O(y^{k-1})$ [12, eqs. 8.911.1 and 8.970.1]. Note that in (3.7), $x = \frac{1}{\sqrt{1-\Delta^2}} \geq 1$. So, the behavior of $P_k(x)$ is dominated by $\frac{1}{2^k}\frac{(2k)!}{(k!)^2}x^k$ as $k \to \infty$. The behavior of $\mathrm{L}_k(y)$ with $y = r^2/2\sigma^2$ is dominated by $\frac{(-1)^k}{k!}y^k$ when $y > 1$ and by 1 when $y < 1$ as $k \to \infty$. So, the ratio test yields

$$\lim_{k\to\infty}\left|\frac{c_{k+1}}{c_k}\right| = \begin{cases} \frac{r^2K}{\sigma^2}\lim\limits_{k\to\infty}\frac{k+1/2}{(k+1)^3}, r^2 > 2\sigma^2 \\ 2K\lim\limits_{k\to\infty}\frac{k+1/2}{(k+1)^2}, r^2 < 2\sigma^2 \end{cases} = 0 < 1. \tag{3.12}$$

From (3.12), it is clear that the series in (3.7) is convergent. Similarly, the convergence of (3.8) can be proved by using $\mathrm{L}_k(y) - \mathrm{L}_{k-1}(y) = \frac{(-1)^k}{k!}y^k + O(y^{k-1})$ and by following almost the same steps. Asymptotically, the terms in the series decay with a rate proportional to $1/k^2$ and $1/k$ when $r^2 > 2\sigma^2$ and $r^2 < 2\sigma^2$, respectively. From (3.12) one expects that the series needs more terms to converge for larger K.

Table 3.2 shows the number of terms required for the series in (3.7) and (3.8) to converge. To obtain these numbers, we defined $F_R^{(n)}(r)$ as the CDF evaluated using (3.8) with the series truncated after summation of its first n terms. Then, we define

$$N_{set.} \triangleq \min n : \max_{0<r<r_{max}} \left|F_R^{(n)}(r) - F_R^{(5n)}(r)\right| < 10^{-12}. \tag{3.13}$$

To find $N_{set.}$, we ran Algorithm 1 for 1000 uniformly spaced values of r in $[0, 15]$ for $n = 1$ to $n = 1000$ and we saved the resulting CDF vectors. Then, we found $N_{set.}$ using criterion (3.13). A similar approach is followed to find $N_{set.}$ for evaluation of the PDF using (3.7). We observe that both series converge fast and evaluation of 105 terms is enough to reach high numerical precision over the practical range of TWDP fading parameters. We also observe that the series in (3.7) and (3.8) require more terms to converge as K or Δ increases.

3.1.4 Integration of the PDF Against the Complementary Error Function

Analysis of wireless fading systems involves integration of the fading PDF against other mathematical functions. Calculation of the BER and the SER of communication systems requires integrations of the form $P_E = \int f_R(r) p_e(r) dr$, where $p_e(r)$ is the probability of error when the received signal amplitude is r. In many cases, $p_e(r)$ is given in terms of the complementary error function [6, 7] defined as $\text{erfc}(x) = \frac{2}{\sqrt{\pi}} \int_x^\infty e^{-t^2} dt$ [12]. So, one needs to evaluate

$$\mathcal{I}(\alpha) \triangleq \int_0^\infty f_R(r) \, \text{erfc}\left(\sqrt{\alpha}\, r\right) \, dr. \tag{3.14}$$

In Appendix 3.B, it is shown that

$$\mathcal{I}(\alpha) = \frac{\left(1 + \frac{1}{2\sigma^2\alpha}\right)^{-\frac{3}{2}}}{4\sigma^2\alpha} \sum_{k=0}^{\infty} \gamma_k \, F\left(\frac{3}{2}, 1-k; 2; \frac{1}{1+2\sigma^2\alpha}\right) \tag{3.15}$$

where γ_k is given by (3.7b). Defining $g_k(x) \triangleq F\left(\frac{3}{2}, 1-k; 2; x\right)$, the hypergeometric function in (3.15) can be evaluated recursively by

$$g_{k+1}(x) = \frac{2k - (k+\frac{1}{2})x}{k+1} g_k(x) + \frac{k-1}{k+1}(x-1) g_{k-1}(x), \; k > 0 \tag{3.16a}$$

$$g_0(x) = \frac{2}{x}\left(\frac{1}{\sqrt{1-x}} - 1\right), \quad g_1(x) = 1 \tag{3.16b}$$

where we have used [12, eqs. 9.137.3 and 9.100] and [13, eq. 7.3.2.156]. So, (3.15) can be calculated efficiently by an algorithm similar to Algorithm 1 using the recursive relationships for the Legendre and the hypergeometric functions given by (3.9) and (3.16).

An immediate application of (3.15) is the calculation of the BER of a BPSK communication system considered in [6]. Using [6, eq. (2)], $Q(x) = \frac{1}{2}\text{erfc}\left(x/\sqrt{2}\right)$ and (3.15) with $\alpha = E_b/N_0$ the exact BER of a BPSK system results as

$$P_{E,\text{BPSK}}\left(E_b/N_0\right) = \frac{1}{2}\mathcal{I}\left(E_b/N_0\right) \tag{3.17}$$

where $N_0/2$ is the power spectral density of additive white Gaussian noise and $r^2 E_b$ is the instantaneous energy received per bit [6]. Fig. 3.3 shows BER curves obtained by evaluating eq. (3.17) and by computer simulations. One observes full agreement between the theoretical and simulation results.

Table 3.3. NUMBER OF TERMS REQUIRED FOR THE ACCURATE COMPUTATION OF(3.17)

K(dB)/Δ	0	0.2	0.4	0.6	0.8	1
-3	10	10	10	11	12	12
0	13	13	14	15	15	16
3	17	18	19	20	21	23
6	24	25	28	30	32	34
9	36	39	44	48	52	56
12	58	65	74	82	91	99

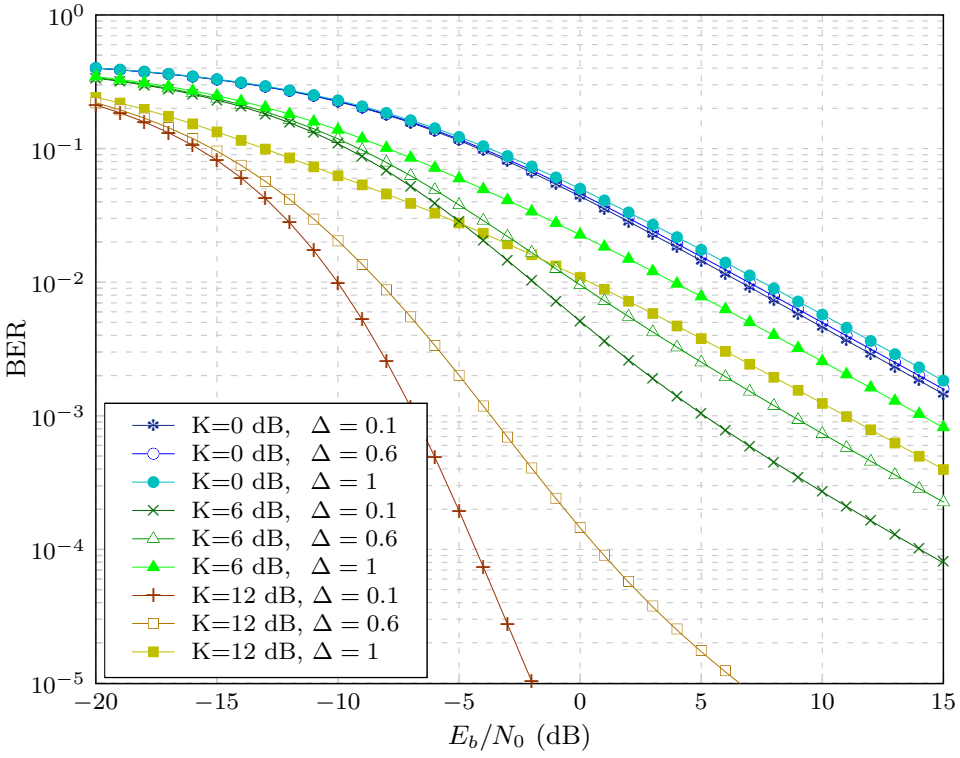

Figure 3.3. The BER of a BPSK system operating in TWDP fading. $N = 100$ terms are used in the summation in (3.17). The markers represent the simulation points and the solid curves are obtained by the theoretical expression in (3.17).

Table 3.3 shows the number of terms required for the series in (3.17) to converge. These numbers are obtained using the criterion in (3.13) with $F_R^{(n)}(r)$ replaced with $P_{E,\text{BPSK}}^{(n)}(\alpha)$ and for $-20\,\text{dB} < \alpha_{\text{dB}} < 20\,\text{dB}$. Note that $\alpha_{\text{dB}} = 10\log_{10}\alpha$. We observe that evaluation of the first 100 terms of the series in (3.17) is sufficient to reach a numerical precision of 10^{-12} for practical TWDP fading parameters.

3.1.5 Conclusion

The PDF and CDF of TWDP fading were expressed as convergent infinite series and a low-complexity algorithm was developed for their evaluation. Efficient infinite series were also given for the TWDP moments and the integral of the TWDP fading PDF against the complementary error function for the performance analysis of wireless systems. The BER of a BPSK system operating in TWDP fading was evaluated.

Appendix 3.A

In this appendix, we prove that (3.7) is equal to (3.2). In (3.2), we use the identity [12, eq. 8.442.2]

$$J_0\left(V_1\nu\right)J_0(V_2\nu)=\sum_{k=0}^{\infty}\frac{(-1)^k\left(\frac{V_1\nu}{2}\right)^{2k}}{(k!)^2}F\left(-k,-k;1;\left(V_2/V_1\right)^2\right) \tag{3.18}$$

where $F(\cdot,\cdot;\cdot;\cdot)$ is the Gauss hypergeometric function [12, Sec. 9.10]. This yields

$$f_R(r)=r\sum_{k=0}^{\infty}\frac{(-1)^k\left(\frac{V_1}{2}\right)^{2k}}{(k!)^2}F\left(-k,-k;1;\left(V_2/V_1\right)^2\right)\underbrace{\int_0^{\infty}\nu^{2k+1}\exp\left(-\frac{\sigma^2\nu^2}{2}\right)J_0(r\nu)d\nu}_{\mathcal{I}_1}. \tag{3.19}$$

Substitution of the solution of the integral $\mathcal{I}_1$ [12, eq. 6.631.1] in (3.19) gives

$$f_R(r)=\frac{r}{\sigma^2}\sum_{k=0}^{\infty}\frac{(-1)^k\left(\frac{V_1^2}{2\sigma^2}\right)^k}{k!}F\left(-k,-k;1;\left(V_2/V_1\right)^2\right)\mathrm{M}\left(k+1,1,-\frac{r^2}{2\sigma^2}\right) \tag{3.20}$$

where $\mathrm{M}(\cdot,\cdot,\cdot)$ is the confluent hypergeometric function [12, Sec. 9.2]. To express (3.20) in terms of K and Δ and to extract the Rayleigh PDF out of the series, we use identities [12, eqs. 8.820.4, 9.212.1 and 8.972.1]

$$F\left(-k,-k;1;\left(V_2/V_1\right)^2\right)=\left(\frac{V_1^2-V_2^2}{V_1^2}\right)^k\mathrm{P}_k\left(\frac{V_1^2+V_2^2}{V_1^2-V_2^2}\right) \tag{3.21}$$

$$\mathrm{M}(a,b,z)=e^z\mathrm{M}(b-a,b,-z) \tag{3.22}$$

$$\mathrm{L}_k(z)=\mathrm{M}(-k,1,z) \tag{3.23}$$

respectively. Substitution of (3.21)-(3.23) in (3.20) gives (3.7).

Appendix 3.B

To evaluate (3.14), we replace $f_R(r)$ in (3.14) with (3.7). This yields

$$\mathcal{I}(\alpha) = \sum_{k=0}^{\infty} \frac{\left(-K\sqrt{1-\Delta^2}\right)^k}{k!} \mathrm{P}_k\left(\frac{1}{\sqrt{1-\Delta^2}}\right) \underbrace{\int_0^{\infty} \frac{r e^{-\frac{r^2}{2\sigma^2}}}{\sigma^2} \mathrm{erfc}(\sqrt{\alpha}\, r) \mathrm{L}_k\left(\frac{r^2}{2\sigma^2}\right) dr}_{\mathcal{I}_2}. \tag{3.24}$$

The integral $\mathcal{I}_2$ has the solution [13, eq. 2.13.8.2]

$$\frac{1}{4\sigma^2\alpha}\, {}_3F_2\left(1, \frac{3}{2}, k+1; 1, 2; -\frac{1}{2\sigma^2\alpha}\right) = \frac{1}{4\sigma^2\alpha}\, F\left(\frac{3}{2}, k+1; 2; -\frac{1}{2\sigma^2\alpha}\right) \tag{3.25}$$

where ${}_3F_2(\cdot,\cdot,\cdot;\cdot,\cdot;\cdot)$ is the generalized hypergeometric function and we have used [12, eqs. 9.14.1 and 9.14.2] to write (3.25). Substituting (3.25) in (3.24) and using the transformation [12, eq. 9.131.1] for the hypergeometric function produces (3.15).

3.2 Supplementary Discussion

In this section, we first propose an efficient algorithm for the evaluation of (3.17). Then we compare the expression in (3.17) for the BER of BPSK systems in TWDP fading, with the BER expressions in [6, eqs. (5) and (6)]. Finally, we will discuss the potential future research based on our contributions in this chapter.

3.2.1 An Algorithm for the Efficient Evaluation of (3.17)

As was discussed in the paper in Sec. (3.1), one can evaluate the BER expression in (3.17) efficiently using basic mathematical operations with no need to evaluate the hypergeometric functions. This can be done using the recursive relationship (3.16) for the Gauss hypergeometric function. The algorithm for evaluation of the BER expression in (3.17) is given below. Note that in this algorithm $\alpha = E_b/N_0$ is the SNR value.

Algorithm 3.2 Evaluation of the BPSK BER operating in TWDP fading using eq. (3.17).

Require: $K \geq 0, 0 \leq \Delta \leq 1, \sigma > 0, N \geq 0, \alpha \geq 0$
  $p'' \leftarrow 0, p' \leftarrow 1$
  $x = 1/(1 + 2\sigma^2\alpha)$
  $g'' \leftarrow 2/x \times (1/\sqrt{1-x} - 1), g' \leftarrow 1$
  $a \leftarrow -K$
  $P \leftarrow p'' \times g'' + a \times p' \times g'$
  for $k = 2$ to N **do**
    $a \leftarrow -\frac{K}{k} \times a$
    $p \leftarrow (2 - \frac{1}{k})p' - (1 - \frac{1}{k})(1 - \Delta^2)p''$
    $g \leftarrow (2 - \frac{2}{k} - (1 - \frac{1}{2k})x)g' + (1 - \frac{1}{2k})(x - 1)g''$
    $P \leftarrow P + a \times p \times g$
    $p'' \leftarrow p', p' \leftarrow p$
    $g'' \leftarrow g', g' \leftarrow g$
  end for
  $P \leftarrow \frac{1}{2} \times \frac{(1+1/(2\sigma^2\alpha))^{-1.5}}{4\sigma^2\alpha} \times P$
  return P

Note that the number of summations and multiplications in Algorithm 3.2 grows linearly with the truncation order N. So one can evaluate (3.17) precisely by selecting large values of N without making the computations lengthy or difficult.

3.2.2 Comparison of (3.17) with the Existing BER Expressions for BPSK Systems Operating in TWDP Fading

As was mentioned in Sec. 3.1, the new expressions derived for TWDP statistics may lead to simpler results in the performance analysis of wireless systems. In this section, we compare the BER expression in (3.17) which is derived using the new PDF expression in (3.7), with

the BER expression for the same system given in [6, eqs. (5) and (6)]. [6, eq. (5)] is

$$P_E = \frac{1}{2\pi}\sum_{i=0}^{M} a_i \left\{ e^{-K(1-\alpha_i)} \int_0^{\frac{\pi}{2}} \frac{\sin^2\theta}{\sin^2\theta + s\sigma^2 E_b/N_0} \exp\left(K(1-\alpha_i) \frac{\sin^2\theta}{\sin^2\theta + s\sigma^2 E_b/N_0} \right) d\theta \right.$$
$$\left. + e^{-K(1+\alpha_i)} \int_0^{\frac{\pi}{2}} \frac{\sin^2\theta}{\sin^2\theta + s\sigma^2 E_b/N_0} \exp\left(K(1+\alpha_i) \frac{\sin^2\theta}{\sin^2\theta + s\sigma^2 E_b/N_0} \right) d\theta \right\} \tag{3.26}$$

where M is the approximation order in (3.6), coefficients a_i are defined in (3.6c) and $\alpha_i = \Delta\cos(\pi(i-1)/(2M-1))$. [6, eq. (6)] is

$$P_E = \frac{1}{2}\sum_{i=0}^{M} a_i \left\{ e^{-K(1-\alpha_i)} \sum_{n=0}^{\infty} H_{n+1}\left(K(1-\alpha_i); 2\sigma^2 E_b/N_0\right) \right.$$
$$\left. + e^{-K(1+\alpha_i)} \sum_{n=0}^{\infty} H_{n+1}\left(K(1+\alpha_i); 2\sigma^2 E_b/N_0\right) \right\} \tag{3.27}$$

where

$$H_{n+1}(b;c) = \frac{b^n}{n!}\left[\frac{1}{2} - \frac{1}{2}\sqrt{\frac{c}{1+c}} \sum_{k=0}^{n} \binom{2k}{k} \frac{1}{[4(1+c)]^k} \right]. \tag{3.28}$$

We believe that the BER expression in (3.17) is superior to the BER expressions in (3.26) and (3.27). The expression in (3.26) requires numerical integration while the solution in eq. (3.17) just requires basic mathematical operations. Although there are no issues with numerical integration, a solution which only requires basic mathematical operations with linear computational complexity is preferred. Similarly, (3.27) requires evaluation of the function $H_{n+1}(\cdot,\cdot)$ defined in (3.28). There is no recursive relation proposed for evaluation of $H_{n+1}(\cdot,\cdot)$ from $H_n(\cdot,\cdot)$. Therefore, evaluation of the n^{th} term of the infinite series in (3.27) requires evaluation of a finite sum with $n+1$ terms. By truncating the infinite series (3.27) to N terms, the total number of operations required for evaluation of (3.27) is $\frac{N^2}{2} + cN$, where c is a constant. So the number of operations required grows as $O(N^2)$ for evaluation of (3.27), while this number grows as $O(N)$ for the solution in eq. (3.17) using Algorithm 2. Also note that the BER solutions in (3.26) and (3.27) require evaluation of the coefficients a_k in eq. (3.6c) of our paper. As is discussed in Secs. 3.1.1 and 3.1.2, this requires numerical integration of polynomials which is not straightforward when high accuracy is needed and therefore large values of M are selected.

Table 3.4 shows the average time required for the evaluation of the BER of a BPSK system operating in TWDP fading for SNR values -20 dB:1 dB:20 dB using (3.26), (3.27) and (3.17). In this table, N_1 and N_2 are the truncation orders of the infinite series in (3.27)

Table 3.4. COMPARISON OF EVALUATION TIMES FOR (3.26), (3.27) AND EQ. (3.17)

Δ	K(dB)	N_1	N_2	t_1	t_2	t_3	t_1/t_3	t_2/t_3
0.2	0	12	10	22 ms	196 μs	16 μs	1.375×10^3	12.25
0.2	6	22	21	33 ms	364 μs	20 μs	1.650×10^3	18.2
0.2	12	47	60	215 ms	901 μs	30 μs	7.167×10^3	30
0.6	0	12	12	23 ms	195 μs	16 μs	1.437×10^3	12.18
0.6	6	22	26	35 ms	363 μs	20 μs	1.75×10^3	18.15
0.6	12	47	76	320 ms	919 μs	39 μs	8.205×10^3	23.5
1	0	12	13	24 ms	197 μs	17 μs	1.411×10^3	11.58
1	6	22	37	38 ms	370 μs	22 μs	1.727×10^3	16.8
1	12	47	93	519 ms	1232 μs	37 μs	14.027×10^3	33.29

and (3.17), respectively. Both N_1 and N_2 are selected such that the evaluated BER values reach numerical precision of order 10^{-9} using the criterion in eq. (3.13) of the paper. For efficient evaluation of (3.27), the number of summations and multiplications is reduced as much as possible. Numerical integrations are performed using MATLAB's `quad` function with its tolerance parameter set to 10^{-9}. In Table 3.4, t_1, t_2 and t_3 show the evaluation times of (3.26), (3.27) and eq. (3.17), respectively. As we observe, the fastest way to compute the BER is evaluation of eq. (3.17) which is as expected from the discussion above. This discussion shows that although evaluation of (3.26), (3.27) is not a problem, evaluation eq. (3.17) is the easiest way to compute the BER of a BPSK systems operating in TWDP fading.

3.2.3 Future Work

As was discussed in Sec. 3.2.2, the new expressions derived for the TWDP fading statistics can be applied in the analysis of fading systems. Compared to the expressions for the performance metrics of TWDP systems available in the literature, the new expressions can be mathematically more tractable and simpler to be evaluated. An example is the performance of BPSK systems operating in TWDP fading, which was investigated in Secs. 3.1.4 and 3.2. In this example, we observed that the new expressions were easier to evaluate compared to the solutions previously proposed in the literature. So, a potential research project for future is to apply the results of Sec. 3.1 to analyze the performance of various TWDP systems.

Bibliography

[1] G. D. Durgin, T. S. Rappaport, and D. A. Wolf, "New analytical models and probability density functions for fading in wireless communications," *IEEE Trans. Commun.,* vol. 50, no. 6, pp. 1005-1015, June 2002.

[2] J. Frolik, "A case for considering hyper-Rayleigh fading channels," *IEEE Trans. Wireless Commun.,* vol. 6, no. 4, pp. 1235-1239, Apr. 2007.

[3] H. Exton, *Multiple Hypergeometric Functions and Applications*, New York: Halsted Press, 1976.

[4] G. P. Efthymoglou, T. Piboongungon, and V. A. Aalo, "Performance of DS-CDMA receivers with MRC in Nakagami-*m* fading channels with arbitrary fading parameters," *IEEE Trans. Veh. Technol.,* vol. 55, no. 1, pp. 104-114, Jan. 2006.

[5] D. Dixit and P. R. Sahu, "Performance of QAM signaling over TWDP fading channels," *IEEE Trans. Wireless Commun.,* vol. 12, no. 4, pp. 1794-1799, Apr. 2013.

[6] S. H. Oh and K. H. Li, "BER performance of BPSK receivers over two-wave with diffuse power fading channels." *IEEE Trans. Wireless Commun.,* vol. 4, no. 4, pp. 1448-1454, July 2005.

[7] H. A. Suraweera, W. S. Lee, and S. H. Oh, "Performance analysis of QAM in a two-wave with diffuse power fading environment," *IEEE Commun. Lett.,* vol. 12, no. 2, pp. 109-111, Feb. 2008.

[8] Y. Lu and N. Yang, "Symbol error probability of QAM with MRC diversity in two-wave with diffuse power fading channels," *IEEE Commun. Lett.,* vol. 15, no. 1, pp. 10-12, Jan. 2011.

[9] Y. Lu and N. Yang, "Symbol error rate of decode-and-forward relaying in two-wave with diffuse power fading channels," *IEEE Trans. Wireless Commun.,* vol. 11, no. 10, pp. 3412-3417, Oct. 2012.

[10] Y. Lu, X. Wang, and N. Yang, "Outage probability of cooperative relay networks in two-wave with diffuse power fading channels," *IEEE Trans. Commun.,* vol. 60, no. 1, pp. 42-47, Jan. 2012.

[11] R. Subadar and A. D. Singh, "Performance of SC receiver over TWDP fading channels," *IEEE Wireless Commun. Lett.,* vol. 2, no. 3, pp. 267-270, June 2013.

[12] I. S. Gradshteyn and I. M. Ryzhik, *Table of Integrals, Series, and Products,* San Diego, CA: Academic Press, seventh ed., 2007.

[13] A. P. Prudnikov, Y. A. Brychkov, and O. I. Marichev, *Integrals and Series, Vol. 3*, Gordon and Breach Science Publishers, 1990.

Chapter 4

Modeling and Analysis of Diffuse Nakagami-*m* with Line-of-Sight Fading

In this chapter, we introduce and analyze diffuse Nakagami-*m* with LOS fading as a new fading model in wireless systems. This chapter includes our paper "A novel line-of-sight plus diffuse fading model" which is submitted to *IEEE Transaction on Information Theory*.

4.1 A Novel Line-of-Sight Plus Diffuse Fading Model[1]

Authors: N. C. Beaulieu and S. A. Saberali

Submitted to IEEE Transactions on Information Theory

4.1.1 Introduction

Multipath propagation in wireless transmission channels gives rise to signal amplitude (and power) fading as the multiple wave components add constructively and destructively. A Rayleigh distribution arises when the number of multipath components is large and none of them is dominant. Based on a central limit theorem argument, the receiver captures a diffuse signal whose envelope is Rayleigh distributed. In the case where there is also a line-of-sight (LOS) component between the transmitter and the receiver, the Rice distribution models the envelope of the received signal [1, 2].

The Nakagami-*m* distribution is a generalized flexible fading model which can characterize various fading environments. The Nakagami-*m* distribution has been shown to fit experimental data in urban multipath channels better than the Rayleigh and Rice distributions [3–5]. The performances of various wireless communication systems operating in Nakagami-*m* fading has been intensively investigated in the literature [6–17].

[1] A version of this chapter has been submitted to the IEEE Transactions on Information Theory, Sep. 2013.

In this paper, we propose the diffuse Nakagami-*m* with LOS fading model. We derive the probability density function (PDF), the cumulative distribution function (CDF) and the characteristic function (CF) of a Nakagami-*m* with LOS distribution. We compare the new fading distribution with Rice, Nakagami-*m* and TWDP fading distributions and find that the new fading model can behave substantially different from Nakagami-*m* fading. It is shown that compared to the Rice and Nakagami-*m* models, TWDP fading shows a closer behavior to the Nakagami-*m* with LOS fading. We also derive an expression for the integral of the product of the Nakagami-*m* with LOS fading PDF, and the complementary error function. This integral is a building block for performance evaluation of many wireless systems operating in diffuse Nakagami-*m* with LOS fading environments. Evaluation of the bit error rate (BER) of an uncoded BPSK wireless system operating in Nakagami-*m* with LOS fading is considered as an example. It is shown that when the LOS wave is strong, the new model leads to diversity orders different from the diversity orders that characterize the Nakagami-*m* and Rice PDFs. We also show that the BER of BPSK systems operating in Nakagami-*m* with LOS fading approaches the BER of a BPSK system operating in TWDP fading for moderate and high power LOS components.

The remainder of this paper is organized as follows. We review the diffuse Nakagami-*m* distribution in Sec. 4.1.2, and discuss heuristically why it does not represent a fading environment with a LOS component. In Sec. 4.1.3, we introduce the Nakagami-*m* with LOS fading model and we derive expressions for its PDF. Derivations of expressions for the CDF, moments and moment generating function of the new fading distribution are presented in Sec. 4.1.4. Secs. 4.1.5 and 4.1.6 present numerical results and discussions about the PDF, CDF and CF of the proposed fading model. These sections also include comparison of the new fading model with the Rice and Nakagami-*m* fading models. In Sec. 4.1.7, the diffuse Nakagami-*m* with LOS fading model is compared to the TWDP fading model. Evaluation of the integral of the Nakagami-*m* with LOS fading PDF against the complementary error function is considered in Sec. 4.1.8. In this section, the BER of a BPSK system operating in Nakagami-*m* with LOS fading is also derived, and it is compared to the BER of BPSK systems operating in Nakagami-*m* and TWDP fading channels. Sec. 4.1.9 concludes the paper.

4.1.2 Diffuse Nakagami-*m* Fading

The Nakagami-*m* distribution has been used to model different fading channels. The distribution of a Nakagami-*m* random variable is determined by the parameters m and Ω, which

are the fading severity and the power, respectively. The Nakagami-*m* PDF is [3]

$$f^{(\text{Nakagami})}(r) = \frac{2}{\Gamma(m)} \left(\frac{m}{\Omega}\right)^m r^{2m-1} e^{-mr^2/\Omega}, \quad , m \geq 0.5,\ r \geq 0 \tag{4.1}$$

where $\Gamma(\cdot)$ is the gamma function. In order to justify our new proposed fading distribution, we need to provide some context for the three common fading models, Nakagami-*m*, Rice, and Rayleigh. A heuristic discussion follows.

The Rayleigh distribution model is derived from physical principles starting from a diffuse scatter propagation environment. The Rice distribution model is derived also starting from physical principles based on a diffuse scatter signal component and a single LOS specular component. The Nakagami-*m* distribution model has only been justified as an amplitude fading model and only by its suitable match to empirical data. The Nakagami-*m* distribution covers a wide range of amplitude fading conditions which are less severe than Rayleigh fading. At the same time, the Rice distribution also covers a wide range of amplitude fading conditions that are less severe than Rayleigh fading [1]. In Nakagami's celebrated paper [3], the author proposes an equivalency between Nakagami-*m* fading and Rice fading. This equivalency has received acceptance in the communications research community [4, 5]. Yet, the basis for such an equivalency seems to be only that Rice channels and Nakagami-*m* channels represent better channels than the Rayleigh channel, without regard to the physical nature of the channel and the presence or absence of a LOS component. We argue here that the Nakagami-*m* channel represents exclusively a diffuse scatter channel.

The central chi-distribution arises when a number of squared, zero-mean Gaussian random variables are summed. As the number increases, the mode moves out, in the direction of larger argument, and the height of the mode of the distribution decreases at the same time. There exists a normalization that identically transforms the central chi-square distribution into the Nakagami-*m* distribution. Effectively, the normalization slows down and stabilizes the location of the mode while the height of the mode grows without bound. This insight into the Nakagami-*m* distribution implies that there is no specular component in the Nakagami-*m* distribution corresponding to the fact that it derives from a particular normalization of the central chi-square distribution which is derived from zero-mean Gaussian random variables (as opposed to the noncentral chi-distribution and the Rice distribution). This mathematical argument that the Nakagami-*m* distribution cannot represent fading with a specular component can be stated in a different, physical way.

The distribution of the signal amplitude in maximal ratio combining diversity (MRC) operating on Rayleigh channels can be identically transformed into the Nakagami-*m* dis-

tribution by the proper equivalency between the diversity order and the Nakagami m parameter for integer and half-integer values of m. Since the Rayleigh channels have no LOS component, the resulting Nakagami-*m* distribution represents a fading channel without LOS component. Finally, it is worth pointing out that the tails of the Nakagami-*m* distribution decay with diversity order m, whereas the tail of the Rice distribution always decays with diversity order 1, the same as for the Rayleigh distribution regardless of the value of the Rice K factor. Hence, a Nakagami-*m* Rice distribution equivalency is flawed, for as wireless engineers and researchers, we work in the tails of the distribution. Hence, one cannot simply transform a Rice distribution, which represents a LOS and a Rayleigh diffuse component, to an equivalent Nakagami-*m* distribution. Nor can a Nakagami-*m* distribution represent a diffuse Nakagami-*m* scatter plus a LOS component.

To recap, the Nakagami-*m* distribution is just a normalized version of the central chi-distribution, so both distributions characterize the same phenomena. The central chi distribution arises when squared zero-mean Gaussian random variables are summed, where none of them is a specular component (which is a diffuse scatter), so the Nakagami-*m* distribution also models a diffuse scatter. Studying the behavior of the modes of these distributions reinforces further our thesis. The mode of a cental chi-distribution moves out which is a characteristic of the PDF of any sum of random variables. The mode of the Nakagami-*m* distribution, however, does not behave like the mode of a sum of random variables (or a diffuse component) as its mode stabilizes as the parameter *m* increases. However, this does not mean that the Nakagami-*m* distribution characterizes a phenomena different from the central chi-distribution; it represents a normalized distribution with a special normalization. Hence, the Nakagami-*m* distribution also characterizes a sum of random variables with no specular component, and there is no contradiction in the behavior of the mode of a Nakagami-*m* distribution and the behavior of the mode of a distribution of a sum of random variables with no specular component. In Secs. 4.1.5 and 4.1.6, we will show in another way that the Nakagami-*m* distribution cannot model the envelope of the received signal when there is a LOS component in the received signal.

The diffuse Nakagami plus LOS fading model is easily justified. In any propagation environment that is well modeled by a suitable Nakagami-*m* distribution, we need only to add a specular wave.

4.1.3 Diffuse Nakagami-*m* with LOS Fading Model

In this section, we introduce the diffuse Nakagami-*m* with LOS fading model and we derive its PDF.

The baseband voltage of the multipath received signal with one LOS component can be modeled as [2, 18]

$$\mathrm{V} = Re^{j\phi} = \underbrace{\mathrm{V}_0 e^{j\phi_0}}_{\text{LOS component}} + \underbrace{\mathrm{V}_d e^{j\phi_d}}_{\text{diffuse component}} \tag{4.2}$$

where V is the received baseband signal with envelope R and phase ϕ. V_0 is the constant magnitude of the LOS component and ϕ_0 is its corresponding random phase, which is uniformly distributed in $[0, 2\pi]$. This assumption is well justified by the discussion in [2, Sec. I]. Following the terminology proposed in [2], the LOS voltage is the specular component of the received signal, while V_d and ϕ_d represent the random magnitude and the random phase of the diffuse component of the received baseband signal, respectively. The diffuse component results from reception of various multipath reflections of the transmitted signal, that have comparable strength. In diffuse Nakagami-*m* with LOS fading, we assume that the magnitude of the diffuse voltage has a Nakagami-*m* distribution with parameters m and Ω, and that the phase ϕ_d is uniformly distributed in $[0, 2\pi]$. Note that in both the Rayleigh and Rice fading models, V_d is Rayleigh distributed. In Rayleigh fading $V_0 = 0$, while $V_0 > 0$ in Rice fading.

The components $X = R\cos\phi$ and $Y = R\sin\phi$ in (4.2) are jointly spherically symmetric random variables and their joint characteristic function, $\Phi_{XY}(\omega_1, \omega_2)$, is a function of $\nu = \sqrt{\omega_1^2 + \omega_2^2}$ [18]. In other words, $\Phi_{XY}(\omega_1, \omega_2) = \Phi(\nu)$. Moreover, the PDF of R, $f_R(r)$, and $\Phi(\nu)$ are Hankel transform pairs; i.e., [2, 18]

$$\Phi(\nu) = \int_0^\infty f_R(r) J_0(\nu r) dr \tag{4.3}$$

$$f_R(r) = r \int_0^\infty \Phi(\nu) J_0(r\nu) \nu d\nu. \tag{4.4}$$

To find $\Phi(\nu)$ we use [18]

$$\Phi(\nu) = \mathrm{E}_{\mathrm{V}_0, \mathrm{V}_d} \left[J_0 \left(\mathrm{V}_0 \nu \right) J_0(\mathrm{V}_d \nu) \right] \tag{4.5}$$

where $E[\cdot]$ is the expectation operator. Since V_0 is deterministic, $\Phi(\nu) = J_0(\mathrm{V}_0\nu)\mathrm{E}_{\mathrm{V}_d}[J_0(\mathrm{V}_d\nu)]$. Moreover,

$$\mathrm{E}_{\mathrm{V}_d}[J_0(\mathrm{V}_d\nu)] = \frac{2}{\Gamma(m)} \left(\frac{m}{\Omega}\right)^m \int_0^\infty x^{2m-1} e^{-\frac{m}{\Omega}x^2} J_0(\nu x) dx \tag{4.6}$$

$$= M\left(m, 1, -\frac{\Omega}{4m}\nu^2\right) \tag{4.7}$$

where $M(\cdot,\cdot,\cdot)$ is the confluent hypergeometric function and we evaluated the last integral using [25, eq. 6.631.1]. Using (4.4)-(4.7), one obtains,

$$f_R(r) = r\int_0^\infty M\left(m,1,-\frac{\Omega}{4m}\nu^2\right)J_0(\mathrm{V}_0\nu)J_0(r\nu)\nu d\nu. \tag{4.8}$$

In Appendix 4.A, it is shown that (4.8) can be expressed as

$$f_R(r) = \frac{2}{\Gamma(m)}\left(\frac{m}{\Omega}\right)^m\left(\mathrm{V}_0^2+r^2\right)^{m-1}re^{-\frac{m}{\Omega}(\mathrm{V}_0^2+r^2)}\times \frac{1}{\pi}\sum_{i=0}^{m-1}\binom{m-1}{i}\left(-\frac{2\mathrm{V}_0 r}{\mathrm{V}_0^2+r^2}\right)^i G_f(r;i) \tag{4.9a}$$

where

$$G_f(r;i) \triangleq \sum_{\substack{k=0\\ k+i\,\text{even}}}^{\infty}\mathrm{B}\left(\frac{k+i+1}{2},\frac{1}{2}\right)\frac{\left(2\frac{m}{\Omega}\mathrm{V}_0 r\right)^k}{k!} \tag{4.9b}$$

$$= \begin{cases} \mathrm{B}\left(\frac{i}{2}+\frac{1}{2},\frac{1}{2}\right)\,{}_1F_2\left(\frac{i}{2}+\frac{1}{2};\frac{1}{2},\frac{i}{2}+1;\left(\frac{m}{\Omega}\mathrm{V}_0 r\right)^2\right), i \text{ even} \\ 2\frac{m}{\Omega}\mathrm{V}_0 r\mathrm{B}\left(\frac{i}{2}+1,\frac{1}{2}\right)\,{}_1F_2\left(\frac{i}{2}+1;\frac{3}{2},\frac{i}{2}+\frac{3}{2};\left(\frac{m}{\Omega}\mathrm{V}_0 r\right)^2\right), i \text{ odd} \end{cases}. \tag{4.9c}$$

In eq. (4.9), $\mathrm{B}(\cdot,\cdot)$ and ${}_1F_2(\cdot;\cdot,\cdot;\cdot)$ represent the beta function [23, Sec. 8.38] and the generalized hypergeometric function [20, Sec. 7.14], respectively. Note that $G_f(r;i) = \sum_{k=0}^{\infty}\mathrm{B}(k+\frac{i+1}{2},\frac{1}{2})\frac{(2\frac{m}{\Omega}V_0 r)^{2k}}{(2k)!}$ when i is even, and $G_f(r;i)=\sum_{k=0}^{\infty}\mathrm{B}(k+\frac{i}{2}+1,\frac{1}{2})\frac{(2\frac{m}{\Omega}V_0 r)^{2k+1}}{(2k+1)!}$ when i is odd. Denoting the k^{th} terms of these series with a_k and b_k, respectively, their successive terms can be computed recursively as

$$a_{k+1} = \frac{(k+\frac{i+1}{2})}{(k+\frac{1}{2})(k+1)(k+\frac{i+2}{2})}\left(\frac{m}{\Omega}V_0 r\right)^2 a_k \tag{4.10a}$$

$$b_{k+1} = \frac{(k+\frac{i}{2}+1)}{(k+1)(k+\frac{3}{2})(k+\frac{i+3}{2})}\left(\frac{m}{\Omega}V_0 r\right)^2 b_k \tag{4.10b}$$

where we have used $\mathrm{B}(x,y) = \Gamma(x)\Gamma(y)/\Gamma(x+y)$ and $\Gamma(k+1) = k!$ [25]. Using (4.10) and the ratio test for convergence of infinite series [25, Sec. 0.22], one can show that (4.9b) is convergent as

$$\lim_{k\to\infty}\frac{a_{k+1}}{a_k} = \lim_{k\to\infty}\frac{b_{k+1}}{b_k} = \left(\frac{m}{\Omega}V_0 r\right)^2\lim_{k\to\infty}\frac{1}{k^2} = 0. \tag{4.11}$$

A recursive algorithm is proposed in Appendix 4.B, for fast and efficient evaluation of the infinite series in (4.9b). Eq. (4.9c) expresses the Nakagami-*m* with LOS fading PDF in terms of the hypergeometric function ${}_1F_2(\cdot;\cdot,\cdot;\cdot)$, which is implemented efficiently in mathematical software packages like Mathematica, Matlab and Maple. Note that performance analysis of wireless fading systems often requires integration of the fading PDF against other

mathematical functions; the derived infinite series PDF expression is more amenable to further analysis than (4.9c) in many of these applications. This is because integration of the hypergeometric function ${}_1F_2(\cdot;\cdot,\cdot;\cdot)$ against other mathematical functions may be difficult.

4.1.4 Properties of the New Probability Distribution

In this section, we investigate the properties of the diffuse Nakagami-*m* with LOS fading distribution. In particular, we derive expressions for its CDF, its moments and its moment generating function.

To facilitate derivation of the Nakagami-*m* with LOS statistics, we use the binomial expansion of $(x+y)^n$ [25, eq. 1.111] to express (4.9) as

$$\begin{aligned} f_R(r) =& \frac{2\left(\frac{m}{\Omega}{\mathrm{V}_0}^2\right)^m}{\pi\Gamma(m){\mathrm{V}_0}^2} e^{-\frac{m}{\Omega}\mathrm{V}_0^2} \sum_{i=0}^{m-1}\sum_{j=0}^{m-1-i} \binom{m-1}{i}\binom{m-1-i}{j} \times \\ & \frac{(-\frac{2}{\mathrm{V}_0})^i}{{\mathrm{V}_0}^{2j}} \sum_{\substack{k=0 \\ k+i \text{ even}}}^{\infty} \frac{\mathrm{B}\left(\frac{k+i+1}{2},\frac{1}{2}\right)\left(2\frac{m}{\Omega}\mathrm{V}_0\right)^k}{k!} r^{i+2j+k+1} e^{-\frac{m}{\Omega}r^2}. \end{aligned} \tag{4.12}$$

One notes that each term of the summation in (4.12) is a combination of powers and exponentials of r. This facilitates integration of (4.12) against other mathematical functions. Using (4.12) and [25, eq. 3.381.4], we evaluate the moments of R as

$$\begin{aligned} \mathrm{E}\left[R^\mu\right] =& \int_0^\infty r^\mu f_R(r) dr \\ =& \frac{\left(\frac{m}{\Omega}\mathrm{V}_0^2\right)^{m-1} e^{-\frac{m}{\Omega}\mathrm{V}_0^2}}{\pi\Gamma(m)\left(\frac{m}{\Omega}\right)^{\frac{\mu}{2}}} \sum_{i=0}^{m-1}\sum_{j=0}^{m-1-i} \binom{m-1}{i}\binom{m-1-i}{j} \times \\ & \frac{(-2)^i}{(\frac{m}{\Omega}{\mathrm{V}_0}^2)^{j+\frac{i}{2}}} \sum_{\substack{k=0 \\ k+i \text{ even}}}^{\infty} \frac{\mathrm{B}\left(\frac{k+i+1}{2},\frac{1}{2}\right)\Gamma(\frac{k+i+\mu}{2}+j+1)}{k!} \left(\frac{4m}{\Omega}{\mathrm{V}_0}^2\right)^{\frac{k}{2}}. \end{aligned} \tag{4.13}$$

Substitution of $\mu = 1$ in (4.13) gives the mean of R. To evaluate the second moment of R, we can find an expression simpler than (4.13) with $\mu = 2$. Since ϕ_0 and ϕ_d are modeled in (4.2) as independent and uniformly distributed random variables in $[0, 2\pi]$, it is straightforward to show

$$\mathrm{E}\left[R^2\right] = \mathrm{E}\left[{\mathrm{V}_0}^2 + 2\mathrm{V}_0\mathrm{V}_d\left(\cos\phi_0\cos\phi_d + \sin\phi_0\sin\phi_d\right) + {\mathrm{V}_d}^2\right] = {\mathrm{V}_0}^2 + \Omega \tag{4.14}$$

where we used $\mathrm{E}\left[V_d^2\right] = \Omega$ [24]. The CDF of R can also be derived by integration of

(4.12), which yields

$$F_R(r) = \int_0^r f_R(x)dx = \frac{\left(\frac{m}{\Omega}{\mathrm{V}_0}^2\right)^{m-1} e^{-\frac{m}{\Omega}\mathrm{V}_0^2}}{\pi\Gamma(m)} \times \sum_{i=0}^{m-1}\sum_{j=0}^{m-1-i} \binom{m-1}{i}\binom{m-1-i}{j} \frac{(-2)^i}{(\frac{m}{\Omega}{\mathrm{V}_0}^2)^{j+\frac{i}{2}}} G_F(r;i,j) \tag{4.15a}$$

$$G_F(r;i,j) = \sum_{\substack{k=0 \\ k+i \text{ even}}}^{\infty} \frac{\mathrm{B}\left(\frac{k+i+1}{2},\frac{1}{2}\right)\left(2\sqrt{\frac{m}{\Omega}}\mathrm{V}_0\right)^k}{k!} \gamma\left(\frac{i+k}{2}+j+1, \frac{m}{\Omega}r^2\right) \tag{4.15b}$$

where $\gamma(\cdot)$ is the incomplete gamma function [25, Sec. 8.35], and we used $\int_0^r x^{\nu-1}e^{-\mu x}dx = \mu^{-\nu}\gamma(\nu,\mu r)$ [25, eq. 3.381.3]. Direct evaluation of the incomplete gamma function in each term of the series is not required as it can be evaluated recursively by [25, 8.356.1]

$$\gamma(n+1,x) = n\gamma(n,x) - x^n e^{-x}. \tag{4.16}$$

Note that the exponential term in (4.16) is independent of n, and therefore it needs to be evaluated only one time. In Appendix 4.B, we propose a recursive algorithm for the efficient evaluation of (4.15b). Note that the beta function and the incomplete gamma function are each computed only once, for $k = 0$ or $k = 1$, to initialize the algorithm. After initialization, the infinite series can be evaluated using basic mathematical operations; i.e., summation and multiplication. The number of required operations grows linearly as $O(N)$, where N is the series truncation order.

One can also derive an expression for the moment generating function of R as

$$\begin{aligned}\Phi(s) &= \int_0^\infty f_R(r)e^{sr}dr \\ &= \frac{2\left(\frac{m}{\Omega}{\mathrm{V}_0}^2\right)^m}{\pi\Gamma(m)} \frac{e^{-\frac{m}{\Omega}\mathrm{V}_0^2}}{{\mathrm{V}_0}^2} \sum_{i=0}^{m-1}\sum_{j=0}^{m-1-i} \binom{m-1}{i}\binom{m-1-i}{j} \times \\ &\frac{(-\frac{2}{\mathrm{V}_0})^i}{{\mathrm{V}_0}^{2j}} \sum_{\substack{k=0 \\ k+i \text{ even}}}^{\infty} \frac{\mathrm{B}\left(\frac{k+i+1}{2},\frac{1}{2}\right)\left(2\frac{m}{\Omega}\mathrm{V}_0\right)^k}{k!} \int_0^\infty r^{i+2j+k+1} e^{-\frac{m}{\Omega}r^2+sr}dr.\end{aligned} \tag{4.17}$$

The integral in (4.17) can be solved using [25, eq. 3.462.1]

$$\int_0^\infty x^{\nu-1}e^{-\beta x^2-\lambda x}dx = (2\beta)^{-\nu/2}\Gamma(\nu)e^{\frac{\lambda^2}{8\beta}}D_{-\nu}\left(\frac{\lambda}{\sqrt{2\beta}}\right), \quad \Re\{\beta\}>0,\ \Re\{\nu\}>0 \tag{4.18}$$

where $D_p(\cdot)$ is the parabolic cylinder function [25, Sec. 9.24]. Substitution of (4.18) in (4.17) gives

$$\Phi(s) = \frac{\left(\frac{m}{\Omega}\mathrm{V_0}^2\right)^{m-1}}{\pi\Gamma(m)} \exp\left(-\frac{m}{\Omega}\mathrm{V}_0^2 + \frac{s^2}{8\frac{m}{\Omega}}\right) \times \sum_{i=0}^{m-1}\sum_{j=0}^{m-1-i}\binom{m-1}{i}\binom{m-1-i}{j}\frac{(-1)^i 2^{\frac{i}{2}-j}}{\left(\frac{m}{\Omega}\mathrm{V_0}^2\right)^{\frac{i}{2}+j}} G_\Phi(s;i,j) \tag{4.19a}$$

$$G_\Phi(s;i,j) = \sum_{\substack{k=0 \\ k+i \text{ even}}}^{\infty} \frac{\mathrm{B}\left(\frac{k+i+1}{2}, \frac{1}{2}\right)\left(2\frac{m}{\Omega}\mathrm{V_0}^2\right)^{\frac{k}{2}}}{k!}\Gamma\left(2j+i+k+2\right) D_{-(2j+i+k+2)}\left(\frac{-s}{\sqrt{2\frac{m}{\Omega}}}\right). \tag{4.19b}$$

The characteristic function of R, $\Phi(j\omega)$, is given by (4.19) with s replaced by $j\omega$, namely by noting that the parabolic cylinder function can be expressed in terms of the Whittaker m-function [25, Sec. 9.24] which is implemented in common mathematical software packages. However, it is not required to evaluate the parabolic cylinder function directly in each term of the series in (4.19b). The parabolic cylinder function can be evaluated recursively by [25, eqs. 9.247.1, 8.250.1 and Sec. 9.254]

$$D_{-n}(z) = -\frac{1}{(n-1)}\left[zD_{-(n-1)}(z) - D_{-(n-2)}(z)\right] \tag{4.20a}$$

$$D_{-2}(z) = e^{-\frac{z^2}{4}} - zD_{-1}(z) \tag{4.20b}$$

$$D_{-1}(z) = e^{\frac{z^2}{4}}\sqrt{\frac{\pi}{2}}\left[1 - \mathrm{erf}\left(\frac{z}{\sqrt{2}}\right)\right]. \tag{4.20c}$$

One can evaluate (4.19b) fast and efficiently using (4.20). In Appendix 4.B, we propose an algorithm for the recursive evaluation of (4.19b) using (4.20). The proposed algorithm only requires basic mathematical operations, and it does not require computation of any special function in each term of the series. In fact, it is required to evaluate the error function only one time to initialize the algorithm. The computational complexity of the algorithm grows linearly with the series truncation order, N.

4.1.5 Numerical Examples and Discussion: PDF

In this section, we provide numerical examples to illustrate the application of the Nakagami-*m* with LOS fading PDF using (4.9). We also compare the exact Nakagami-*m* with LOS fading PDF with the Rice and Nakagami-*m* PDFs.

Fig. 4.1 shows the Nakagami-*m* with LOS fading PDF for $m = 3$, $\Omega = 1$ and four different LOS magnitudes. Note that the PDF reduces to the Nakagami-*m* PDF when $V_0 = 0$.

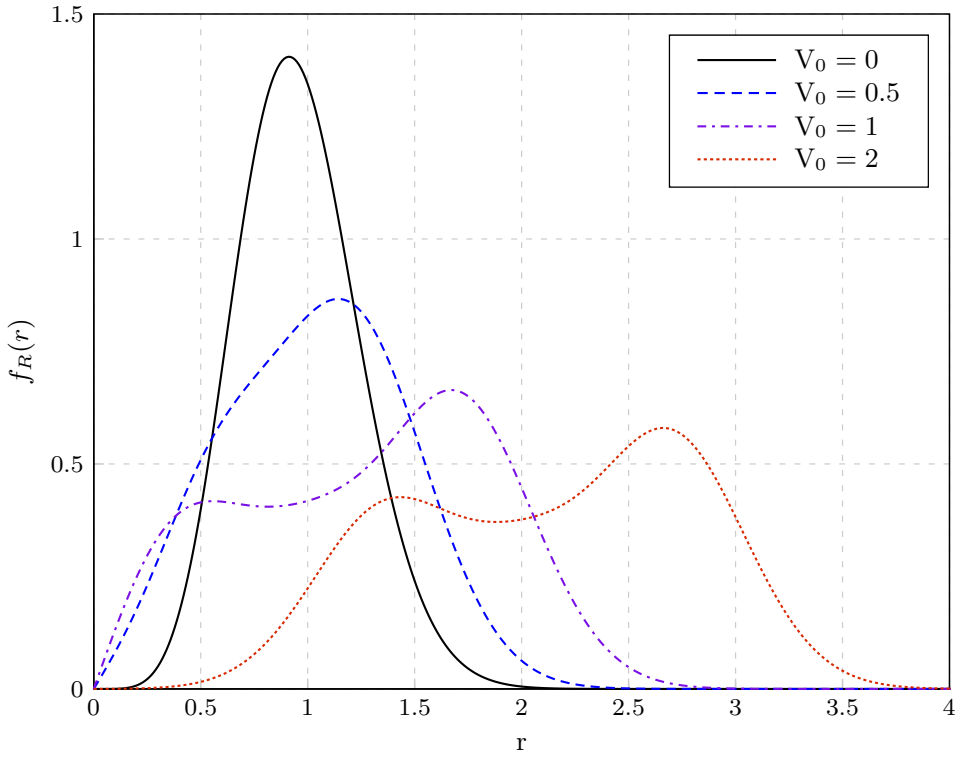

Figure 4.1. The Nakagami-*m* with LOS fading PDF for $m = 3$, $\Omega = 1$ and different choices of the LOS magnitude V_0.

We observe that as the LOS component gets stronger, the PDF gets more different from the Nakagami-*m* PDF. In fact, when the LOS power is on the order of the diffuse power Ω, the PDF becomes bimodal. From Fig. 4.1, one can realize that in general, the Nakagami-*m* distribution cannot model or approximate the behavior of the received signal envelope when there is a LOS component in the received signal. Such an approximation can be valid only when the LOS power is negligible compared to the diffuse power. This is consistent with our model in (4.2), where the non-specular multipath waves were absorbed in the diffuse component of the received signal.

To show that the Rice and Nakagami-*m* distributions cannot model the envelope of the received signal in (4.2), we compare their PDFs with the diffuse Nakagami-*m* with LOS PDF in Fig. 4.2. In this figure, the black curves show the Nakagami-*m* with LOS PDF with parameters $m = 4$, $\Omega = 1$ and $V_0 = 2$. We compare this distribution with three approximate distributions for the envelope of the received signal in model (4.2). The first candidate is the Rice distribution $R_R \sim \text{Rice}(V_R, \sigma_R^2)$. The PDF of R_R is [24]

$$f^{(\text{Rice})}(r) = \frac{r}{\sigma_R^2} e^{-\frac{r^2+V_R^2}{2\sigma_R^2}} I_0\left(\frac{V_R}{\sigma_R^2} r\right) \tag{4.21}$$

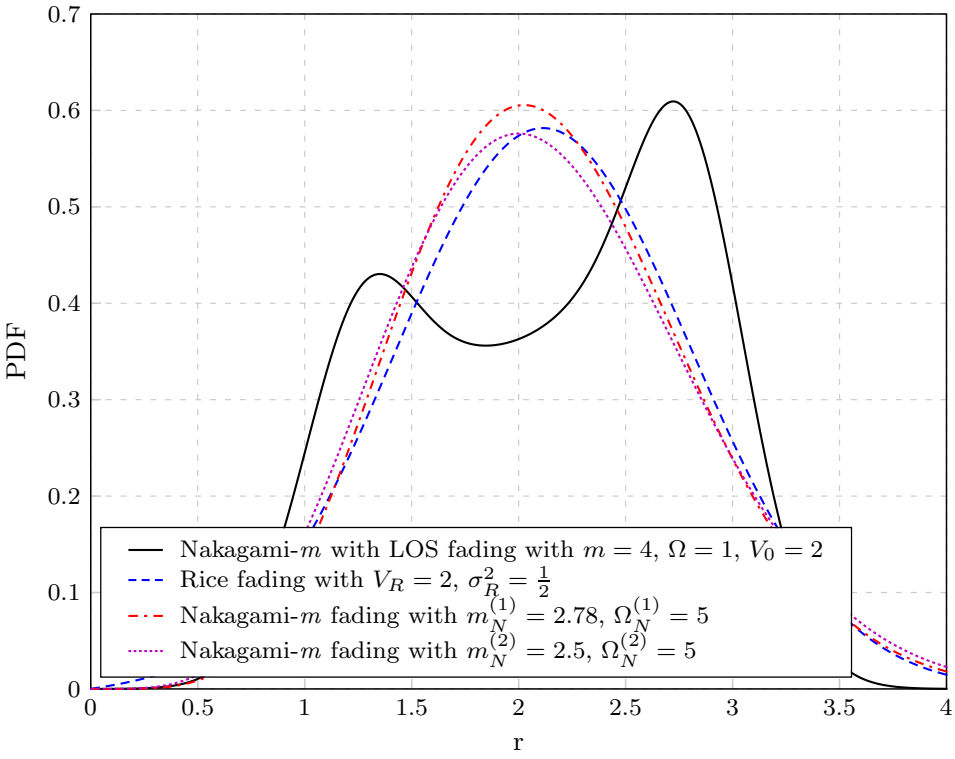

(a) Linear scaling

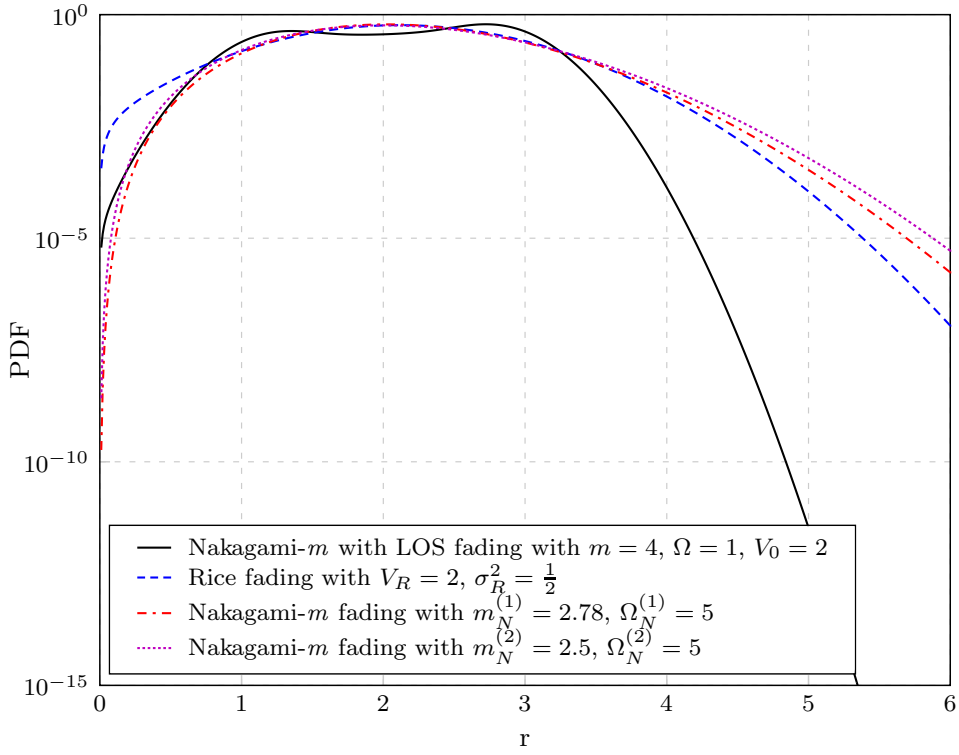

(b) Logarithmic scaling

Figure 4.2. Comparison of the Nakagami-m with LOS PDF with the Rice and Nakagami-m PDFs with the equivalency parameters in (4.22)-(4.24).

where $I_0(\cdot)$ is the zeroth-order modified Bessel function of the first kind, V_R is the magnitude of the LOS component and $2\sigma_R^2$ is the mean-squared voltage of the diffuse component [24]. So, the parameters of the Rice distribution corresponding to model (4.2) are

$$V_R = V_0 \tag{4.22a}$$

$$\sigma_R^2 = \frac{\Omega}{2}. \tag{4.22b}$$

For the Nakagami-*m* with LOS distribution with parameters $m = 4$, $\Omega = 1$ and $\mathrm{V}_0 = 2$, the equivalency Rice parameters are $V_R = 2$ and $\sigma_R^2 = \frac{1}{2}$. The blue curves in Fig. 4.2 show this PDF. The second candidate for comparison is the Nakagami-*m* distribution $R_N^{(1)} \sim \text{Nakagami}(m_N^{(1)}, \Omega_N^{(1)})$ corresponding to the Rice distribution with the parameters in (4.22). The parameters of this distribution are determined by the widely used Rice to Nakagami-*m* parameter transformation [3, 5, 24]

$$m_N^{(1)} = \frac{\left(\frac{V_R^2}{2\sigma_R^2} + 1\right)^2}{\left(\frac{V_R^2}{\sigma_R^2} + 1\right)} \tag{4.23a}$$

$$\Omega_N^{(1)} = V_R^2 + 2\sigma_R^2 \tag{4.23b}$$

which gives $\Omega_N^{(1)} = 5$ and $m_N^{(1)} \approx 2.78$. The resulting PDF is shown in Fig. 4.2 with red color. The last candidate is also a Nakagami-*m* distribution, $R_N^{(2)} \sim \text{Nakagami}(m_N^{(2)}, \Omega_N^{(2)})$, whose parameters are chosen such that its first and second moments match the first and second moments of the Nakagami-*m* with LOS distribution. The first and second moments of the latter are given by (4.13) and (4.14). Equating these moments with the first and second moments of the Nakagami-*m* distribution gives [3]

$$\Omega_N^{(2)} = \Omega + V_0^2 \tag{4.24a}$$

$$\frac{\Gamma\left(m_N^{(2)} + \frac{1}{2}\right)}{\Gamma\left(m_N^{(2)}\right)} \sqrt{\frac{\Omega_N^{(2)}}{m_N^{(2)}}} = E\left[R\right]. \tag{4.24b}$$

By solving (4.24) for $m_N^{(2)}$ and $\Omega_N^{(2)}$, we obtain the Nakagami-*m* equivalency parameters. In our example, solving (4.24) yields $m_N^{(2)} = 2.50$ and $\Omega_N^{(2)} = 5$. The purple curves in Fig. 4.2 correspond to this PDF. Note that unlike the Rice fading and the Nakagami-*m* fading models with parameters in (4.22) and (4.23), the parameters of the last Nakagami-*m* fading model given by (4.24), are sensitive to parameter m of the Nakagami-*m* with LOS fading model. This is because $E[R]$ in (4.24b) is a function of m.

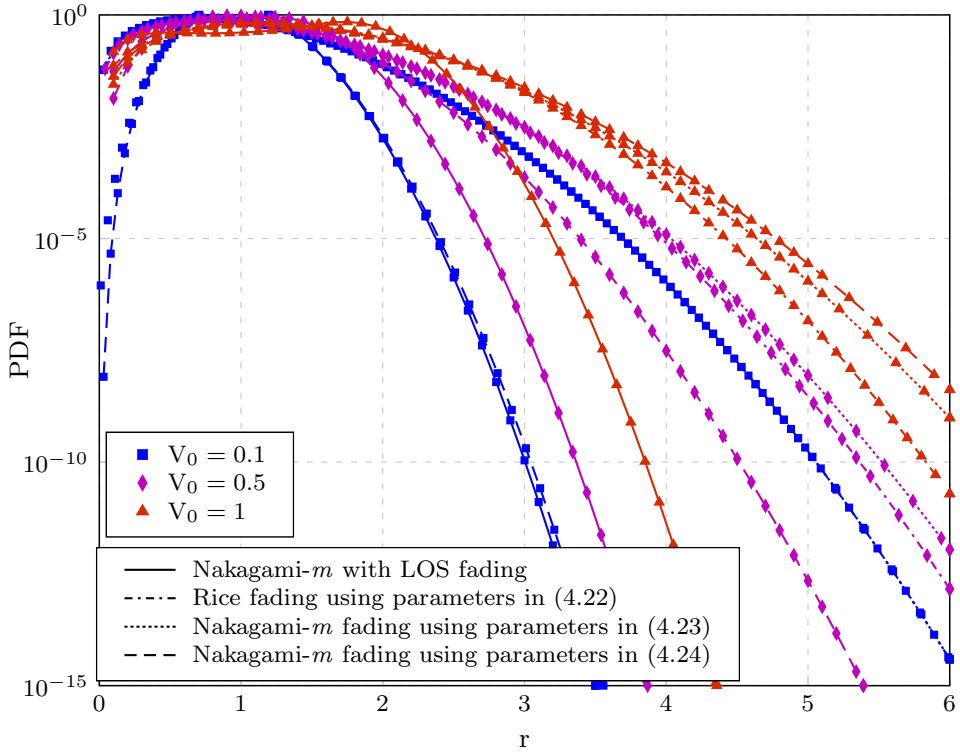

Figure 4.3. Comparison of the decay rate of the tail of the Nakagami-*m* with LOS fading PDF with the decay rates of the tails of the Rice and Nakagami-*m* PDFs with the equivalency parameters for $m = 4$, $\Omega = 1$ and various LOS amplitudes.

In Fig. 4.2, we observe that the shape of the PDF of the new model is substantially different from all the proposed approximate PDFs. In particular, the PDF of R has two modes while the approximate PDFs have just a single mode for the considered parameters. Another very significant observation is that in Fig. 4.2b, the tail of the Nakagami-*m* with LOS fading PDF decays much faster than the other PDFs. This is significant as the performance analysis of wireless fading systems involves integrations on the tail of the fading PDF. This observation shows that for performance analysis, it is not always possible to approximate the Nakagami-*m* with LOS fading PDF with Nakagami-*m* or Rice PDFs. This fact is more clear in Fig. 4.3 which shows the tail of the Nakagami-*m* with LOS distribution and the approximate distributions for different LOS magnitudes. As we observe in this figure, when the LOS power is much smaller than the diffuse power, the Nakagami-*m* distribution with parameters given by (4.24) can approximate the Nakagami-*m* with LOS distribution. However, the Rice and the Nakagami-*m* approximations with parameters in (4.22) and (4.23) are not precise even for low-power LOS components. More significantly, none of the proposed approximations remains useful for moderate and high-power LOS waves.

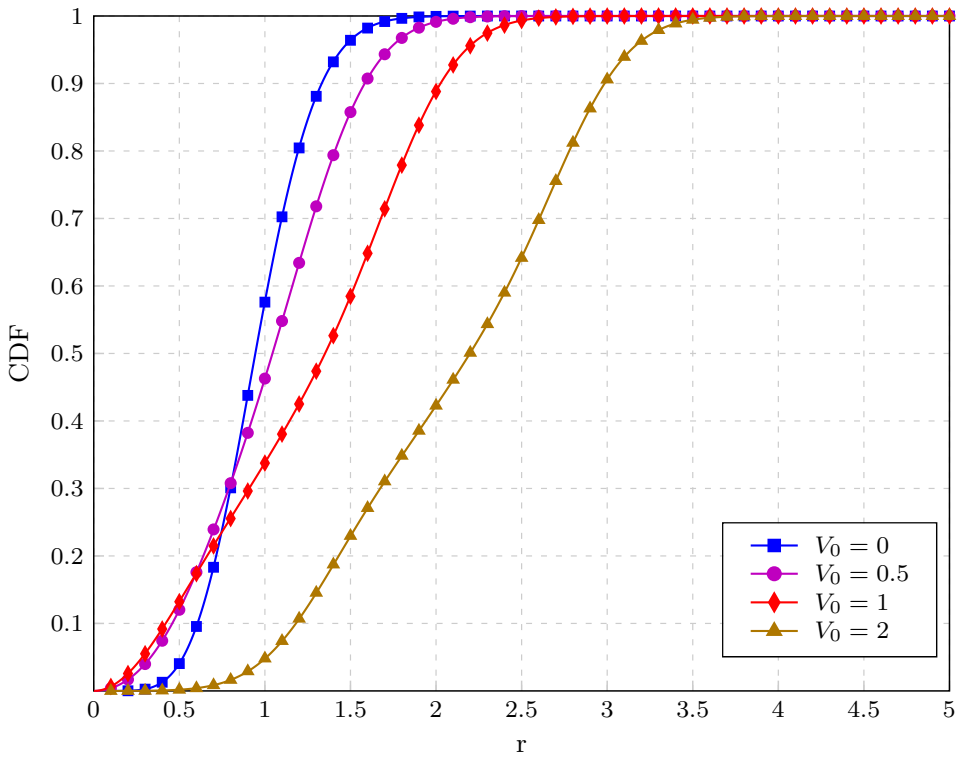

Figure 4.4. The diffuse Nakagami-*m* with LOS fading CDF for $m = 3, \Omega = 1$ and different values of V_0. The markers represent the Monte-Carlo simulation points and the solid curves are obtained by the theoretical expression in (4.15).

4.1.6 Numerical Examples and Discussion: CDF and CF

The fading CDF is required for the evaluation of the outage probability of wireless fading systems. In this section, we present numerical examples for the CDF of diffuse Nakagami-*m* with LOS fading. We also provide the CF curves of the new distribution using eqs. (4.19) and (4.20). The theoretical results are verified by computer simulations.

Fig. 4.4 shows the CDF of diffuse Nakagami-*m* with LOS fading obtained by evaluation of eq. (4.15) and by computer simulations. The simulation results are obtained by generating $N_s = 10^6$ samples of the diffuse Nakagami-*m* with LOS distribution. The simulation CDF at point r is evaluated as the ratio of the number of samples smaller than r to N_s. In Fig. 4.4, we observe full agreement between the theoretical and computer simulation results. We also observe that for fixed values of m and Ω, the CDF increases to one more slowly as the LOS component V_0 gets stronger. This is consistent with our observation in Fig. 4.1, where the modes of the PDF locate at larger values of r as V_0 increases. In Fig. 4.5, we look at the lower tails of the CDFs of the diffuse Nakagami-*m* with LOS distribution and the corresponding Rice and Nakagami-*m* distributions derived in Sec. 4.1.5. Note that the

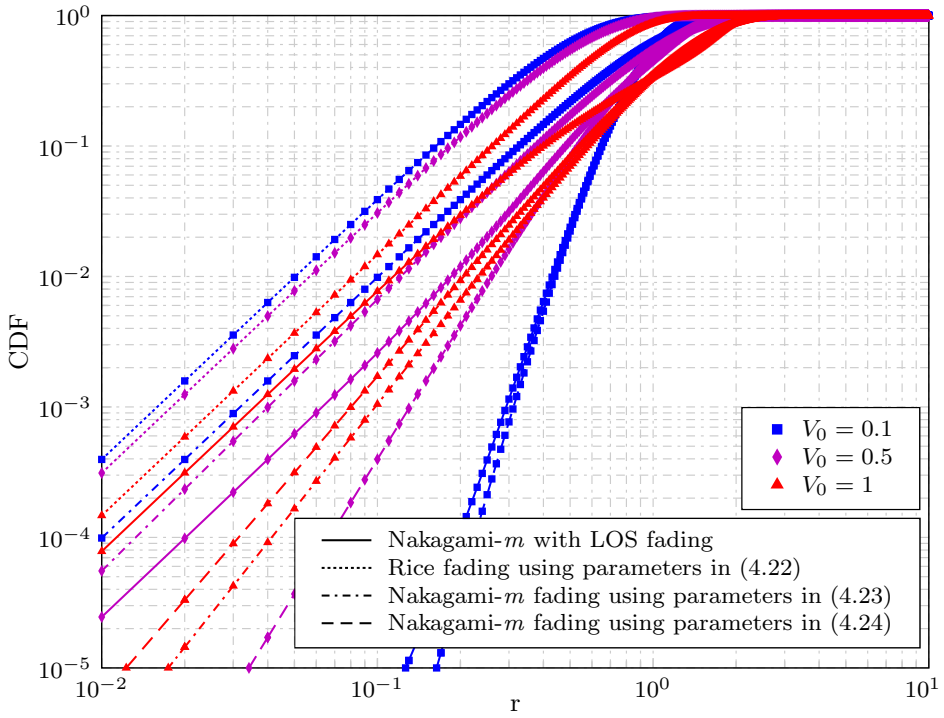

Figure 4.5. Comparison of the of diffuse Nakagami-*m* with LOS fading CDF and the CDFs of the corresponding Rice and Nakagami-*m* distributions for $m = 4$, $\Omega = 1$ and various LOS amplitudes.

behavior of the fading CDF in the lower tail is significant, as it is closely connected to the outage probability of wireless fading systems. In this figure, the diffuse Nakagami-*m* with LOS CDF is plotted for parameters $m = 4$, $\Omega = 1$ and three LOS values 0.1, 0.5 and 1. Fig. 4.5 also shows the Rice and Nakagami-*m* CDFs with the equivalency parameters in (4.22)-(4.24). Note that the Rice and Nakagami-*m* CDF expressions corresponding to the PDF expressions in (4.21) and (4.1) are [1, 24]

$$F^{(\text{Rice})}(r) = 1 - Q\left(\frac{V_R}{\sigma_R}, \frac{r}{\sigma_R}\right) \tag{4.25}$$

$$F^{(\text{Nakagami})}(r) = \frac{\gamma\left(m, \frac{m}{\Omega}r^2\right)}{\Gamma(m)} \tag{4.26}$$

respectively, where $Q(\cdot, \cdot)$ is the Marcum Q function. We observe that, in general, the CDF of none of these distributions can closely approximate the CDF of the Nakagami-*m* with LOS distribution. Also note that when the LOS component is weak, the second Nakagami-*m* distribution with parameters in (4.24), has the closest CDF curve to $F_R(r)$.

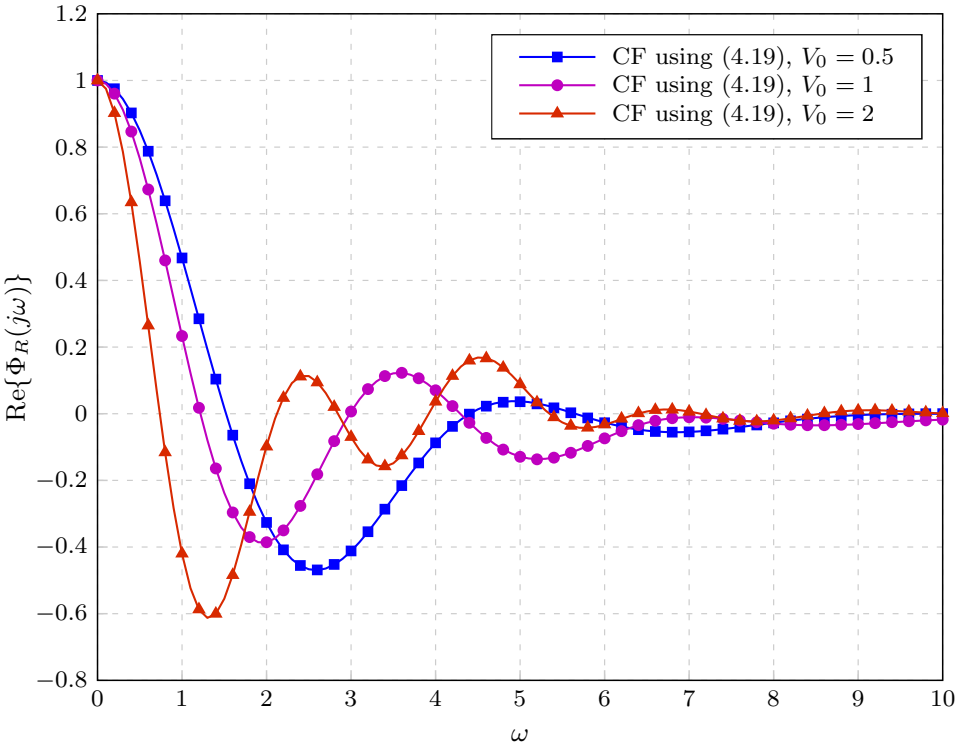

(a) Real part

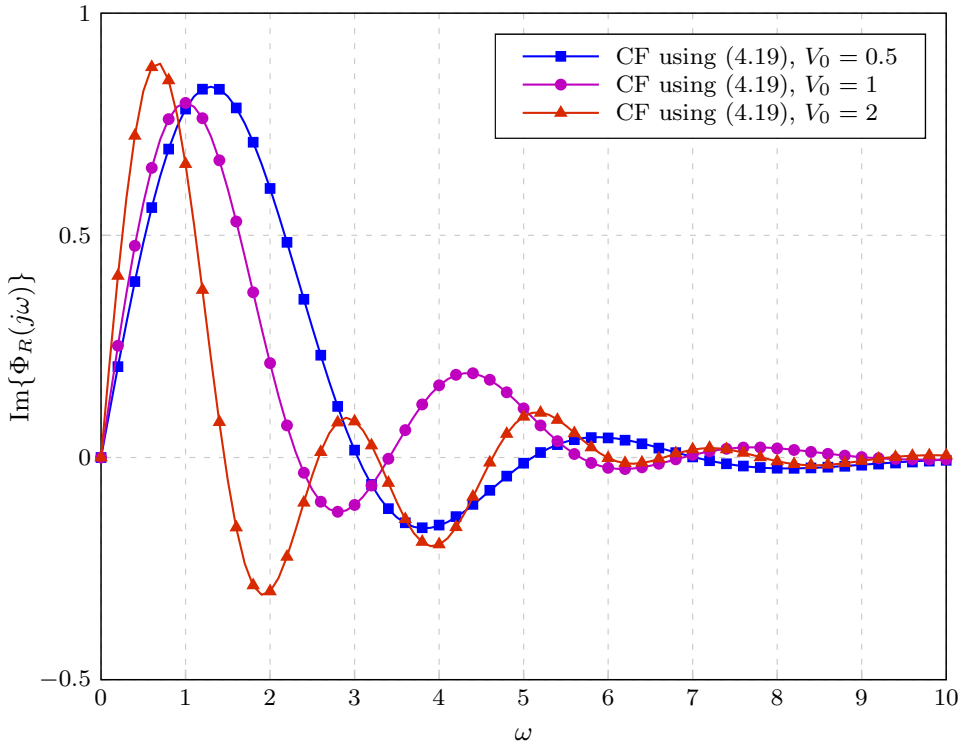

(b) Imaginary part

Figure 4.6. The Nakagami-*m* with LOS fading CF for $m = 3, \Omega = 1$ and different choices of V_0. The markers represent the Monte-Carlo simulation points and the solid curves are obtained by the theoretical expression in (4.19).

Fig. 4.6 shows the Nakagami-*m* with LOS fading CF evaluated both by using (4.19) and by computer simulations. Using the recursive algorithm proposed in Appendix B, each of the CF curves was evaluated in fractions of a second. As we observe, the Nakagami-*m* with LOS CF becomes more oscillatory as the LOS component gets stronger. Moreover, the envelopes of the real and imaginary parts of the CF are not always decreasing. This is clear for the CF curves for $V_0 = 2$,

4.1.7 Comparison to TWDP Fading

In this section, we compare the diffuse Nakagami-*m* with LOS and TWDP fading behaviors. As was discussed in Sec. 4.1.3, the received signal in Nakagami-*m* with LOS fading has one LOS component and a Nakagami-*m* distributed diffuse component. In TWDP fading, however, the received signal has two LOS components and a Rayleigh distributed diffuse component. The mathematical model for the received baseband signal in TWDP fading is [2, 22]

$$\tilde{V} = V_1 e^{j\psi_1} + V_2 e^{j\psi_2} + \tilde{V}_d e^{j\psi_d} \tag{4.27}$$

where V_1, V_2 and V_d are magnitudes of the two LOS components and the diffuse component, respectively. ψ_1, ψ_2 and ψ_d are the corresponding phases which are independent and uniformly distributed in $[0, 2\pi]$. The real and imaginary parts of the diffuse component are normally distributed with zero mean and variance σ^2. So, $\tilde{V}_d$ is Rayleigh distributed and its mean-squared voltage is $2\sigma^2$ [2, 21, 22]. Defining

$$K = \frac{V_1^2 + V_2^2}{2\sigma^2} \tag{4.28}$$

$$\Delta = \frac{2V_1V_2}{V_1^2 + V_2^2} \tag{4.29}$$

the TWDP PDF has the approximate solution [2]

$$f_R(r) \approx \frac{r}{\sigma^2} \exp\left(-\frac{r^2}{2\sigma^2} - K\right) \sum_{i=1}^{M} a_i D\left(\frac{r}{\sigma}; K, \Delta \cos\frac{\pi(i-1)}{2M-1}\right) \tag{4.30a}$$

where

$$D(x; K; \alpha) = \frac{e^{\alpha K}}{2} I_0\left(x\sqrt{2K(1-\alpha)}\right) + \frac{e^{-\alpha K}}{2} I_0\left(x\sqrt{2K(1+\alpha)}\right). \tag{4.30b}$$

Another solution for the TWDP fading PDF is also available in [22], which gives the PDF as an infinite series. As is clear from (4.27) and (4.30), TWDP fading is totally described by three parameters V_1, V_2 and σ^2, or equivalently, by parameters K, Δ and σ^2. So, compared to the Rice and Nakagami-*m* distributions considered in Secs. 4.1.5 and 4.1.6, TWDP

fading provides more degrees of freedom to behave similar to diffuse Nakagami-*m* with LOS fading. To compare the TWDP statistics with the Nakagami-*m* with LOS statistics, we follow two methods to derive the TWDP fading equivalency parameters. In the first method, we approximate the distribution of the envelope of the diffuse Nakagami-*m* component in (4.2) with Rice distribution Rice(V_2, σ^2). Note that the resulting Rice distribution models the envelope of the combination of a LOS component with magnitude V_2 with a Rayleigh distributed diffuse component with power $2\sigma^2$. Therefore, the Rice approximation for the diffuse component in (4.2) can be used to approximate (4.2) with the TWDP fading model in (4.27). To derive the equivalency parameters of the Rice distribution, we use the Nakagami-*m* to Rice transformation [24, eq. (2.26)]

$$m = \left(\frac{V_2^2}{2\sigma^2} + 1\right)^2 / \left(\frac{V_2^2}{\sigma^2} + 1\right) \tag{4.31a}$$

$$\Omega = V_2^2 + 2\sigma^2. \tag{4.31b}$$

By solving (4.31), the Rice approximation for the diffuse Nakagami-*m* component gives the TWDP equivalency parameters

$$V_1 = V_0 \tag{4.32a}$$

$$V_2 = \sqrt{\sqrt{1 - \frac{1}{m}}\Omega} \tag{4.32b}$$

$$\sigma^2 = \frac{\Omega}{2}\left(1 - \sqrt{1 - \frac{1}{m}}\right). \tag{4.32c}$$

An important benefit of the Rice approximation for the diffuse power is that it gives all the equivalency parameters analytically. We insist that the resulting TWDP model with the equivalency parameters in (4.32) is an approximate model for (4.2) as the Rice distribution obtained by the Nakagami-*m* to Rice transformation is an approximate model for the Nakagami-*m* distribution.

A second approach we use to derive the TWDP parameters is the moment matching method. Since the TWDP model is described by three parameters, we need to equate three moments of the TWDP distribution with the corresponding three moments of the Nakagami-*m* with LOS distribution. Infinite series expressions are given for the n-th moments of the TWDP and Nakagami-*m* with LOS distributions in [22, eq. (11)] and (4.13), respectively. Note that a simpler expression for the second moment of the Nakagami-*m* with LOS distribution was given in (4.14). The second moment of the TWDP distribution can also be obtained as $V_1^2 + V_2^2 + 2\sigma^2$, by following the same method we used to derive (4.14). Except for the second moments, all the other moments are given by infinite series expressions,

Table 4.1. TWDP EQUIVALENCY PARAMETERS.

Nakagami-m parameters	TWDP parameters	Rice Approx.	Moments Matching		
			1st, 2nd, 3rd	1st, 2nd, 10th	1st, 2nd, 20th
Case I: $m = 2$, $V_0 = 1, \Omega = 1$	K(dB)	7.655	7.674	7.488	5.784
	Δ	0.985	0.985	0.996	0.717
	σ	0.383	0.382	0.389	0.457
Case II: $m = 4$, $V_0 = \frac{1}{2}, \Omega = 1$	K(dB)	9.206	9.087	7.406	6.885
	Δ	0.834	0.829	0.672	0.493
	σ	0.259	0.262	0.310	0.326

and therefore, the TWDP equivalency parameters must be evaluated numerically. Equating the second moments gives

$$V_1^2 + V_2^2 + 2\sigma^2 = V_0^2 + \Omega. \tag{4.33}$$

The other required identities are given by equating two other moments. Note that choosing a high order moment increases the contribution of the upper tail of the distribution, and therefore, the resulting PDF is more likely to match the diffuse Nakagami-*m* with LOS fading PDF at its upper tail. However, this may lead to a looser match at the lower tail of the distribution (near zero).

Table 4.1 shows the equivalency TWDP parameters for a Nakagami-*m* with LOS distribution using the Rice approximation for the diffuse component and the moment matching method. Note that the parameters obtained by the Rice approximation are very close to the parameters obtained by matching the first, second and third moments. However, the former values are given analytically while the latter values must be computed numerically. Fig. 4.7 shows the TWDP PDFs with the parameters in Table 4.1, as well as the corresponding Nakagami-*m* with LOS fading PDFs. We observe that the PDFs obtained by the Rice approximation and the moments matching method behave almost the same, when low order moments are matched. Moreover, the PDFs resulting from matching high order moments show a loose fit at the lower tail of the PDF and a better fit at the upper tail, which is expected as was discussed before. Note that none of the derived TWDP fading PDFs coincides the Nakagami-*m* with LOS fading PDF, specially near the modes of the distribution.

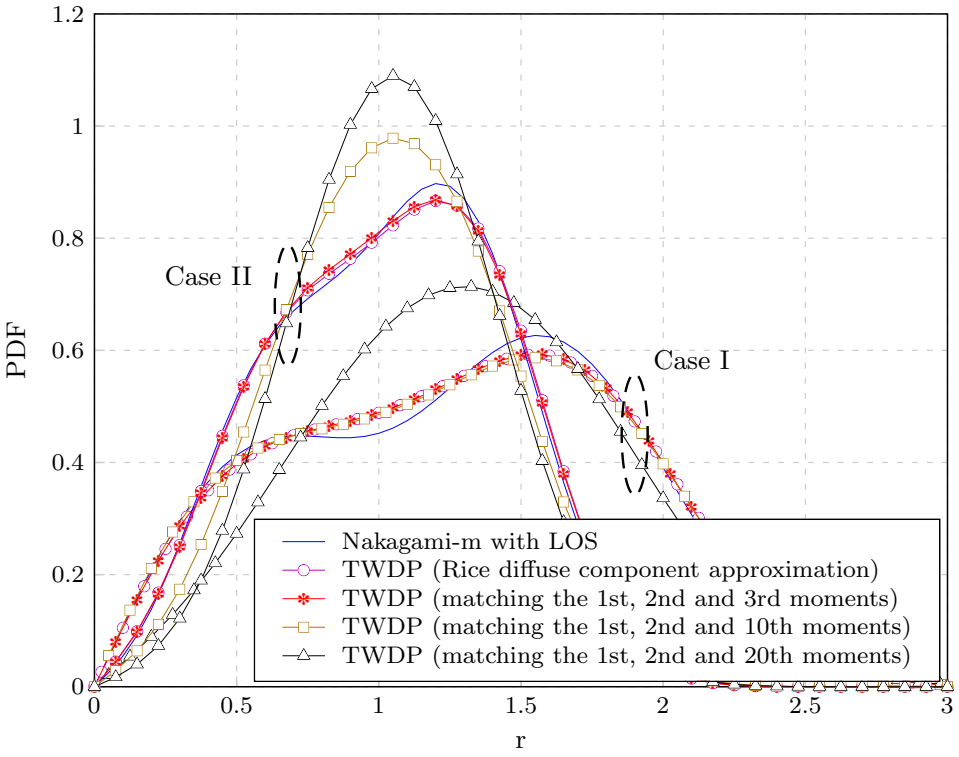

(a) Linear scaling

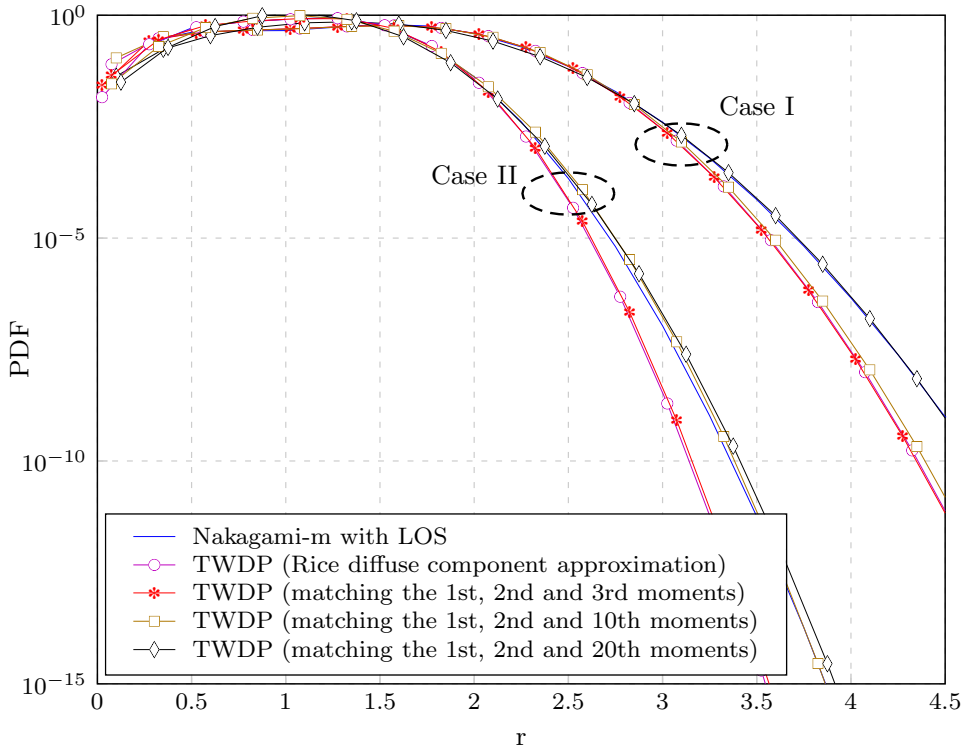

(b) Logarithmic scaling

Figure 4.7. Comparison between the diffuse Nakagami-*m* with LOS fading PDF and the TWDP fading PDFs with the equivalency parameters in Table 4.1.

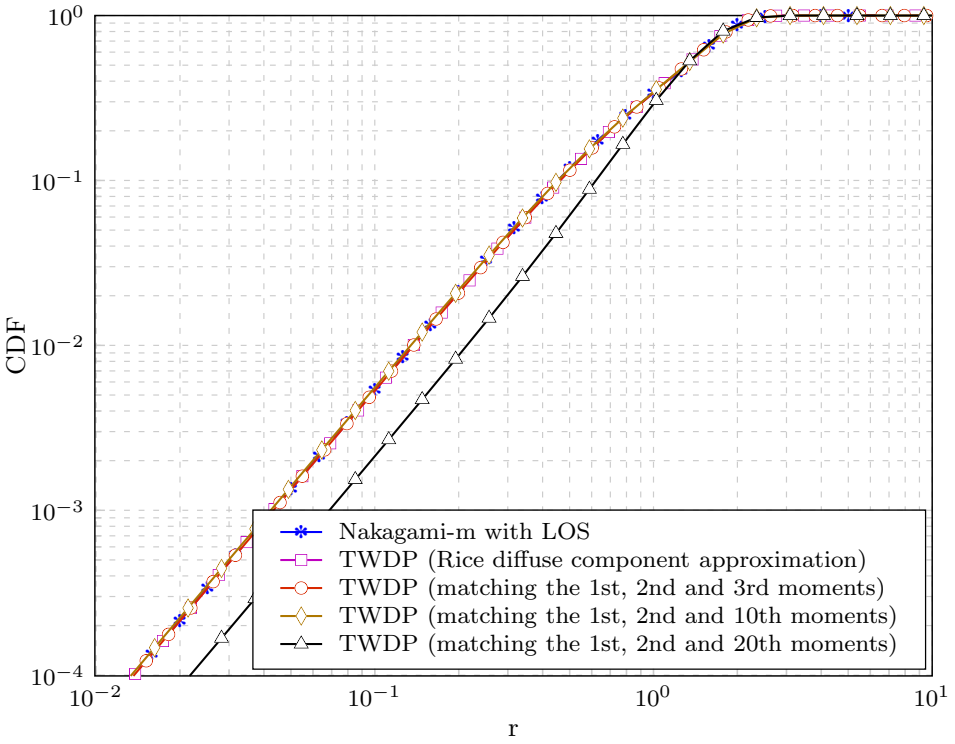

(a) Case I

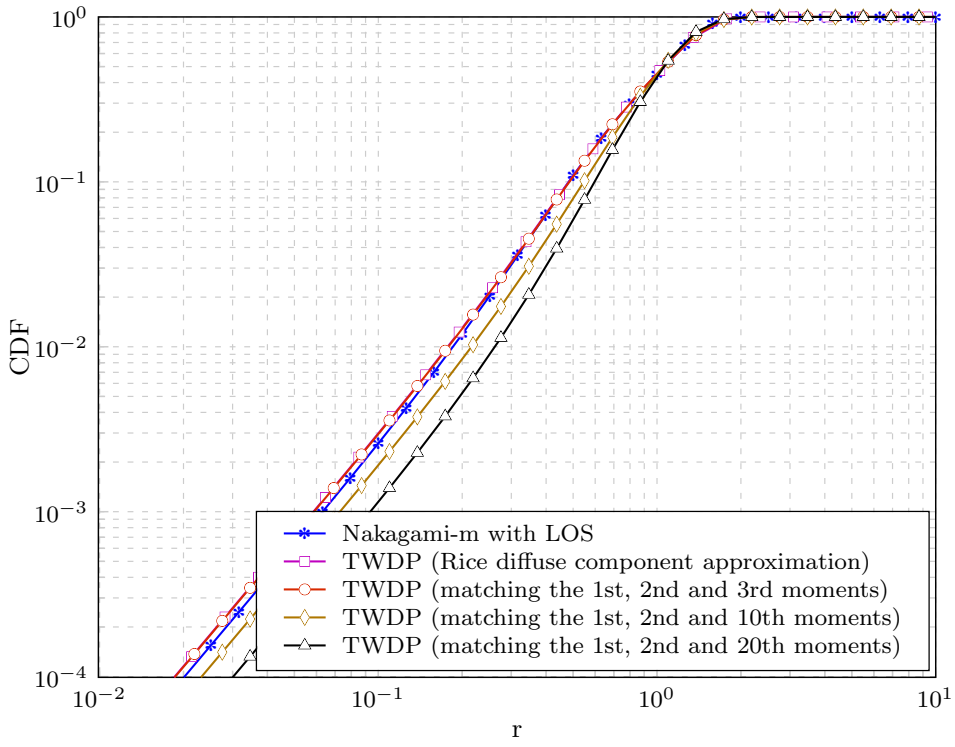

(b) Case II

Figure 4.8. Comparison between the diffuse Nakagami-*m* with LOS fading CDF and the TWDP fading CDFs with the equivalency parameters in Table 4.1.

Fig. 4.8 shows the CDFs of the distributions in Table 4.1. We observe that the CDFs of the TWDP distributions obtained by the Rice approximation and by matching the low-order moments, are close to the Nakagami-*m* with LOS fading CDF.

Moreover, the TWDP CDF obtained by the Rice approximation for the diffuse component behaves not worse than the CDFs obtained by the moments matching method. Since the parameters of the Rice approximation are given analytically it is worthy to investigate its CDF behavior more thoroughly. Fig. 4.9 shows the CDFs of two Nakagami-*m* with LOS distributions and the corresponding TWDP fading CDFs obtained by the Rice approximation for the diffuse component. We observe that the resulting TWDP CDFs are very close to the Nakagami-*m* with LOS CDFs for $r > 0.1$. However, for $r < 0.1$, they deviate from the Nakagami-*m* with LOS CDFs, specially when the LOS power V_0^2 is much smaller than the diffuse power, Ω.

As the last point, note that approximating diffuse Nakagami-*m* with LOS fading with TWDP fading may lead to very large values of K. This can be shown clearly for TWDP fading with parameters given by the Rice approximation in (4.32). Substitution of (4.32) in (4.28) yields

$$K = \frac{\frac{V_0^2}{\Omega} + \sqrt{1 - \frac{1}{m}}}{1 - \sqrt{1 - \frac{1}{m}}}. \tag{4.34}$$

From (4.34), it is clear that K gets larger either when m increases or when the ratio of the LOS power to the diffuse power increases. When K is large, the TWDP approximate PDF expression in (4.30) deviates from the true TWDP fading PDF [2]. Moreover, evaluation of the coefficients a_i in (4.30) gets very difficult for large values of K [22]. For example, precise evaluation of the polynomial integrals required for computation of coefficients a_i are not straightforward for $K > 12$ dB and $\Delta = 1$ as it leads to $M = \frac{1}{2}\Delta K > 8$ [22]. Similarly, evaluation of the TWDP fading PDF and CDF expressions given in [22] is not straightforward for $K > 12$ dB [22]. To show how restrictive this fact is, we use (4.34) to determine the range of values of V_0^2 which leads to $K < 12$ dB. For $\Omega = 1$ and $m = 5$, this range is (0, 0.778), which is very small and only covers low-power LOS components. For the same value of Ω and $m = 7$, this range reduces to $(0, 0.25)$. For $m \geq 9$ and $\Omega = 1$, any positive value for V_0^2 leads to $K > 12$ dB. So, the use of the TWDP fading model to approximate the Nakagami-*m* with LOS fading model is very restricted, particularly when m is large.

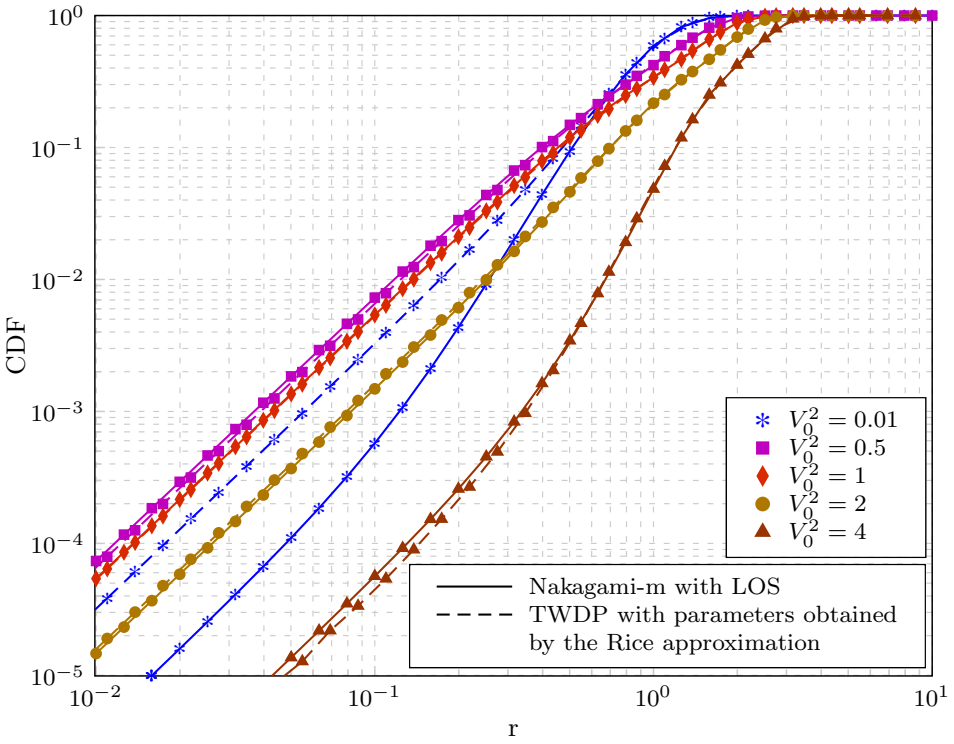

(a) $m = 2$ and $\Omega = 1$

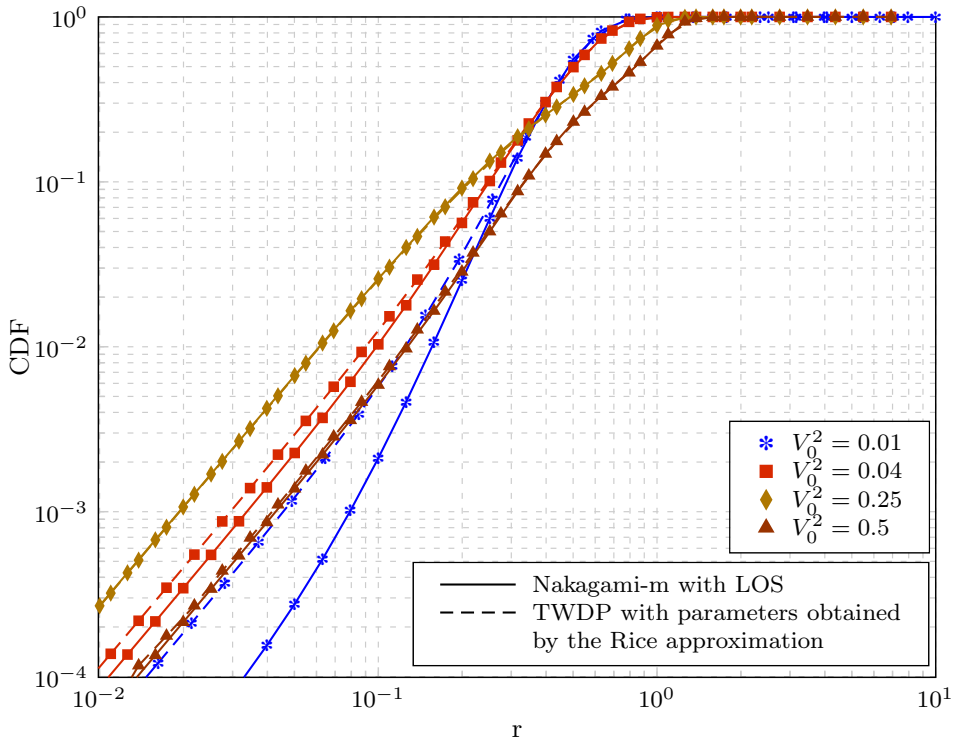

(b) $m = 4, \Omega = 1/2$

Figure 4.9. Comparison between the diffuse Nakagami-*m* with LOS fading CDF and the TWDP fading CDFs with the equivalency parameters given by the Rice approximation in (4.32) for different LOS powers.

4.1.8 Integration of the PDF Against the Complementary Error Function

A significant application of the fading PDF is in calculation of performance metrics of wireless communication systems. Evaluation of the symbol error rate (SER) of many communication systems involve integrals of the form $\mathcal{P}(\lambda) = \int_0^\infty f_R(r)\text{erfc}(ar)dr$, where $\text{erfc}(x) = \frac{2}{\sqrt{\pi}}\int_x^\infty e^{-t^2}dt$ is the complementary error function [23]. In Appendix 4.C, it is shown that

$$\mathcal{P}(\lambda) = \frac{\left(\frac{m}{\Omega}\mathrm{V}_0^2\right)^{m-1} e^{-\frac{m}{\Omega}\mathrm{V}_0^2}}{\pi\sqrt{\pi}\Gamma(m)} \sum_{i=0}^{m-1}\sum_{j=0}^{m-1-i} \frac{\binom{m-1}{i}\binom{m-1-i}{j}}{\left(\frac{m}{\Omega}V_0^2\right)^{\frac{i}{2}+j}}(-2)^i \mathrm{H}(\lambda; i, j) \tag{4.35a}$$

where

$$\mathrm{H}(\lambda; i, j) = \sum_{\substack{k=0 \\ k+i \text{ even}}}^{\infty} \frac{\left(2\sqrt{\frac{m}{\Omega}}\mathrm{V}_0\right)^k}{k!}\mathrm{B}\left(\frac{k+i+1}{2}, \frac{1}{2}\right)\Gamma\left(\frac{i+2j+k+3}{2}\right) \times \mathrm{B}_{\frac{1}{1+\frac{\Omega\lambda^2}{m}}}\left(\frac{i+k}{2}+j+1, \frac{1}{2}\right) \tag{4.35b}$$

and $B_x(\cdot,\cdot)$ is the incomplete beta function [25, Sec. 8.39]. Note that in (4.35b), the incomplete beta function can be computed recursively using

$$\mathrm{B}_x\left(n, 1/2\right) = \frac{1}{n-\frac{1}{2}}\left[(n-1)\mathrm{B}_x\left(n-1, 1/2\right) - x^{n-1}\sqrt{1-x}\right]. \tag{4.36}$$

In Appendix 4.B, we propose an efficient algorithm for evaluation of (4.35b) using (4.36).

As an example of application of (4.35), we calculate the BER of a BPSK system operating in diffuse Nakagami-*m* with LOS fading. In non-fading conditions, the BER of an optimal detector for a BPSK signal is given by $P_e(r) = \frac{1}{2}\text{erfc}\left(\sqrt{\frac{E_b}{N_0}}r\right)$, where $\frac{E_b}{N_0}$ is the signal-to-noise ratio per bit [1]. So, under diffuse Nakagami-*m* with LOS fading the BER is given by

$$\begin{aligned}\mathcal{P}_e^{\text{BPSK}}\left(\sqrt{\frac{E_b}{N_0}}\right) &= \int_0^\infty f_R(r)P_e(r)dr = \frac{1}{2}\int_0^\infty f_R(r)\text{erfc}\left(\sqrt{\frac{E_b}{N_0}}r\right)dr \\ &= \frac{1}{2}\mathcal{P}\left(\sqrt{\frac{E_b}{N_0}}\right)\end{aligned} \tag{4.37}$$

where $\mathcal{P}(\cdot)$ is defined in (4.35). The resulting BER curves are shown in Fig. 4.10 for different choices of Nakagami-*m* with LOS fading parameters. Also shown in this figure are the BER curves of BPSK systems operating in Nakagami-*m* fading and TWDP fading, with the equivalency parameters given by (4.24) and (4.32). As we observe, when $V_0^2 \ll \Omega$; i.e.,

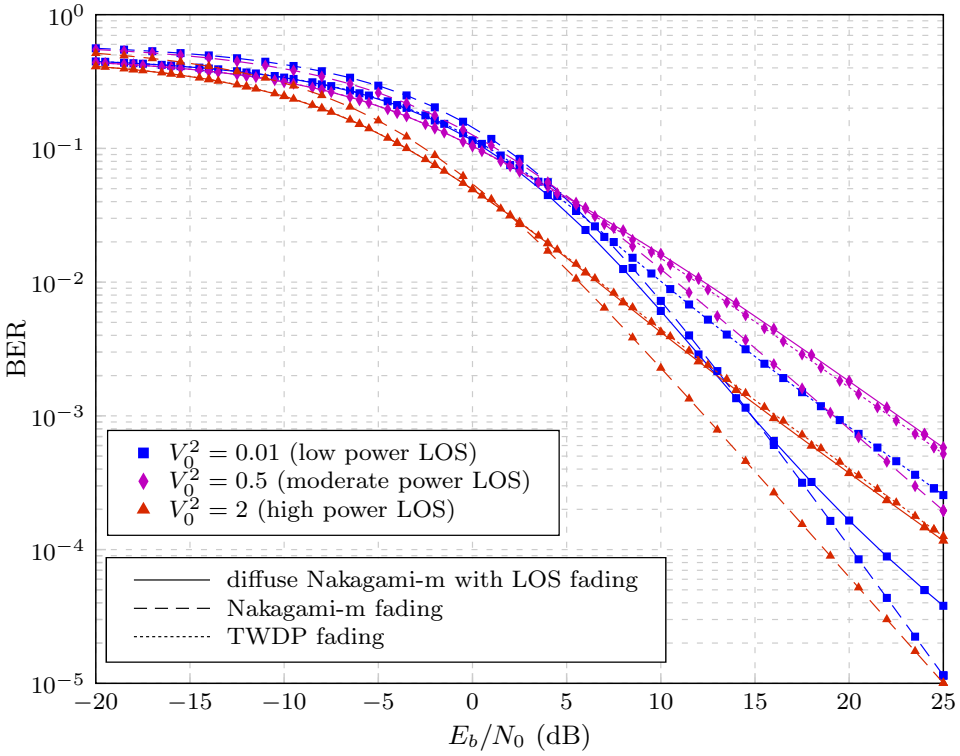

(a) $m = 2, \Omega = 1$

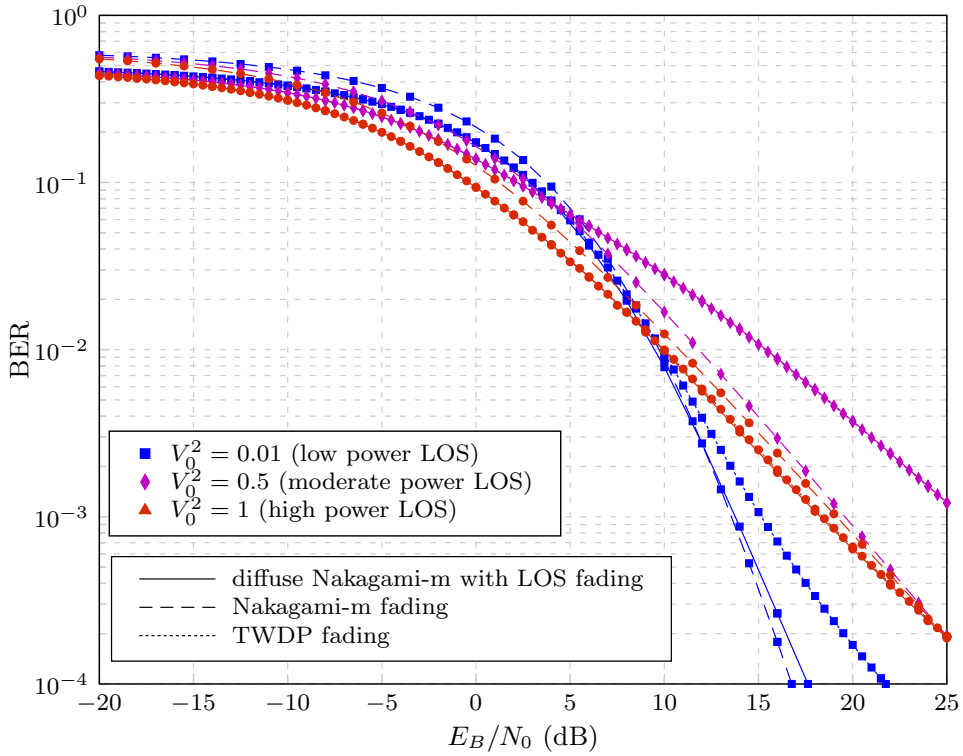

(b) $m = 4, \Omega = \frac{1}{2}$

Figure 4.10. The BER of a BPSK system operating in Nakagami-*m* with LOS fading, and Nakagami-*m* and TWDP fadings with the equivalency parameters in (4.24) and (4.32). The markers represent the Monte-Carlo simulation points.

when the LOS power is much smaller than the diffuse power, the BER curves of Nakagami-*m* with LOS fading and Nakagami-*m* fading show a similar behavior. This is expected as the presence of a LOS component is the only difference between these two fading models. As the LOS gets stronger, the Nakagami-*m* fading curves deviate from the Nakagami-*m* with LOS fading curves. We observe an exactly opposite trend in the behavior of the BER curves in TWDP fading. As the LOS power increases, the BER curves in TWDP fading show a closer fit to the BER curves in Nakagami-*m* with LOS fading. Also note that the slope of the BER curves in diffuse Nakagami-*m* with LOS fading can be different from the BER curves in Nakagami-*m* fading and TWDP fading. Among other things, this difference leads to different predictions of diversity order.

4.1.9 Conclusion

A diffuse Nakagami-*m* with LOS fading model was introduced. Expressions were derived for the PDF, CDF, moments and moment generating function of the new fading model. The Nakagami-*m* with LOS fading was compared to Nakagami-*m*, Rice and TWDP fading models. An expression was derived for the integral of the PDF of the new fading model against the complementary error function. The BER of an BPSK wireless system operating in TWDP fading was derived and its behavior was compared to the BER of BPSK systems operating in Nakagami-*m* and TWDP fading channels.

Appendix 4.A

In this appendix, we prove that (4.9) is the solution of (4.8). Using (4.6)-(4.8), we write

$$f_R(r) = \frac{2}{\Gamma(m)}\left(\frac{m}{\Omega}\right)^m r \times \int_0^\infty x^{2m-1} e^{-\frac{m}{\Omega}x^2} \underbrace{\int_0^\infty J_0(V_0\nu)J_0(r\nu)J_0(x\nu)\nu d\nu}_{\mathcal{I}_1} dx. \tag{4.38}$$

Substitution of the closed-form solution of $\mathcal{I}_1$ [19, eq. 2.12.42.16] in (4.38) gives

$$f_R(r) = \frac{2}{\pi V_0 \Gamma(m)}\left(\frac{m}{\Omega}\right)^m \int_{|V_0-r|}^{V_0+r} \frac{x^{2m-1}e^{-\frac{m}{\Omega}x^2}}{\sqrt{1-\left(\frac{v_0^2+r^2-x^2}{2V_0 r}\right)^2}} dx. \tag{4.39}$$

The change of variable $y = x^2 - (V_0^2 + r^2)$ simplifies (4.39) to

$$f_R(r) = \frac{2}{\pi\Gamma(m)}\left(\frac{m}{\Omega}\right)^m r e^{-\frac{m}{\Omega}(V_0^2+r^2)} \times \int_{-2V_0 r}^{2V_0 r} \frac{\left(y+V_0^2+r^2\right)^{m-1} e^{-\frac{m}{\Omega}y}}{\sqrt{4V_0^2 r^2 - y^2}} dy. \tag{4.40}$$

Using the binomial expansion of $(x+y)^n$ [25] in (4.40) yields

$$f_R(r) = \frac{2}{\pi\Gamma(m)}\left(\frac{m}{\Omega}\right)^m r e^{-\frac{m}{\Omega}(V_0^2+r^2)} \times \sum_{i=0}^{m-1}\binom{m-1}{i}(V_0^2+r^2)^{m-i-1}\underbrace{\int_{-2V_0r}^{2V_0r}\frac{y^i e^{-\frac{m}{\Omega}y}}{\sqrt{4V_0^2r^2-y^2}}dy}_{\mathcal{I}_2}. \tag{4.41}$$

We use [25, eq. 3.389.1] to solve the integral $\mathcal{I}_2$. This yields

$$\begin{aligned}\int_{-2V_0r}^{2V_0r}&\frac{y^i e^{-\frac{m}{\Omega}y}}{\sqrt{4V_0^2r^2-y^2}}dy \\ &= \frac{1}{2}\mathrm{B}\left(\frac{i}{2}+\frac{1}{2},\frac{1}{2}\right)(2V_0r)^i\,{}_1F_2\left(\frac{i}{2}+\frac{1}{2};\frac{1}{2},\frac{i}{2}+1;(\frac{m}{\Omega}\mathrm{V}_0r)^2\right) \\ &\quad -\frac{m}{\Omega}\mathrm{B}\left(\frac{i}{2}+1,\frac{1}{2}\right)(2V_0r)^{i+1}\,{}_1F_2\left(\frac{i}{2}+1;\frac{3}{2},\frac{i}{2}+\frac{3}{2};(\frac{m}{\Omega}\mathrm{V}_0r)^2\right).\end{aligned} \tag{4.42}$$

Substitution of (4.42) in (4.41) gives (4.9). To express the PDF as an infinite series, we use [25, eq. 9.14.1]

$${}_1F_2(a;b_1,b_2;x) = \sum_{k=0}^{\infty}\frac{(a)_k}{(b_1)_k(b_2)_k k!}x^k. \tag{4.43}$$

By substituting (4.43) in (4.9c) and using the identities [25]

$$k! = \Gamma(k+1) \tag{4.44}$$

$$\mathrm{B}(x,y) = \frac{\Gamma(x)\Gamma(y)}{\Gamma(x+y)} \tag{4.45}$$

$$\Gamma(x)\Gamma(x+\frac{1}{2}) = \frac{\sqrt{\pi}\Gamma(2x)}{2^{2x-1}} \tag{4.46}$$

$$(a)_k\Gamma(a) = \Gamma(a+k) \tag{4.47}$$

we can show that (4.9c) and (4.9b) are equal.

Appendix 4.B

In this appendix, we propose efficient algorithms for fast and accurate evaluation of the infinite series in (4.9b), (4.15b), (4.19b) and (4.35b). These algorithms highly facilitate evaluation of the derived expressions for the Nakagami-*m* with LOS fading PDF, CDF and CF, and the BER of a BPSK system operating in diffuse Nakagami-*m* with LOS fading. To derive Algorithms 4.1-4.4, we have used the recurrence relations in (4.10), (4.16), (4.20) and (4.36), respectively.

Algorithm 4.1 Efficient computation of the infinite series in (4.9b)

Require: $m \geq 0.5, \Omega > 0, V_0 \geq 0, N \geq 0, i \geq 0, r \geq 0$

$c \leftarrow \text{mod}(i, 2)$
$z \leftarrow (m/\Omega \times V_0 \times r)^2$
$a \leftarrow B(i/2 + 1/2 + c/2, 1/2) \times (4 \times z)^{c/2}$
$G_f \leftarrow a$
for $k = 0$ to N **do**
  $a \leftarrow \frac{k+i/2+1/2+c/2}{(k+1/2+c/2)(k+1+c/2)(k+i/2+1+c/2)} \times z \times a$
  $G_f \leftarrow G_f + a$
end for
return G_f

Algorithm 4.2 Efficient computation of the infinite series in (4.15b)

Require: $m \geq 0.5, \Omega > 0, V_0 \geq 0, N \geq 0, i \geq 0, j \geq 0, r \geq 0$

$c \leftarrow \text{mod}(i, 2)$
$u \leftarrow (m/\Omega \times V_0)^2$
$z \leftarrow m/\Omega \times r^2$
$w \leftarrow z^{ii/2+jj+c/2} \times \exp(-m/\Omega \times r^2)$
$a \leftarrow B(i/2 + 1/2 + c/2, 1/2) \times (4 \times u)^{c/2}$
$b \leftarrow \gamma(i/2 + j + 1 + c/2, z)$
$G_F \leftarrow a \times b$
for $k = 0$ to N **do**
  $a \leftarrow \frac{k+i/2+1/2+c/2}{(k+1/2+c/2)(k+1+c/2)(k+i/2+1+c/2)} \times u \times a$
  $w \leftarrow z \times w$
  $b \leftarrow (ii/2 + jj + k + 1 + c/2) \times b - w$
  $G_F \leftarrow G_F + a \times b$
end for
return G_F

In these algorithms, $\text{mod}(\cdot, \cdot)$ is the modulus after division function and is used to determine whether i is even or odd. Note that evaluation of the initial values of some variables in Algorithms 4.2, 4.3 and 4.4 requires computation of some special functions, namely, the beta function, the incomplete gamma function and the incomplete beta function. These functions are implemented in common mathematical softwares and they need to be evaluated just once to initialize the algorithm. Once the initial values of the variables are computed, they will update recursively. The updates only require basic mathematical operations. The number of required operations grows linearly with the series truncation order, N, in all the proposed algorithms. This allows calculating the series to high accuracy levels without making the computations time consuming and difficult, by simply increasing N.

Algorithm 4.3 Efficient computation of the infinite series in (4.19b)

Require: $m \geq 0.5, \Omega > 0, V_0 \geq 0, N \geq 0, i \geq 0, j \geq 0, r \geq 0$

$c \leftarrow \text{mod}(i, 2)$
$u \leftarrow 2 \times m/\Omega \times V_0^2$
$z \leftarrow -s/\sqrt{2 \times m/\Omega}$
$d'' \leftarrow \exp(z^2/4) \times \sqrt{\pi/2} \times (1 - \text{erf}(z/\sqrt{2}))$
$d' \leftarrow \exp(-z^2/4) - z \times d''$
$d \leftarrow d'$
$L \leftarrow i + 2j + 2 + c$
$a \leftarrow B(i/2 + 1/2 + c/2, 1/2) \times \Gamma(L) \times u^{c/2}$
for *l*=3 to L **do**
  $d \leftarrow -\frac{1}{l-1}(z \times d' - d'')$
  $d'' \leftarrow d'$
  $d' \leftarrow d$
end for
$G_\Phi \leftarrow a \times d$
for $k = 0$ to N **do**
  $a \leftarrow \frac{(k+i/2+1/2+c/2)(k+i/2+j+1+c/2)(k+i/2+j+3/2+c/2)}{(k+1/2+c/2)(k+1+c/2)(k+i/2+1+c/2)} \times u \times a$
  for $l = (L + 2 \times k + 1)$ to $(L + 2 \times k + 2)$ **do**
    $d \leftarrow -\frac{1}{l-1}(z \times d' - d'')$
    $d'' \leftarrow d'$
    $d' \leftarrow d$
  end for
  $G_\Phi \leftarrow G_\Phi + a \times d$
end for
return G_Φ

Algorithm 4.4 Efficient computation of the infinite series in (4.35b)

Require: $m \geq 0.5, \Omega > 0, V_0 \geq 0, \lambda \geq 0, N \geq 0, i \geq 0, j \geq 0$

$c \leftarrow \text{mod}(i, 2)$
$u \leftarrow m/\Omega \times V_0^2$
$z \leftarrow 1/(1 + \Omega/m \times \lambda^2)$
$n \leftarrow i/2 + j + c/2$
$w \leftarrow z^n \times \sqrt{1 - z}$
$a \leftarrow B(i/2 + 1/2 + c/2, 1/2) \times \Gamma(i/2 + j + 3/2 + c/2) \times (4 \times u)^{c/2}$
$b \leftarrow B_z(i/2 + j + 1 + c/2, 1/2)$
$H \leftarrow a \times b$
for $k = 0$ to N **do**
  $a \leftarrow \frac{(k+i/2+1/2+c/2)(k+i/2+j+3/2+c/2)}{(k+1/2+c/2)(k+1+c/2)(k+i/2+1+c/2)} \times u \times a$
  $w \leftarrow z \times w$
  $n \leftarrow n + 1$
  $b \leftarrow \frac{1}{n-\frac{1}{2}}((n-1) \times b - w)$
  $H \leftarrow H + a \times b$
end for
return H

Appendix 4.C

In this appendix, we derive an infinite series expression for the integral of the diffuse Nakagami-*m* with LOS fading PDF against the complementary error function. Define

$$\mathcal{P}(\lambda) = \int_0^\infty f_R(r)\text{erfc}(\lambda r)dr. \tag{4.48}$$

Substitution of (4.9) with (4.9b) in (4.48) yields

$$\begin{aligned}\mathcal{P}(\lambda) =& \frac{2}{\pi\Gamma(m)}\left(\frac{m}{\Omega}\right)^m e^{-\frac{m}{\Omega}\mathrm{V}_0^2}\sum_{i=0}^{m-1}\binom{m-1}{i}(-2\mathrm{V}_0)^i \times \\ & \sum_{\substack{k=0\\ k+i\,\text{even}}}^{\infty}\frac{\left(2\frac{m}{\Omega}\mathrm{V}_0\right)^k}{k!}\mathrm{B}\left(\frac{i+k+1}{2},\frac{1}{2}\right)\times \\ & \underbrace{\int_0^\infty r^{i+k+1}\left(\mathrm{V}_0^2+r^2\right)^{m-1-i}e^{-\frac{m}{\Omega}r^2}\text{erfc}(\lambda r)dr}_{\mathcal{I}_3}.\end{aligned} \tag{4.49}$$

By using the binomial expansion of $(x+y)^n$ and [19, eq. 2.8.5.7], we solve $\mathcal{I}_3$ as

$$\begin{aligned}\mathcal{I}_3 = & \sum_{j=0}^{m-1-i}\binom{m-1-i}{j}V_0^{2(m-1-i-j)}\frac{\lambda^{-\alpha}}{\alpha\sqrt{\pi}}\Gamma\left(\frac{\alpha+1}{2}\right)\times \\ & {}_2F_1\left(\frac{\alpha}{2},\frac{\alpha+1}{2};\frac{\alpha}{2}+1;-\frac{m}{\Omega\lambda^2}\right)\end{aligned} \tag{4.50a}$$

where

$$\alpha \triangleq i+2j+k+2. \tag{4.50b}$$

Moreover, we can express the hypergeometric function in (4.50a) in terms of the incomplete beta function as

$${}_2F_1\left(\frac{\alpha}{2},\frac{\alpha+1}{2};\frac{\alpha}{2}+1;-\frac{m}{\Omega\lambda^2}\right) = \left(1+\frac{m}{\Omega\lambda^2}\right)^{-\frac{a+1}{2}}{}_2F_1\left(1,\frac{\alpha+1}{2};\frac{\alpha}{2}+1;\frac{1}{1+\frac{\Omega\lambda^2}{m}}\right) \tag{4.51}$$

$$= \frac{a}{2}\left(\frac{m}{\Omega\lambda^2}\right)^{-\frac{a}{2}}\mathrm{B}_{\frac{1}{1+\frac{\Omega\lambda^2}{m}}}\left(\frac{a}{2},\frac{1}{2}\right) \tag{4.52}$$

where we have used [20, eqs. 7.3.1.3 and 7.3.1.119] to write (4.51) and (4.52), respectively.

Bibliography

[1] J. G. Proakis, *Digital Communications,* 4th ed., New York: McGraw-Hill, 2001.

[2] G. D. Durgin, T. S. Rappaport, and D. A. Wolf, "New analytical models and probability density functions for fading in wireless communications," *IEEE Trans. Commun.,* vol. 50, no. 6, pp. 1005-1015, June 2002.

[3] M. Nakagami, " The m-distribution, a general formula of intensity of rapid fading," in *Statistical Methods in Radio Wave Propgation,* W. G. Hoffman, Ed. Oxford, England Pergamon, 1960.

[4] H. Suzuki, "A statistical model for urban radio propagation" *IEEE Trans. Commun.,* vol. 25, no. 7, pp. 673-680, July 1977.

[5] W. R. Braun and U. Dersch, "A physical mobile radio channel model" *IEEE Trans. Veh. Technol.,* vol. 40, no. 2, pp. 472-482, May 1991.

[6] N. C. Beaulieu and A. A. Abu-Dayya, "Analysis of equal gain diversity on Nakagami fading channels," *IEEE Trans. Commun.,* vol. 39, no. 2, pp. 225-234, Feb. 1991.

[7] A. A. Abu-Dayya and N. C. Beaulieu, "Outage probabilities of cellular mobile radio systems with multiple Nakagami interferers," *IEEE Trans. Veh. Technol.,* vol. 40, no. 4, pp. 757-768, Nov. 1991.

[8] E. Al-Hussaini and A. Al-Bassiouni, "Performance of MRC diversity systems for the detection of signals with Nakagami fading," *IEEE Trans. Commun.,* vol. 33, no. 12, pp. 1315-1319, Feb. 1985.

[9] V. A. Aalo, "Performance of maximal-ratio diversity systems in a correlated Nakagami-fading environment," *IEEE Trans. Commun.,* vol. 43, no. 8, pp. 2360-2369, Aug. 1995.

[10] V. A. Aalo, O. Ugweje, and R. Sudhakar, "Performance analysis of a DS/CDMA system with noncoherent M-ary orthogonal modulation in Nakagami fading," *IEEE Trans. Veh. Technol.,* vol. 47, no. 1, pp. 20-29, Feb. 1998.

[11] Q. T. Zhang, "Maximal-ratio combining over Nakagami fading channels with an arbitrary branch covariance matrix," *IEEE Trans. Veh. Technol.,* vol. 48, no. 4, pp. 1141-1150, July 1999.

[12] P. Lombardo, G. Fedele, and M. M. Rao, "MRC performance for binary signals in Nakagami fading with general branch correlation," *IEEE Trans. Commun.,* vol. 47, no. 1, pp. 44-52, Jan. 1999.

[13] M. D. Yacoub, C. R. C. M. Da Silva, and J. E. Varga Bautista, "Second-order statistics for diversity-combining techniques in Nakagami-fading channels," *IEEE Trans. Veh. Technol.,* vol. 50, no. 6, pp. 1464-1470, Nov. 2001.

[14] M. O. Hansna and M. S. Alouini, "Outage probability of multihop transmission over Nakagami fading channels," *IEEE Commun., Lett.* vol. 7, no. 5, pp. 216-218, May 2003.

[15] G. K. Karagiannidis, "Moments-based approach to the performance analysis of equal gain diversity in Nakagami-*m* fading," *IEEE Trans. Commun.,* vol. 52, no. 5, pp. 685-690, May 2004.

[16] N. C. Beaulieu and J. Cheng, "Precise error-rate analysis of bandwidth-efficient BPSK in Nakagami fading and cochannel interference," *IEEE Trans. Commun.,* vol. 52, no. 1, pp. 149-158, Jan. 2004.

[17] G. K. Karagiannidis, "On the symbol error probability of general order rectangular qam in Nakagami-*m* fading," *IEEE Commun., Lett.* vol. 10, no. 11, pp. 745-747, Nov. 2006.

[18] A. Abdi, H. Hashemi, and S. Nader-Esfahani, "On the PDF of the sum of random vectors," *IEEE Trans. Commun.,* vol. 48, no. 1, pp. 7-12, Jan. 2000.

[19] A. P. Prudnikov, Y. A. Brychkov, and O. I. Marichev, *Integrals and Series, Vol. 2*, Gordon and Breach Science Publishers, 1986.

[20] A. P. Prudnikov, Y. A. Brychkov, and O. I. Marichev, *Integrals and Series, Vol. 3*, Gordon and Breach Science Publishers, 1986.

[21] A. Papoulis and S. U. Pillai, *Probability, Random Variables and Stochastic Processes*, New York: McGraw-Hill, 2002.

[22] S. A. Saberali and N. C. Beaulieu, "New expressions for TWDP fading statistics," *Accepted for publication in IEEE Wireless Commun. Letts.*

[23] M. Abramowitz and I. A. Stegun, *Handbook of Mathematical Functions with Formulas, Graphs, and Mathematical Tables*, New York: Dover, 1970.

[24] M. K. Simon and M. S. Alouini, *Digital Communications over Fading Channels*, Wiley, 2005.

[25] I. S. Gradshteyn and I. M. Ryzhik, *Table of Integrals, Series, and Products,* San Diego, CA: Academic Press, seventh ed., 2007.

Chapter 5

Conclusion

In this chapter, we summarize the contributions of this thesis. The main focus of this thesis was to improve the existing mathematical tools for the statistical modeling and mathematical analysis of shadowing and multipath fading systems.

In Chapter 2, we investigated the problem of approximating the lognormal CF. We developed a novel method for deriving limiting expressions for the lognormal CF. Unlike most of the previous work in the literature that has looked at this problem from a numerical analysis point of view, we looked at the problem from a statistical theory perspective, by means of the CLT. Using the new framework, we derived two limiting expressions for the lognormal CF. Among the derived expressions, one is only of theoretical significance, while the other is also useful in practice for approximating the lognormal CF. Although we obtained only two limiting expressions for the lognormal CF, application of the proposed framework is not limited to our results in this thesis. An outline of our future research plans regarding the materials in Chapter 2 was also sketched.

In Chapter 3 of this thesis, we focused on improving the mathematical tools for the analysis of TWDP fading systems. We derived an alternative expression for the TWDP fading PDF. The new expression was used to derive new formulas for the TWDP fading CDF and moments. It was shown that application of the proposed PDF expression in the performance analysis of BPSK systems is straightforward. Algorithms were developed for fast, accurate and efficient evaluation of the TWDP fading PDF and CDF as well as the BER of a BPSK system operating in TWDP fading. It was shown that the new BER expression obtained for BPSK systems in TWDP fading is superior to the existing BPSK BER expressions in the TWDP literature. Potential future research directions were also discussed.

Finally, we investigated a novel multipath fading model in Chapter 4. The new model combines a LOS component and a Nakagami-*m* diffuse component at the receiver. At the

first part of our contributions in Chapter 4, we justified the new fading model and we derived expressions for evaluating its PDF, CDF, CF and moments. We also proposed efficient algorithms for evaluating the derived expressions with low computational complexity. Then, we compared the new fading model with some of the existing fading models, namely the Rice, Nakagami-*m* and TWDP fading models. We showed that TWDP fading exhibits a closer behavior to diffuse Nakagami-*m* with LOS fading. However, none of the considered models can perfectly represent the behavior of the new fading model. We also discussed the application of the results in the performance analysis of fading systems and we derived the BER of a BPSK system operating in diffuse Nakagami-*m* with LOS fading.